

DEVELOPMENT OF INFRARED SPECTROSCOPIC METHODS FOR
ASSESSMENT OF EXTRACELLULAR MATRIX CHANGES IN
CARDIOVASCULAR DISEASES

A Dissertation
Submitted to
the Temple University Graduate Board

In Partial Fulfillment
of the Requirements for the Degree
DOCTOR OF PHILOSOPHY

by
Rabee Cheheltani
May 2014

Examining Committee Members:

Mohammad F. Kiani, Department of Mechanical Engineering
Nancy Pleshko, Department of Bioengineering
Abdel Karim Sabri, Department of Physiology
David A. Vorp, Department of Bioengineering, University of Pittsburgh
Bin Wang, Department of Biomedical Engineering, Widener University
Mary F. Barbe, Department of Anatomy and Cell Biology

ABSTRACT

Extracellular matrix (ECM) is a key component and regulator of many biological tissues. Several cardiovascular pathologies are associated with significant changes in the composition of the matrix. Better understanding of these pathologies and the physiological phenomenon behind their development depends on reliable methods that can measure and characterize ECM content and structure. In this dissertation, infrared spectroscopic methodologies are developed to study the changes in extracellular matrix of cardiovascular tissue in two cardiovascular pathologies; myocardial infarction and abdominal aortic aneurysm.

The specific aims of this dissertation were:

1. To develop a Fourier transform infrared imaging spectroscopy (FT-IRIS) methodology for creating distribution maps of collagen in remodeled cardiac tissue sections after myocardial infarction, and to quantitatively compare maps created by FT-IRIS with conventional staining techniques.
2. To develop an FT-IRIS method to assess elastin and collagen composition in the aortic wall. This will be accomplished using ex vivo animal aorta samples, where the primary ECM components of the wall will be systematically enzymatically degraded.
3. To apply the newly developed FTIR imaging methodology to evaluate changes in the primary ECM components (collagen and elastin) in the wall of human AAA tissues.

The infrared absorbance band centered at 1338 cm^{-1} , was used to map collagen deposition across heart tissue sections of a rat model of myocardial infarction, and was correlated strongly in the size of the scar ($R=0.93$) and local intensity of collagen deposition ($R=0.86$).

In enzymatically degraded pig aorta samples, as a model of ECM degradation in abdominal aortic aneurysm (AAA), partial least squares (PLS) models were created to predict collagen and elastin content in aorta based on collected FTIR spectra and biochemically measured values. PLS models based on FT-IRIS spectra were able to predict elastin and collagen content of the samples with strong correlations ($R^2=0.90$ and 0.70 respectively). Elastin content prediction from IFOP spectra was successful through a PLS regression model with high correlation ($R^2=0.81$).

The PLS regression coefficient from the FT-IRIS models were used to map collagen and elastin human AAA biopsy tissue sections, creating a similar map of each component compared to histologically stained images. The mean value of collagen deposition in each tissue was calculated for 13 pairs of AAA samples where stress had been calculated using finite element modeling. In most pairs with stress values higher than 5 N/m^2 , collagen content was lower in the sample with higher stress value. Collagen maturity had a weak negative correlation ($R=-0.35$) with collagen content in these samples.

These results confirm that infrared spectroscopy is a powerful tool that can be applied to replace or complement conventional methods such as histology and biochemical analysis to characterize ECM components in cardiovascular tissues. Furthermore, infrared spectroscopy has the potential for translation to a clinical environment to examine ECM changes in aorta in a minimally invasive fashion using fiber optic technology.

This dissertation is dedicated to my parents,
for their endless love and support, even from thousands of miles away.

And to Soroush,
for his love, friendship and partnership, which ever inspires me.

ACKNOWLEDGMENTS

I would like to thank my advisors Dr. Mohammad Kiani and Dr. Nancy Pleshko for their continuous help and support during the development of this dissertation. It has been a great pleasure and honor being their student. Dr. Kiani has been my teacher and mentor from the very first steps of developing myself as a scientist. He has been giving me unrestricted guidance and support in all aspects of my training. He is a real role model. Dr. Pleshko generously adopted me as an honorary member of her group, offering her facilities and her time for the past few years, teaching me, encouraging me and hugely inspiring me. I am extremely grateful for everything I learnt from them.

I would like to thank all members of my advisory committee. Dr. Bin Wang has been kindly offering his time and expertise during various stages of my project. Dr. Abdel Karim Sabri patiently worked with me for several months as I was resolving one of the biggest challenges of this project. Dr. David Vorp has been a generous collaborator, supporting me with his expertise and his resources, and his original ideas in developing the in vitro aneurysm model. I would also like to thank Dr. Mary Barbe who kindly accepted to provide her expertise as the external reader.

I would like to acknowledge Jenna Rosano, Jennifer Marmion, Giuseppina Lamberti and Dr. Yuan Tang in Temple Biofluidics Laboratory, and Mugdha Padalkar and Uday Palukuru in Tissue Imaging and Spectroscopy Laboratory, and all my friends and colleagues in the College of Engineering who have been kindly supporting me for the past few years. Special thanks go to Dr. Cushla McGoverin and Dr. Arash Hanifi for their tremendous help as I was learning infrared spectroscopy data collection and analysis.

TABLE OF CONTENTS

ABSTRACT.....	II
DEDICATION.....	IV
ACKNOWLEDGMENTS.....	V
LIST OF TABLES.....	IX
LIST OF FIGURES.....	X
CHAPTER 1 INTRODUCTION.....	1
1.1 Overview.....	1
1.2 Specific Aims.....	2
1.3 Organization of the Dissertation.....	3
1.4 Extracellular Matrix.....	4
1.4.1 Collagen.....	4
1.4.2 Elastin and Elastic Fibers.....	7
1.5 Cardiovascular ECM in Health and Disease.....	8
1.5.1 Cardiac ECM and Cardiac Remodeling.....	8
1.5.2 Arterial ECM and Abdominal Aortic Aneurysm.....	10
1.6 Fourier Transform Infrared Spectroscopy.....	12
1.6.1 Basics.....	12
1.6.2 Sampling Techniques.....	13
1.6.3 Pre-Processing of FTIR Spectra.....	15
1.6.4 FTIR Data Analysis.....	17
1.7 Application of FTIR in cardiovascular tissues.....	19
1.7.1 FTIR Studies of Cardiac Tissue.....	19
1.7.2 FTIR Studies of Arterial Tissue.....	20
1.7.3 The Contribution of this Dissertation.....	24
CHAPTER 2 FOURIER TRANSFORM INFRARED SPECTROSCOPIC IMAGING OF CARDIAC TISSUE TO DETECT COLLAGEN DEPOSITION AFTER MYOCARDIAL INFARCTION.....	25
2.1 Abstract.....	25
2.2 Introduction.....	26
2.3 Materials and Methods.....	29
2.3.1 Induction of MI.....	29

2.3.2	Targeted Delivery of VEGF Treatment	29
2.3.3	Extraction of Heart Samples and Cryopreservation.....	30
2.3.4	Cryo-sectioning	30
2.3.5	FT-IRIS Data Acquisition and Analysis	31
2.3.6	Immunohistochemical staining for collagen type I.....	31
2.3.7	Histological Staining.....	32
2.3.8	Image Processing	34
2.3.9	Statistical Data Analysis	36
2.4	Results.....	36
2.4.1	Qualitative Correlation of FT-IRIS Data vs Staining Methods	36
2.4.2	FT-IRIS to Map Collagen Deposition Density	37
2.5	Discussion.....	38
CHAPTER 3 INFRARED SPECTROSCOPY TO MEASURE COLLAGEN AND ELASTIN IN AORTA USING MULTIVARIATE ANALYSIS		45
3.1	Abstract.....	45
3.2	Introduction	46
3.3	Materials and Methods.....	47
3.3.1	Pure Component Pellets	47
3.3.2	Porcine Aorta Pellets.....	47
3.3.3	Enzymatic Degradation of Aorta Specimens.....	47
3.3.4	Data processing.....	48
3.4	Results and Discussion	48
CHAPTER 4 FOURIER TRANSFORM INFRARED SPECTROSCOPY TO QUANTIFY COLLAGEN AND ELASTIN DEGRADATION IN AN IN VITRO MODEL OF ABDOMINAL AORTIC ANEURYSM.....		51
4.1	Abstract.....	51
4.2	Introduction	52
4.3	Material and Methods	55
4.3.1	Preparation of the aorta samples	55
4.3.2	Enzymatic degradation of the aorta samples	55
4.3.3	Biochemical analysis for quantification of elastin and collagen	56
4.3.4	FTIR Fiber optic probe (IFOP) data collection	57
4.3.5	FT-IRIS data collection and analysis	58
4.3.6	PLS models	58
4.3.7	Pure component pellets.....	59
4.3.8	Mapping components in aorta and human AAA sections	60
4.3.9	Histological staining	61
4.4	Results and Discussion	61

4.4.1	Measured collagen and elastin content in aorta	61
4.4.2	FTIR Spectral features of Elastin, Collagen and Aorta Samples	63
4.4.3	PLS Models.....	66
4.4.4	Mapping components in aorta sections and human AAA section.....	69
4.4.5	Conclusion.....	70
CHAPTER 5 CORRELATION OF FOURIER TRANSFORM INFRARED SPECTROSCOPIC IMAGING-DERIVED PARAMETERS WITH MECHANICAL PROPERTIES OF ABDOMINAL AORTIC ANEURYSM.....		72
5.1	Introduction	72
5.1.1	Abdominal Aortic Aneurysm	72
5.1.2	AAA Extracellular Matrix.....	73
5.1.3	Intraluminal Thrombus	75
5.1.4	Mechanical Properties in AAA	76
5.2	Material and Methods	77
5.2.1	AAA Tissue Preparation.....	77
5.2.2	Mechanical Properties	77
5.2.3	FT-IRIS Data Collection and Analysis.....	78
5.3	Results.....	79
5.3.1	Elastin Distribution.....	79
5.3.2	Collagen Distribution	80
5.3.3	Relationship between Collagen and Stress.....	81
5.3.4	Relationship between Collagen and ILT Thickness	82
5.3.5	Relationship between Collagen Maturity and Content	84
5.4	Discussion.....	85
CHAPTER 6 SUMMARY AND CONCLUSION		88
REFERENCES.....		91

LIST OF TABLES

Table 1-1 Amino acid composition of collagen in mammalian bone and skin	5
Table 1-2 Amino acid composition of mammalian elastin	8
Table 1-3 Amino acid composition of mammalian elastin	23
Table 3-1 Collagen and elastin content in aorta specimens	48
Table 3-2 Summary of PLS results in collagen-elastin and degraded aorta KBr pellets	49
Table 4-1 Summary of the four PLS models and their abbreviations in chapter 4.....	58

LIST OF FIGURES

Figure 1.1 Triple helical structure of collagen.....	5
Figure 1.2 Fibrillar procollagens and collagen assembly and formation of covalent crosslinks.....	6
Figure 1.3 Elastic recoil property of elastic fibers.....	7
Figure 1.4 Idealization of a healthy elastic artery.....	11
Figure 1.5 Conceptual illustration for PLS.....	19
Figure 2.1 FTIR spectra of myocardial tissue	33
Figure 2.2 FT-IRIS and immunohistochemical staining (IHC) in cardiac tissue	35
Figure 2.3 Collagen deposition in infarcted left ventricle using FT-IRIS and other methods	37
Figure 2.4 Correlation of collagen intensity between FT-IRIS and IHC staining.	38
Figure 2.5 Comparison of FT-IRIS and trichrome staining.	40
Figure 3.1 Score plots of the PLS model on KBr Pellets	50
Figure 4.1 Experimental procedure for in vitro AAA mode.	57
Figure 4.2 Experimental procedure for in vitro AAA mode	62
Figure 4.3 Average spectra of samples with low, medium and high elastin content.....	65
Figure 4.4 Predicted vs. reference values for the developed PLS models.....	68
Figure 4.5 Comparison of factor 1 in PLS models predicting collagen and elastin.....	69
Figure 4.6 Histological and FT-IRIS images of aorta samples.....	71
Figure 5.1 Proposed stages of AAA progression [121].....	74
Figure 5.2 FT-IRIS mapping of elastin in a neovessel formed in a human AAA wall.....	80
Figure 5.3 FT-IRIS mapping of collagen in an example AAA sample.....	81
Figure 5.4 Collagen quantity vs. Stress in AAA samples.	82
Figure 5.5 Collagen quantity vs. Stress in the media of AAA samples.	83
Figure 5.6 Collagen quantity in the media vs. ILT Thickness of AAA samples.	83
Figure 5.7 Relationship between collagen content and maturity	84

CHAPTER 1

INTRODUCTION

1.1 Overview

Extracellular matrix (ECM) is a key component of biological tissues. It is a material synthesized by cells, is found between the cells, and is crucial for the structure and function of tissues [1]. ECM provides a structure for the cells to grow in and affects their function through cell-matrix interactions [2], [3]. One of the major features of cardiovascular pathologies is significant changes in the composition of the extracellular matrix. Better understanding of these pathologies and the physiological phenomenon behind their development depends on reliable methods that can measure and characterize ECM content and structure. Several methodologies have been developed to assess the content and composition of ECM in biological tissues. Histochemical assays are some of the most common methods for visualizing components in tissue sections. Immunohistochemical staining methods provide a more specific, sensitive and quantifiable staining technique but they use expensive reagents and achieving reliable results require substantial preparation and experimentation. Biochemical assays are available that provide quantitative measurement of components, but they are destructive methods. In this dissertation, methodologies based on Fourier transform infrared spectroscopy (FTIR) are developed as alternative or complementary methods to these conventional assays, and the applicability of the developed methods are compared with conventional methods.

1.2 Specific Aims

The specific aims of this dissertation are:

1. To develop a Fourier transform infrared imaging spectroscopy (FT-IRIS) methodology for creating distribution maps of collagen in remodeled cardiac tissue sections after myocardial infarction and quantitatively compare maps created by FT-IRIS with conventional staining techniques.
2. To develop an FTIR method to assess elastin and collagen composition in the aortic wall. This will be accomplished using ex vivo animal aorta samples, where the primary ECM components of the wall will be enzymatically degraded in a systematic manner.
 - a. The level of degradation will be assessed by FT-IRIS in terms of the relative amounts of elastin and collagen in the samples. The FT-IRIS results will be validated using established histological techniques.
 - b. Infrared fiber optic probe data will be collected from the degraded tissues to validate the feasibility of this data collection mode.
3. To apply the newly developed FTIR imaging methodology to evaluate changes in the primary ECM components (collagen and elastin) in the wall of human AAA tissues.
 - a. FT-IRIS data collection and analysis will be performed on tissue sections from human biopsies of patients with abdominal aortic aneurysm, and will be validated using established histological techniques.

- b. The results from FT-IRIS will be used to study correlations between ECM components and mechanical properties of the tissue.

1.3 Organization of the Dissertation

In this dissertation, novel infrared spectroscopic methods have been developed for the characterization of extracellular matrix (ECM) proteins in cardiovascular tissues. The methods of and findings from Specific Aim 1 is covered in CHAPTER 2 which is focused on cardiac tissue. CHAPTER 3 covers the first step in development of infrared spectroscopic methods in measuring collagen and elastin in aorta tissue using potassium bromide pellets. CHAPTER 4 and CHAPTER 5 address Specific Aims 2 and 3 and the development of the methodology in aortic tissue in the context of abdominal aortic aneurysm and the application of the methodology in correlating the ECM component quantity with mechanical properties.

In this chapter, first tissue extracellular matrix is described and a review of the structure and function of major cardiovascular extracellular matrix components are provided (section 1.4). The following section (section 1.5) introduces cardiac and arterial extracellular matrix components and structure, and two cardiovascular pathologies that are the focus of this dissertation; cardiac remodeling following myocardial infarction and abdominal aortic aneurysm. After a general overview of the pathology, the effect and importance of extracellular matrix changes in each of the described pathologies is reviewed. The next section (section 1.6), is devoted to Fourier transform infrared spectroscopy, its basics, its different modalities and spectral processing methods. In the final section (section 1.7) a review of current literature on applying infrared spectroscopy in characterization of extracellular matrix in cardiovascular tissues is presented.

1.4 Extracellular Matrix

ECM in animals consist of three major classes of molecules: (1) structural proteins such as collagen and elastin, which provide the strength and flexibility; (2) protein-polysaccharide complexes called proteoglycans, which provide an embedding structure for structural proteins; and (3) adhesive glycoproteins such as fibronectins and laminins, which anchor cells to the ECM [1]. The difference in the ECM properties in different tissues arise from the difference in the composition of these molecules as well as the relative ratio of these classes in the tissue [1]. ECM proteins are large and complex molecules with several highly specific and distinct domains necessary for their function [2], [4]. In cardiovascular tissue, ECM proteins are mainly collagen and elastin macromolecules.

1.4.1 Collagen

Collagen is the most abundant protein with various functions in different tissues. It has a variety of forms and functions and is present in tendon, ligament, bone, dentin, skin, arteries and cartilage [5]. The collagen family of proteins is composed of 28 different types of collagen that assemble into suprastructures in the form of fibrils, micro-fibrils or network-like structures [3].

The hallmark of collagen molecule is its triple helix structure. Stabilized by hydrogen bonds, this right-handed helix is composed of three polypeptide chains called α -chains. Each α -chain contains a repeating $(\text{Gly-X-Y})_n$ structure with the X and Y being each of the 21 amino acids. Proline and hydroxyproline are the most frequent amino acids in X and Y positions respectively (Figure 1.1) [6]. Collagen formation and regulation is a complex process that includes several

post-translational modifications [6]–[8]. The mean amino acid composition of collagen in mammalian bone and skin is listed in Table 1-1.

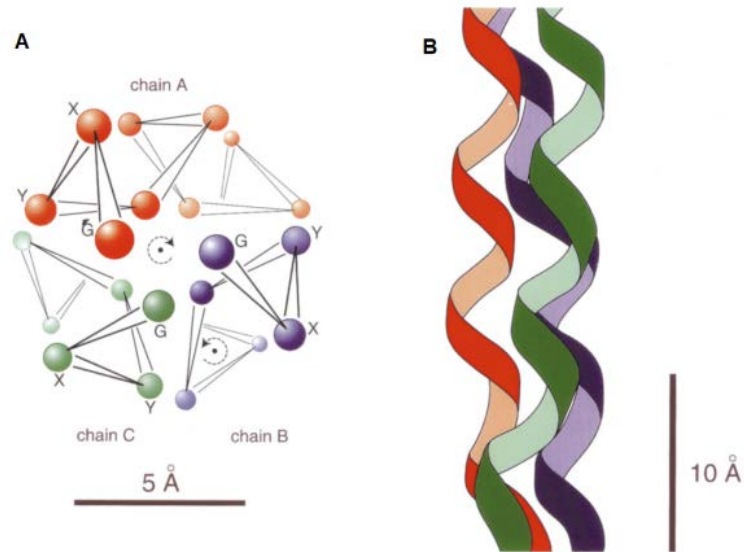


Figure 1.1 Triple helical structure of collagen. A) Cross-section view (G=Gly). B) longitudinal view [9]

Table 1-1		
<i>Amino acid composition of collagen in mammalian bone and skin presented as residues per 1000 residues [10]</i>		
	Bone	Skin
Aspartic Acid	48 ± 3	47 ± 3
Hydroxyproline	95 ± 8	95 ± 7
Threonine	19 ± 2	19 ± 4
Serine	35 ± 4	36 ± 5
Glutamic acid	75 ± 4	74 ± 3
Proline	119 ± 7	126 ± 6
Glycine	330 ± 11	329 ± 18
Alanine	115 ± 9	109 ± 8
Valine	23 ± 2	22 ± 3
Methionine	4 ± 2	6 ± 2
Isoleucine	11 ± 2	11 ± 2
Leucine	26 ± 2	24 ± 3
Tyrosine	3 ± 2	3 ± 2
Phenylalanine	14 ± 1	13 ± 2
Hydroxylysine	6 ± 3	6 ± 1
Lysine	26 ± 3	29 ± 4
Histidine	5 ± 1	5 ± 3
Arginine	49 ± 4	49 ± 3

One of the major subfamilies of collagen molecule is fibrillar collagens that include collagen types I, II, III and V. Fibrillar collagens are of most interest from the biomechanical point of view due to their role in the tissue structural integrity and resistance to tensile stress [6], [8]. All fibrillar collagens are synthesized as soluble precursors called procollagens that undergo subsequent biosynthesis processes to form collagen fibrils. Collagen fibrils are subsequently stabilized by the formation of covalent cross-links (Figure 1.2), which for the most part are initiated by members of the lysyl oxidase family of copper-dependent amine oxidases [6]. The formation of the crosslinks and the tissue-specific alignment of the cross-linked fibers have a direct effect in mechanical properties necessary in each tissue. Examples include longitudinal strength in tendon due to parallel alignment of the fibers, tensile strength in bone due to concentric layers, compliance in skin due to random organization and strength and transparency in cornea due to precise layered organization [3], [11].

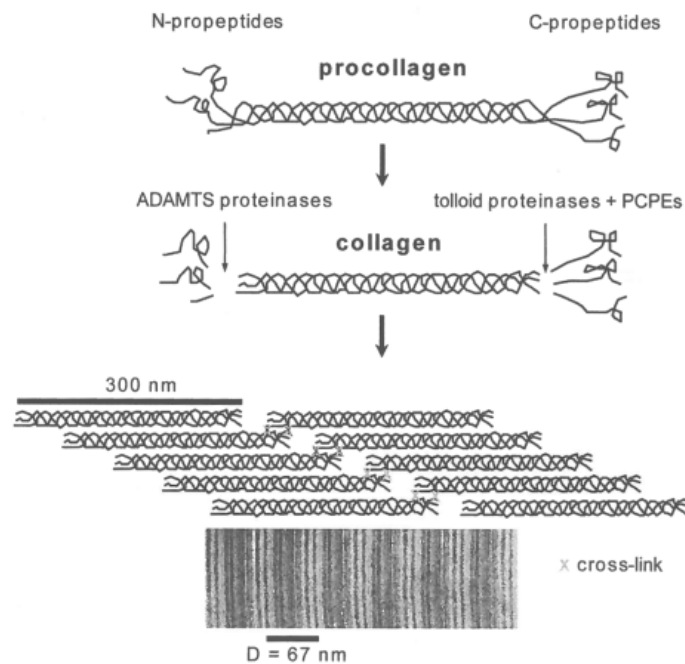


Figure 1.2 Fibrillar procollagens and collagen assembly and formation of covalent crosslinks. (Adapted from [6])

1.4.2 Elastin and Elastic Fibers

Elastic fibers provide elasticity in tissues that are subject to repeated stretching such as lungs and blood vessels. Unlike collagen, elastic fibers are highly elastic proteins that can stretch up to twice their length and retain elastic recoil. The major constituent of elastic fibers is elastin.

Elastin is an amorphous protein, but when it is laid on a network of microfibrils of 10-12nm diameter (consisting of several proteins), the mature elastic fibers are formed [12]–[14], which are capable of elastic recoil (Figure 1.3). The amino acid composition of elastin is provided in Table 1-2.

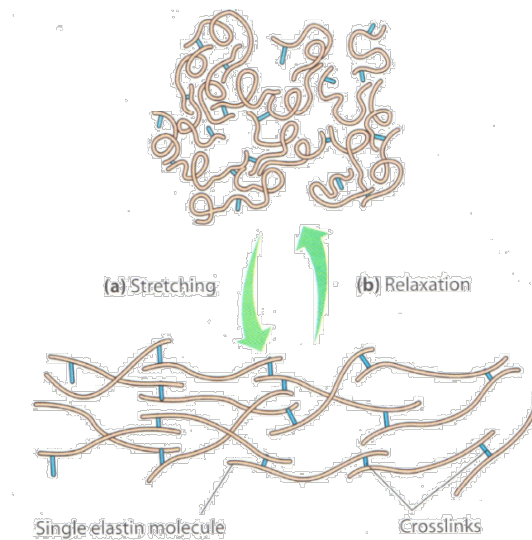


Figure 1.3 Elastic recoil property of elastic fibers. (Adapted from Becker et al. [1])

Elastin turnover is very low and elastic fibers are considered to last the lifetime of the organism [15], [16]. It is however subject to proteolytic degradation and chemical alterations due to aging and disease that change its mechanical properties [15], [17], [18]. Purified elastin is highly insoluble in aqueous solutions [16]. Tropoelastin is the soluble precursor of elastin. Pre-tropoelastin is the precursor of tropoelastin that is synthesized in the ribosome of specific cells.

Elastin binding protein (EBP) transports tropoelastin to outside the cell and the EBP-tropoelastin complex outside the cell binds itself to a structure of fibrillin-rich microfibrils [19]. The interaction between microfibrillar molecules and tropoelastin has been discussed by Kielty et al [20]. Elastin is a highly cross-linked polymer with the crosslinking initiated by lysyl oxidase family which is also responsible for the crosslinking of collagen. Crosslinking per unit protein in elastin is 1.5-2 times higher than collagen [13].

Table 1-2		
<i>Amino acid composition of mammalian elastin presented as residues per 1000. [14]</i>		
	Bovine Lung Parenchyma	Human Aorta
Aspartic Acid	8	10
Hydroxyproline	10	8
Threonine	10	7
Serine	10	9
Glutamic acid	24	17
Proline	108	104
Glycine	302	324
Alanine	213	224
Valine	148	143
Methionine	1	0
Isoleucine	17	27
Leucine	66	65
Tyrosine	7	9
Phenylalanine	38	26
Hydroxylysine	0	ND
Lysine	13	5
Histidine	3	1
Arginine	10	5

1.5 Cardiovascular ECM in Health and Disease

1.5.1 Cardiac ECM and Cardiac Remodeling

The heart pumps the blood into the blood vessels of the body, with its pumping function mostly performed by cardiac myocytes, the muscle cells in the cardiac tissue. The viability and functionality of myocardium, among other factors, depends to a large extent on its extracellular matrix which includes the interstitial matrix and the basement membranes [21], [22]. The major

structural proteins of this matrix are collagen fibers of type I and III. These collagen fibers provide the supporting scaffold for maintaining the shape and functionality of the cardiac tissue, coordinate the pumping force and resilience of the myocytes, and are determining factors in diastolic and systolic stiffness of the cardiac tissue[21], [22].

One of the most critical cases of cardiac ECM alteration is cardiac remodeling, defined as the change in size, shape and function of the heart after injury. This adverse remodeling can occur as a result of several diseases such as myocardial infarction (MI), hypertension and inflammatory heart muscle disease (myocarditis). This remodeling is accompanied by a progressive increase in the mass and volume of the left ventricle and a change in its shape, ultimately resulting in ischemic heart disease and cardiac dysfunction[23].

In myocardial infarction (MI), a blockage of coronary arteries that feed the cardiac myocytes results in necrosis and death of cardiomyocytes. In the complex physiological processes that follow an MI, the dead cardiomyocytes are replaced with fibrillar collagen which results in formation of scar tissue in the infarct zone as well as excessive deposition of fibrous tissue in interstitium remote to infarction site [21], [24]. These changes lead to increased stiffness and eventually cardiac dysfunction [24], [25]. Advancements in the clinical management of MI, especially in high income countries, has resulted in the higher survival rates from this acute condition; however, the subsequent cardiac remodeling and resulting ischemic heart disease has become one of the leading causes of death in these countries [26].

Several assays have been developed to assess the excess collagen deposition in cardiac tissue. Histochemical assays such as trichrome or picrosirius red staining protocols are some of the most common methods of visualizing collagen deposition in heart sections [24], [27].

Immunohistochemical staining methods provide a more specific, sensitive and quantifiable staining technique but they use expensive reagents and achieving reliable results require substantial preparation and experimentation [28], [29]. In Specific Aim 1 of this dissertation (CHAPTER 2), we develop a Fourier transform infrared imaging spectroscopy (FT-IRIS) method as an alternative or complementary method to these conventional assays. In this specific aim, we create distribution maps of collagen in remodeled cardiac tissue sections and create a map by FT-IRIS which will be compared to conventional staining techniques.

1.5.2 Arterial ECM and Abdominal Aortic Aneurysm

Arterial wall is composed of three distinct layers: the intima, media and adventitia (Figure 1.4). The cellular and extracellular composition of these layers is related to their functionality. The innermost layer, tunica intima, is essentially composed of a single layer of endothelial cells that are in direct contact with the blood flow. Tunica media is composed of smooth muscle cells surrounded by an elastic extra-cellular matrix (ECM) of fibrous proteins, elastin and collagen. Elastin fibers provide the elastic properties and tensile strength of the aorta necessary for propulsion of the blood downstream. These fibers are arranged in concentric plates called elastic lamellae with a network of finer elastic fibers between lamellae. Collagen fibers, which are dispersed in the space between the lamellae, contribute to the strength and structural integrity of the aorta. The outermost layer, tunica adventitia, is surrounded by loose connective tissue and mostly consists of bundles of thick collagen fibrils[30]–[32]. In aging and disease, the fibrous structure and content of collagen and elastin in the aortic ECM undergo significant changes [15], [17], [31], [33], [34].

Left untreated, the aorta wall gradually expands until stress and the resultant strain due to the blood pressure acting on the wall exceeds the strength of the wall at which point rupture and consequent death may happen [35]. Several major and minor surgical repair procedures to treat at risk AAA's before rupturing exist; however, a decision to surgically intervene is complicated by the mortality risk of the surgical procedure itself, cost and post-procedural complications. Presently, the maximum diameter of the aneurysm is used as the screening factor to identify at risk aneurysms, with 5-5.5cm being the limit. Several studies however, have questioned the suitability of maximum diameter criterion with reports of larger than 5 cm aneurysm that are stable, and a considerable percentage of smaller aneurysms rupturing. Thus, a current clinical challenge is to find a more reliable method for diagnosing at risk AAAs [36].

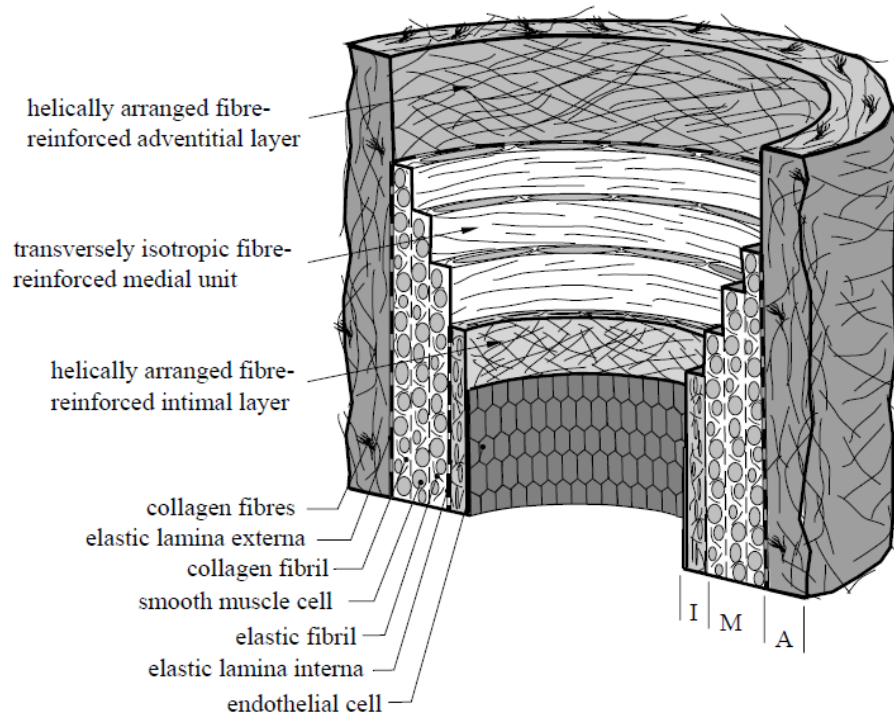


Figure 1.4 Idealization of a healthy elastic artery, composed of three layers: intima (I), media (M), adventitia (A). (Adapted from Gasser et al. [30])

In order to predict rupture, several studies have used computational methods, such as finite elements, to model the structure of aorta and to assess the mechanical strength of the aorta vs. the applied stress [37]. Although the patient-specific dimensions of the aorta can be rendered using current imaging techniques and implemented in these models, the technology to assess the molecular composition of the aorta in individual patients is not available. On the other hand, there have been some studies on the relationship between level of ECM protein degradation in aortic samples and their mechanical properties [38]. In specific aims 2 and 3 (CHAPTER 4 and CHAPTER 5), a methodology will be established to detect levels of elastin and collagen degradation in aortic aneurisms with the ultimate goal of translating this knowledge to developing an infrared fiber optic technology for clinical diagnosis of AAA. In specific aim 2, porcine aortic tissues will be used to both develop the methodology and validate the feasibility of fiber optic data collection. In specific aim 3, this methodology will be applied to assess collagen and elastin content and quality in human AAA tissue sections.

1.6 Fourier Transform Infrared Spectroscopy

1.6.1 Basics

Infrared spectroscopy is the study of the interaction of infrared light with matter. When infrared light, or heat, interacts with the molecules, they absorb infrared radiation and vibrate. Different chemical structures in molecules, known as functional groups, tend to absorb infrared radiation at specific frequencies (wavenumbers, cm^{-1}). With this coherent correlation between the infrared radiation and molecular structures, unknown molecules can be identified using their infrared spectrum. A measured infrared spectrum of a sample shows how well the sample absorbs infrared light at each wavenumber of the infrared radiation [39].

Any quantitative analysis in infrared spectroscopy is based on Beer's law, which is a relation between the absorbance and concentration in the following form:

$$A = \epsilon lc \quad (1.1)$$

where A is the absorbance, ϵ is the wavelength dependent absorptivity for the specific molecule, l is the optical path length, and c is the concentration. Variable A can be measured as peak height, peak height ratio, peak area, or peak area ratio from the FTIR spectrum and is a unitless quantity [39].

The fundamental measurement performed in an FTIR spectrometer is obtaining the sample's interferogram, defined as the intensity of the infrared light versus optical path difference. For obtaining the interferogram of a sample, a beam containing many frequencies of light (broadband source) is used. The beam from the broadband infrared light is split in a beam splitter, creating an optical path difference using a fixed and a moving mirror. The intensity at each optical path difference (each position of the moving mirror) is recorded. The interferogram is then Fourier transformed to obtain the infrared spectrum of the sample.

1.6.2 Sampling Techniques

Different methods and instrumentation are available for FTIR spectral collection. In this section, an overview of the FTIR sampling techniques used in our studies will be presented.

1.6.2.1 KBr Pellets

Using potassium bromide (KBr) pellets is one of the simplest methods for obtaining the FTIR spectra of solid samples. KBr is transparent to infrared spectra and can be used to dilute the sample to create a pellet from which the infrared beam passes and FTIR spectra are recorded in

transmission mode. For preparing KBr Pellets of a sample, both sample and KBr must be ground to have particle sizes less than 2 microns in diameter [39]. Sample powder should be completely mixed with KBr powder in 1:100 proportions, and pressed to produce a transparent pellet. To achieve good quality spectra, sample powder should be homogeneously dispersed in the KBr powder, and the pellet should be free of cracks and opaque areas.

1.6.2.2 Fourier Transform Infrared Imaging Spectroscopy (FT-IRIS)

The coupling of an FTIR spectrometer to an optical microscope with an array detector provides a system capable of creating FTIR hyper-spectral images of sample sections. Through proper processing of the spectra across the section, images of relative amount, molecular nature, distribution, and orientation of the components of tissue sections can be created [40].

FT-IRIS is performed on histological tissue sections and has several advantages over conventional histochemical and immunohistochemical methods. The spectra are acquired in a single microscopic scanning step after sectioning, thus it requires minimal tissue preparation and no additional reagents or hazardous histology chemicals. Furthermore, after an initial identification and analysis of the corresponding band (or bands, in multivariate analysis) for molecules of interest, the procedure can be repeated with additional tissue samples without variability among batches. In addition, since no target-specific staining is required, several different tissue components (e.g. different proteins, lipids, proteoglycans, etc.) can be studied on the same sample section as long as the corresponding absorbance bands are known. FT-IRIS spectra can be acquired at pixel resolutions of up to ~6.25 microns, which can be further enhanced in conjunction with an attenuated total reflectance (ATR) accessory, where pixel resolutions of up to 3-4 microns can be achieved [41].

1.6.2.3 Infrared fiber Optic Probe

Infrared fiber optic probe (IFOP) technology enables flexible *in situ* sampling of tissue composition [42]. The sampling tip, attached to the spectrometer via a fiber optic probe, collects the FTIR spectra from the point of contact with the sample. Various combinations of sampling tips and fiber optic materials have been developed in the near- and mid-IR spectral regions [43]. The flexible nature of IFOP technology makes it a valuable sampling tool with potential for *in vivo* sampling and transfer to clinical environment.

1.6.3 Pre-Processing of FTIR Spectra

An FTIR spectrum of a sample is a fingerprint of the sample's component. Depending on the complexity of the sample or the sampling technique used to obtain the spectra, preprocessing techniques may be necessary to manipulate the spectra to enhance the information hidden in the spectra without destroying the integrity of the original spectral data. A summary of different preprocessing methods used in this study is discussed in this section.

1.6.3.1 Baseline Correction

Several factors such as sample scattering, inappropriate choice of background and instrument drift can result in spectra that have curved or sloping baseline. An appropriate baseline correction is applied to these spectra by generating a function in the form of a straight line or a curve that parallels the baseline in the sample spectrum and subtracting the generated function from the sample spectrum, yielding results that should be void of curved or sloped baseline [39]. Depending on the application, baseline correction can be applied to the whole range of the spectrum of the sample or in the range that a specific processing is performed. In this study,

where the area below a peak is integrated to quantify the peak, a baseline correction is applied such that a horizontal line would connect higher and lower limits of the peak.

1.6.3.2 Spectral Derivative

In many FTIR applications, there is a region of the spectrum where several bands overlap to form a broader band. One method to differentiate the overlapping bands and their peak position is to calculate the second derivative of the spectra. Individual peaks that are overlapping in a broader band in the original spectra show up as individual downward peaks in its second derivative [39]. Different methods have been developed to calculate the second derivative of FTIR spectra. In this study, second derivative spectra were calculated using the Savitzky-Golay algorithm. This algorithm numerically calculates second derivative of the spectra by first fitting a polynomial in a symmetrical window on the raw data, and then calculating the derivative of the polynomial analytically [44].

1.6.3.3 Multiplicative Scatter correction

Scattering effects such as path length variations, offset shifts and interferences can be treated with a multiplicative scatter correction (MSC). The correction is done by two transformations. Two correction coefficients, a and b , are computed from a regression of each individual sample's spectrum onto a reference spectrum (usually the average spectrum in the data set). Variable a is the intercept to account for offset effects that are additive and chemical in nature, and variable b is the slope to account for amplification effects that are multiplicative and scattering effects. Extended multiplicative scatter correction (EMSC), is an extension to conventional MSC, which is not limited to only removing multiplicative and additive effects from the spectra. In EMSC, three new parameters are introduced to account for physical and chemical

phenomena that affect the measured spectra. One of the primary advantages of EMSC is that it corrects the wavelength dependent aspects of scattering [44].

1.6.4 FTIR Data Analysis

After necessary pre-processing manipulations, data analysis methods are performed to extract the necessary qualitative or quantitative information from the spectral data. In this section, a summary of different methods applied in this study to analyze or quantify FTIR spectra is presented. These methods can be categorized into two groups of univariate and multivariate data analysis methods. In univariate analysis, the quantification or characterization of the molecule or structural group of interest is acquired based on one peak or one spectral band in the spectrum. Peak integration mapping method is a univariate analysis method. In multivariate analysis, a range of the spectra containing several peaks is used in the analysis to extract necessary information by decomposing the data to detect and model the “hidden phenomena” that would characterize or quantifying the chemical structures of interest [45].

1.6.4.1 Peak Integration Mapping

Most quantitative spectroscopic analyses are based on the Beer’s law discussed in section 1.6.1. This law relates the concentration of absorbing structure in the sample to the amount of light absorbed by the structure. The amount of light absorbed is observable as peak height or integrated peak area of in sample’s spectra. Thus, the peak heights or areas in the absorbance spectrum of an analyte (the molecule whose concentration is measured) are directly proportional to the concentration of the analyte [46].

1.6.4.2 Principal Component Analysis (PCA)

Principal component analysis (PCA) is a multivariate analysis method. In PCA the data matrix, X , is decomposed into a “structure” part and a “noise” part. The X -matrix is usually composed of n objects and p variables. When performing PCA on FTIR spectra, objects are different samples, observations, experiments, etc., and variables are measured spectral absorbance at each wavenumber [45]. PCA transforms the data into a new coordinate system of principal components or PC's that are linearly orthogonal. The resulting PCA model can be represented in matrix format as:

$$X = TP^T + E \quad (1.2)$$

Where T is the score matrix, P is the loading matrix and E the error matrix. The combination of score and loading matrices creates the structural part of the model that is the most informative of the data. In other words, by multiplying the scores and loading, the entire structure of the original data set is reconstructed and separated from the error [47]. In spectroscopy, each loading matrix is a linear combination of wavenumbers. A successful PCA model would only need a few scores (and their corresponding loading matrices) to model the structure of the data.

1.6.4.3 Partial Least Squares Regression

Partial least squares - or projection to latent structures- (PLS) is a useful regression modeling techniques that models two matrices of X and Y to find the latent variables in X that will best predict the latent variables in Y by maximizing the covariance between X and Y . Similar to other regression models, the regression coefficient in PLS (regression coefficient spectra) can be applied to matrix of predictors, X , to predict matrix of responses Y . Figure 1.5 shows a conceptual illustration for PLS.

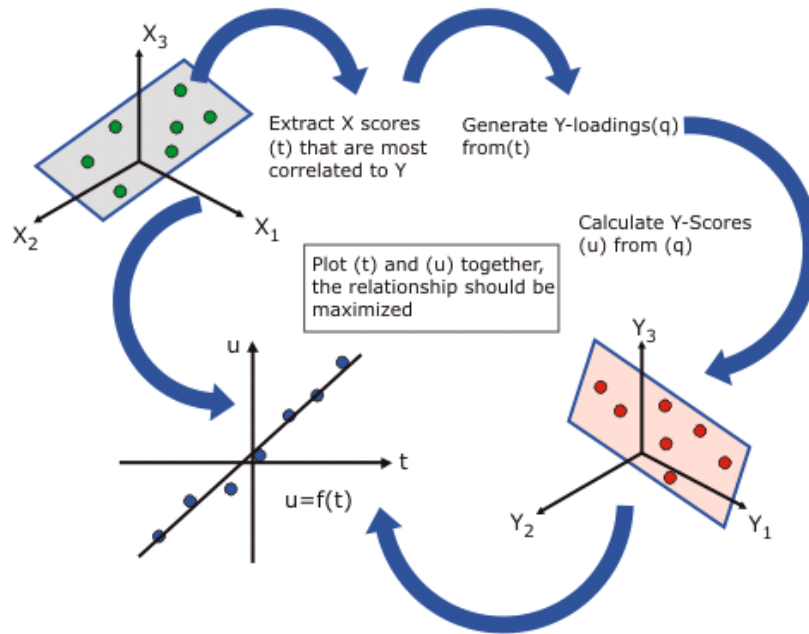


Figure 1.5 Conceptual illustration for PLS [47]

1.7 Application of FTIR in cardiovascular tissues

In this section a review of the current literature on application of FTIR in characterizing cardiovascular tissue components is presented.

1.7.1 FTIR Studies of Cardiac Tissue

FTIR and FT-IRIS have been applied in the study of several tissue types; however, the study of their applicability to cardiac tissue has been limited so far. Liu et al. identified a number of IR absorption peaks that are characteristic of collagen using single point mid-infrared spectra of infarcted rat left ventricle compared with sham control [48], but no quantitative analysis was performed. In a later study [49] the authors used an absorbance band at 1204 cm^{-1} as the representative band for collagen deposition. They used the intensity of the inverted second derivative of the 1204 cm^{-1} band to qualitatively show similar collagen localization between the

spectroscopic analysis and trichrome staining of the tissue. However, the 1204 cm^{-1} band is part of the Amide III absorbance which is present in some form in all proteins, including myosin which is the major component of cardiac tissue, and therefore is not necessarily a very specific spectroscopic marker. Another group [50] used attenuated total reflectance (ATR) spectroscopy to classify normal and cardiomyopathic hamster heart tissue through linear discrimination analysis aided by genetic algorithm selection of spectroscopically diagnostic mid-IR regions. In that study, specific absorbances attributable to cardiac collagen were not identified. In a later study by the same group [51], synchrotron FTIR was utilized to assess cardiomyopathic hamster heart for collagen expression in focal microdomains based on similarities in the tissue spectra and that of pure collagen in the amide II range ($1167\text{-}1355\text{ cm}^{-1}$). Here again, no specific collagen absorbances were identified in the cardiac tissue spectra. Finally, a recent FTIR imaging study by Yang et al. [52] evaluated collagen deposition in a human heart post-MI based on the 1638 cm^{-1} absorbance found in the amide I region. In this study, qualitative comparisons were made to H&E staining, but no comparisons to histologic staining specific for collagen were performed.

1.7.2 FTIR Studies of Arterial Tissue

FTIR studies of arterial tissue have been performed in the context of different arterial diseases. In the following sections a review of these studies is presented, categorized based on the disease model.

1.7.2.1 FTIR Studies of Atherosclerotic Arteries and Arterial Plaques

In rabbit atherosclerotic aorta sections [53] macro-ATR imaging was used to create images based on integrated area of cholesterol ester C-O band at $\sim 1170\text{ cm}^{-1}$, and integrated area of Amide II band at 1530 cm^{-1} . This study presented different band assignments for spectra of

media and the atherosclerotic region. Higher spatial resolution (ca. 3–4 μ m) images of arterial cross sections was made possible using micro-ATR imaging with a germanium objective.

Palombo et al. [54] studied diet induced atherosclerotic lesions in the descending thoracic segment of rabbit aorta. They applied peak integration mapping of amide I and II for visualization of proteins and (C=O) ester band (1753–1707 cm^{-1}) for visualization of atherosclerotic lesions. Using PCA and Factor Analysis (FA) they created FTIR images that differentiated structural motifs in the vascular wall.

Mamarelis et al. [55] performed FTIR on carotid atheromatic plaque samples from patients who underwent carotid endarterectomy. They studied the role of oxidative stress on atherogenesis by investigating FTIR spectral features of pathogenic compounds in the plaque. The pathogenic components they studied included foam cells, hemorrhagic regions and a region rich in calcium carbonate.

1.5.2.2. FTIR Studies of Aortic Aneurysms

Near-IR has been applied to study an apolipoprotein E-deficient (apoE^{-/-}) mouse model of AAA to predict the level of Ang II using PCR on near-IR spectra of aorta samples [56].

Bonnier et al. [57] studied the FTIR imaging of human ascending aorta tissues from four groups of subjects; normal, patients with bicuspid valves, aneurysmal tissues and aneurysmal tissues from patients with bicuspid valves. They calculated the ratio of band areas from the second derivative spectra of 1643-1667 cm^{-1} over 1628-1642 cm^{-1} corresponding respectively to alpha helical and beta-sheet secondary structures and showed that normal tissue has a value of about 4, with bicuspid valve patients having values lower and aneurysmal tissues values higher. This study reported that the decrease in beta-sheet structures in aneurysmal patients was related to

elastin degradation in this pathology. They also showed that they PCA on second derivative of the spectra in the frequency range of 950-1750 cm^{-1} can be used to differentiate tissues from normal, bicuspid and aneurysmal patients.

Rubin et al. have compared the spectra of normal and aneurysmal ascending human aortas [58]. They noticed the amide I peak at 1653 cm^{-1} is higher in normal tissues but is shifted to 1648 cm^{-1} and is broader in aneurysmal tissues. They showed that they can discriminate between the two tissue types by hierarchical cluster analysis (HCA).

Bonnier et al. applied curve fitting procedures to study the protein secondary structure of ascending aorta samples and their reorganization as a predictor of the outcome of aneurysm[59]. In the six samples they studied (3 normal and 3 aneurysmal) they were able to resolve five and four components for amide I and amide II respectively. The band at 1655 cm^{-1} , assigned to alpha helical structures and the peak related to beta sheet conformation was located between 1610 and 1635 cm^{-1} . The results of their band assignments is consistent with a previous study [60]. A summary of these band assignments for Amide I is presented in Table 1-3. They attributed the spectral band at 1658 cm^{-1} , assigned to alpha helical structures [61], [62], to be exclusive of alpha-helical structure of collagen. They noted that in aneurysmal tissues, the band at 1635 cm^{-1} (assigned to beta sheet structures) decreased, while the band at 1629 cm^{-1} (another beta sheet band) and alpha-helical increased. Globally, they observed a decrease in beta structures and they concluded this is consisted with aneurysm conditions. In aneurysm, elastin degrades faster than collagen, and since elastin is made up of repetition of beta domains, the decrease in beta structures could be correlated to degradation of elastin in aneurysm.

Table 1-3	
<i>Amide I Band assignments for protein secondary structures</i> [59], [60]	
Peak position	Band assignment
1620, 1635	β -strands
1645 \pm 4	Unordered structures
1658	α -helix
1660-1700	β -turns

Another study [63] used images acquired from human ascending aorta from 15 patients. For each tissue section they selected 2-4 spectral images to collect a total of 42 images for the study. After necessary pre-processing steps, they performed two different separation methods. Factorial discriminant analysis (FDA) separated 42 images into two groups of normal and pathological tissue. They also applied K-means clustering to the imaging spectra by considering an initial number of 20 unsupervised groups to account for different components of the ECM, and they were able to identify two types of spectral populations that they assigned to be representative of images from healthy and pathological samples. They later applied ANOVA to this data and, by using the Fisher F value, found 15 proportions among 20 to be significantly different and clustered the unsupervised groups into three groups of neutral, healthy and aneurysmal and color coded image spectra according to group affiliation. In the reconstructed images, healthy tissues had a dominance of color assigned to healthy tissues and pathological tissues had a dominance of color assigned to pathological tissues.

1.5.2.3. FTIR Study of Arterial Remodeling

Spectral clustering was applied to FTIR images of arterial sections from rat carotid balloon injury model to qualitatively and quantitatively differentiate between arterial layers, comparable to histology based methodologies [64]. For qualitative analysis histomorphometric measurement of lumen area and the area enclosed by the external elastic lamina was used.

1.7.3 The Contribution of this Dissertation

The studies mentioned above set the groundwork for applying FTIR to studying changes in pathologic cardiovascular tissues or differentiation of healthy from diseased tissue. The quantification of ECM components however, has not been addressed. This dissertation is aimed at developing methods that quantify collagen and elastin in cardiac and aortic tissue using FTIR.

CHAPTER 2

FOURIER TRANSFORM INFRARED SPECTROSCOPIC IMAGING OF CARDIAC TISSUE TO DETECT COLLAGEN DEPOSITION AFTER MYOCARDIAL INFARCTION

For the most part, sections presented in this chapter were published in Cheheltani et al. (2012) Fourier transform infrared spectroscopic imaging of cardiac tissue to detect collagen deposition after myocardial infarction. Journal of biomedical optics, 17(5), 056014 [65]. Copyright 2012, Society of Photo-Optical Instrumentation Engineers.

2.1 Abstract

Myocardial infarction often leads to an increase in deposition of fibrillar collagen. Detection and characterization of this cardiac fibrosis is of great interest to investigators and clinicians. Motivated by the significant limitations of conventional staining techniques to visualize collagen deposition in cardiac tissue sections, we have developed a Fourier Transform Infrared Imaging Spectroscopy (FT-IRIS) methodology for collagen assessment. The infrared absorbance band centered at 1338 cm^{-1} , which arises from collagen amino acid side chain vibrations, was used to map collagen deposition across heart tissue sections of a rat model of myocardial infarction, and was compared to conventional staining techniques. Comparison of the size of the collagen scar in heart tissue sections as measured with this methodology and that of trichrome staining showed a strong correlation ($R=0.93$). A Pearson correlation model between local intensity values in FT-IRIS and immuno-histochemical staining of collagen type I also showed a strong correlation ($R=0.86$). This study demonstrates that FT-IRIS methodology can be utilized to

visualize cardiac collagen deposition. In addition, given that vibrational spectroscopic data on proteins reflect molecular features, it also has the potential to provide additional information about the molecular structure of cardiac extracellular matrix proteins and their alterations.

2.2 Introduction

In cardiac tissue, ECM supports, connects and coordinates cardiac myocytes and the forces generated by them [21], [66]. Several cardiac pathologies are associated with significant changes in the composition of the matrix [21], [66]. Therefore, detection and quantitative measurement of these matrix changes play an important role in experimental assessment of novel treatment methods and drug delivery systems for treating cardiac diseases. Adverse cardiac remodeling and cardiac fibrosis after myocardial infarction is one of the most commonly studied aspects of ECM alteration in cardiac tissue. This fibrosis may be characterized by replacement of dead cardiomyocytes with fibrillar collagen and formation of scar tissue in the infarct zone as well as excessive deposition of fibrous tissue in interstitium remote to infarction site [21], [24]. This change in tissue composition leads to increased stiffness and eventually cardiac dysfunction [24], [25].

Several assays have been developed to assess the excess collagen deposition in cardiac tissue. Histochemical assays such as trichrome or picrosirius red staining protocols are some of the most common methods of visualizing collagen deposition in heart sections [24], [27]. Immunohistochemical staining methods provide a more specific, sensitive and quantifiable staining technique but they use expensive reagents and achieving reliable results require substantial preparation and experimentation [28], [29]. In this study,

Fourier Transform Infrared Imaging Spectroscopy (FT-IRIS) is proposed as an alternative or complementary method to these conventional assays.

In Fourier transform infrared (FTIR) spectroscopy, the interaction of molecular bonds with varying wavelengths of infrared light are measured. Molecular structures inside the matter under study (such as biological tissues) can be characterized based on signature spectral absorbances [39]. The coupling of an FTIR spectrometer to a microscope and array detector provides an imaging system for creation of maps of molecular bond vibrations, known as hyperspectral imaging, or Fourier transform infrared imaging spectroscopy, FT-IRIS [67]. Data collection in FT-IRIS does not require staining or labeling prior to imaging, and thus is not prone to batch to batch variability. Furthermore, unlike histochemical techniques, this technology has the potential for in vivo use through fiber optic applications [42], [68]. FTIR and FT-IRIS have been applied to analyze several soft [69] and hard[70] tissue types including bone and cartilage [67], skin [71] and arteries [64]; however, the study of their applicability to cardiac tissue has been limited so far.

Liu et al. identified a number of IR absorption peaks that are characteristic of collagen using single point mid-infrared spectra of infarcted rat left ventricle compared with sham control [48], but no quantitative analysis was performed. In a later study [49] the authors used an absorbance band at 1204 cm^{-1} as the representative band for collagen deposition. They used the intensity of the inverted second derivative of the 1204 cm^{-1} band to qualitatively show similar collagen localization between the spectroscopic

analysis and trichrome staining of the tissue. However, the 1204 cm^{-1} band is part of the Amide III absorbance which is present in some form in all proteins, including the major component of cardiac tissue, myosin, and therefore is not necessarily a very specific spectroscopic marker. In another study [50], attenuated total reflectance (ATR) spectroscopy was used to classify normal and cardiomyopathic hamster heart tissue through linear discrimination analysis aided by genetic algorithm selection of spectroscopically diagnostic mid-IR regions. In that study, specific absorbances attributable to cardiac collagen were not identified. In a later study by the same author [51], synchrotron FTIR was utilized to assess cardiomyopathic hamster heart for collagen expression in focal microdomains based on similarities in the tissue spectra and that of pure collagen in the amide II range ($1167\text{-}1355\text{ cm}^{-1}$). Here again, no specific collagen absorbances were identified in the cardiac tissue spectra. Finally, a recent FTIR imaging study by Yang et al [52] evaluated collagen deposition in a human heart post-MI based on the 1638 cm^{-1} absorbance found in the amide I region. In this study, qualitative comparisons were made to H&E staining, but no comparisons to histologic staining specific for collagen were performed. Overall, these prior studies that utilized FTIR to qualitatively assess collagen demonstrate the potential for quantitative characterization of collagen deposition in cardiac tissue using FTIR technology.

The objective of the current study was to (a) introduce standard FT-IRIS methodology for creating distribution maps of collagen in remodeled cardiac tissue sections and (b) quantitatively compare maps created by FT-IRIS with conventional staining techniques.

This distribution mapping can be utilized to visualize collagen deposition when assessing the results of treatment strategies involving ECM. Therefore, this methodology was also applied to map collagen deposition in infarcted rat cardiac tissues which showed moderated cardiac remodeling after treatment with targeted delivery of vascular endothelial growth factor (VEGF) [72], [73].

2.3 Materials and Methods

2.3.1 Induction of MI

All animal procedures were performed under an IACUC-approved protocol. Myocardial infarction was surgically induced in six-week old male Sprague-Dawley rats (Harlan Laboratories, Indianapolis, Indiana) as described previously [74]. Briefly, rats were anesthetized with 4% isoflurane and maintained with 2% isoflurane using a rodent respirator. After a left thoracotomy, and pericardiotomy, the heart was exteriorized and a 6.0 silk suture was placed around the left anterior descending coronary artery and ligated. The heart was placed back and the chest was closed. The lungs were then re-inflated using positive end-expiratory pressure. Animals were then allowed to recover.

2.3.2 Targeted Delivery of VEGF Treatment

To demonstrate the applicability of our methodology to drug delivery and treatment development, a group of infarcted rats were treated by targeted delivery of VEGF to infarcted myocardium and the extent of collagen deposition in their cardiac tissue was compared to control group (n=6 in each group). For treatment group, upon completion of the surgical procedure, animals received targeted delivery of VEGF-encapsulated immunoliposomes via tail

vein injection. We have previously shown that this treatment improves cardiac function and vascular structure in MI rats [72].

2.3.3 Extraction of Heart Samples and Cryopreservation

Four weeks after the induction of MI, rats were anesthetized with ketamine/xylazine 87/13 mg/kg S.C. and euthanized by cardiectomy. Excised hearts were washed in saline solution, placed in embedding medium (Tissue-Tek O.C.T Compound, Sakura Finetek, Torrance, CA), and flash frozen in a mixture of dry ice and isopentane. Fresh frozen tissues were kept at -80°C until sectioning.

2.3.4 Cryo-sectioning

For FT-IRIS analysis, 9 µm sections of unfixed frozen tissue embedded in embedding medium were mounted on low-e reflective-coated infrared microscope slides (MirrIR slides, Kevley Technologies, Chesterland, OH). Sections were then air-dried for 30 minutes, embedding medium dissolved in deionized water, and sections fixed in 10% formalin and air dried completely. For immunohistochemical and histologic analysis, 9 µm sections of unfixed frozen tissue were mounted on polylysine coated slides. All sections used in immunohistochemical staining were collected consecutively after the corresponding section used for FT-IRIS analysis. For some histochemical staining samples, sections were not consecutive to their paired sections obtained for FT-IRIS.

2.3.5 FT-IRIS Data Acquisition and Analysis

FT-IRIS images of a section of the heart on low-e slides were acquired at 25 μm (partial tissue sections) or 50 μm (whole tissue sections) pixel resolution and 8 cm^{-1} spectral resolution with 2 co-added scans using a Perkin Elmer Spotlight 400 spectrometer (Shelton, CT). The spectrometer source is an electrically heated silicon carbide light source with high emissivity and a quasi-blackbody emission spectrum with an effective temperature of $\sim 1300^\circ\text{K}$. Data were analyzed with Isys 5.0 software (Spectral Dimensions Inc, Onley, MD). The integrated area of the amide I absorbance band, centered near 1650 cm^{-1} , that arises from the C=O stretching vibration [67], was used to mask each sample such that only tissue regions of the image were included in analyses. The baselined, integrated area of the absorbance band centered at 1338 cm^{-1} , arising from collagen CH₂ side chain vibrations [42], was mapped across the tissue section, creating an intensity image of collagen deposition (Figure 2.1-A-E). As the 1338 cm^{-1} is a very small absorbance band, we also performed second derivative analysis on the spectra to confirm the distribution at that wavenumber (Figure 2.1 F,G). Second derivative spectra can be utilized to improve the resolution of absorbance bands, while maintaining a relationship to intensity of the original raw spectral absorbance band [75]. The results of these analyses were similar to the integrated absorbance band analysis, and thus only the integrated band areas are presented in the Results section.

2.3.6 Immunohistochemical staining for collagen type I

Immunohistochemical staining was used to visualize the distribution of collagen type I in the infarct zone of rat heart sections. Since cardiac collagen type I is the primary collagen type in cardiac fibrosis [23], [66], collagen type I was selected as the target molecule for the staining.

Briefly, 9 μm cross-sections of fresh frozen heart tissue on polylysine coated slides were incubated with 5% BSA in PBS to block unspecific binding, and then incubated at 4°C overnight with mouse monoclonal to Collagen I antibody (abcam Ab90395, 1:200 dilution) diluted in 5% BSA in PBS. Slides were then washed in PBS, incubated with Alexa Fluor 594 donkey anti-mouse IgG (Invitrogen A21203, 1:200 dilution in PBS), washed in PBS, incubated with DAPI, washed in PBS and mounted with glass coverslips using mounting medium for fluorescence (Vectashield, Vector Laboratories, Burlington, CA). Images of the stained slides were taken using a Retiga 1300 microscope camera (QImaging, Surrey, BC) and Mac 5000 motorized stage controller (Ludl Electronics, Hawthorne, NY) coupled to a Nikon Eclipse TE200 (Nikon Instruments Inc., Mellville, NY) fluorescent microscope.

2.3.7 Histological Staining

Gomori's trichrome stain (Richard Allen Scientific, Kalamazoo, MI) was used to histochemically distinguish collagen (blue) from muscle tissue (red). Nine micrometer cross-sections of fresh frozen heart tissue mounted on histology slides were fixed with Bouin's solution at 56 °C for 1 hour, and then stained according to the manufacturer's directions. Stained heart sections were dehydrated using various grades of alcohol and xylenes, and then mounted with glass coverslips. Images of sequential regions within each section were obtained using a Nikon DS-Fi1 color microscope camera and Nikon Element software (Nikon Instruments Inc., Mellville, NY). A mosaic image of the area of interest was created using Adobe Photoshop CS software.

Picrosirius Red (Polysciences, Inc.) stains thick collagen fibers bright yellow to red when viewed under polarized light [76] and was also used to show collagen deposition in the infarct zone.

Nine micrometer sections of fresh frozen heart tissue were obtained on polylysine coated slides.

Heart sections were fixed with 4% formaldehyde for 10 minutes, and then stained according to the manufacturer's directions, dehydrated and mounted with glass slides. Images of sequential regions within each section were obtained under polarized light using a Nikon Digital DS-Fi1 color camera and Nikon Element software. A mosaic image of the area of interest was created using Adobe Photoshop CS software.

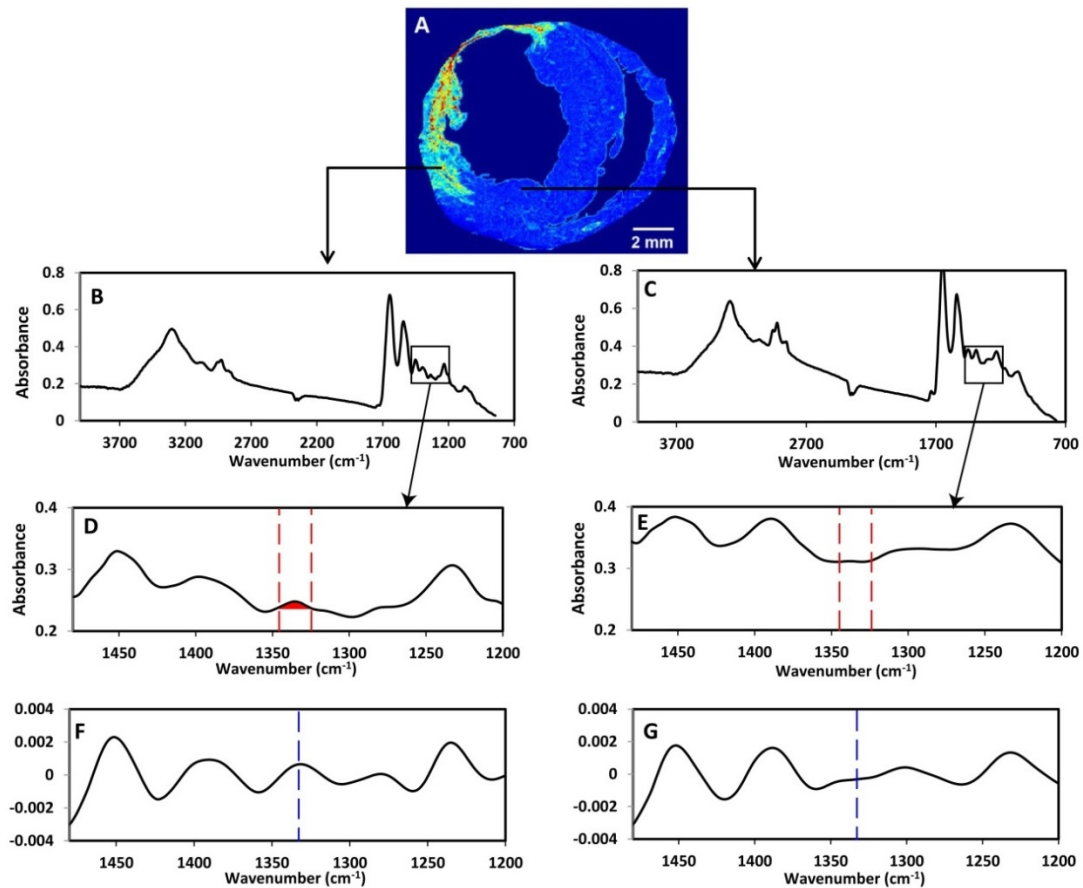


Figure 2.1 FTIR spectra of myocardial tissue. **A:** intensity image created by peak integration mapping of the 1338 cm^{-1} absorbance band that arises from collagen sidechain vibrations. **B:** Representative spectra for left ventricle within the infarct region. **C:** Representative spectra for left ventricle remote to the infarct region. **D** and **E:** Expanded spectra in the infarcted myocardium (**D**) and myocardium remote to the infarct region (**E**) showing the area of integration for 1338 cm^{-1} absorbance in (**D**), and the absence of the absorbance in (**E**). **F** and **G:** Expanded inverted second derivative spectra (multiplied by negative one to facilitate peak identification) in the infarcted myocardium (**F**) and myocardium remote to the infarct region (**G**)

2.3.8 Image Processing

Six infarcted heart tissue samples were used to compare FT-IRIS local intensity of collagen deposition with immunohistochemical staining. Collagen intensity maps were created on two consecutive 9 μm sections of infarcted myocardium using FT-IRIS and fluorescent microscopic imaging of immuno-histochemical staining as described above. Images from both techniques were imported into ImageJ software as 8 bit grey-scale intensity images, resized and aligned to match. The same area of 6250 μm x 1875 μm containing the scar region was selected in both images, and after normalizing the intensity by adjusting the minimum to 0 and maximum to 255 in both, each were divided into a 5x4 grid (Figure 2.2-A). The mean grey value in each element of the grid was measured and the grey values from two methods were compared for 20 grid elements in a Pearson's correlation analysis (Figure 2.2-B).

Nine samples (4 targeted VEGF-treated and 5 untreated control MI animals) were used to compare area of collagen deposition in cardiac sections from FT-IRIS images with trichrome staining results by correlating the number of pixels denoting collagen deposition in each section from both methods. In FT-IRIS intensity images, the 1338 cm^{-1} peak integration values above zero were used as a threshold to create a binary image of the cross section, isolating areas of collagen deposition from the rest of the tissue. These images were processed in ImageJ software (National Institute of Health, USA) to measure the percentage area of the scar region in each tissue cross section. In trichrome images, scar region was isolated using imageJ software. First a color deconvolution routine [76] was performed (using the ImageJ plug-in) to separate RGB channels. In the blue channel, a threshold was applied at a level that distinguished stained areas

(denoting scar region) from the unstained background followed by noise reduction procedures. The percentage area of stained regions (collagen deposition) within each sample was measured.

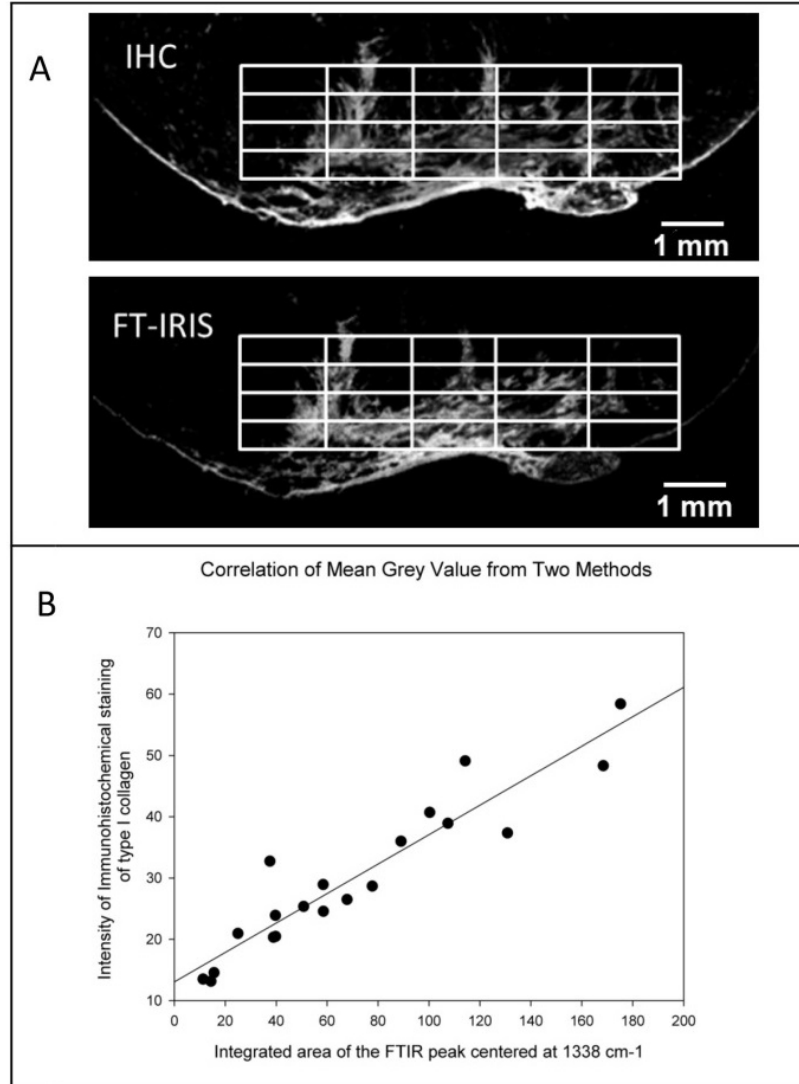


Figure 2.2 Comparison of intensity maps from FT-IRIS and immunohistochemical staining (IHC) in a representative sample. Panel A shows the image of the infarct region from both techniques after being resized and aligned to match. A grid of 5x4 was applied to the same area of 6250 μm x 1875 μm in both images. Mean grey values in each grid element were compared between two methods in a Pearson correlation model as shown in panel B.

2.3.9 Statistical Data Analysis

Data analysis was performed with statistical software Sigmaplot (Systac Software Inc., San Jose, CA). Correlation coefficients (R values) were calculated from a Pearson's correlation model with P values less than 0.05 considered to be statistically significant. Comparison of treatment groups was performed using a student's T-test.

2.4 Results

2.4.1 Qualitative Correlation of FT-IRIS Data vs Staining Methods

Peak integration mapping of the band centered at 1338 cm^{-1} creates a map of collagen deposition consistent with images created by three different staining techniques in serial sections of the infarct zone in the same rat heart sample (Figure 2.3). Panel A shows an FT-IRIS obtained color map of the collagen deposition density with red being the highest and blue the lowest. In Gmori's trichrome staining of an adjacent section from the same tissue (Panel B) collagen deposition stained in blue, distinguished from red stained muscle tissue, appears in the same areas as in the FT-IRIS image. Immunohistochemical staining of collagen type I of the same tissue (panel C), demonstrates the same density distribution as the FT-IRIS image. For panel D, a section from the same tissue was stained using a Picrosirius red staining protocol as described above and imaged under polarized light. The bright red and yellow collagen fibers again show a similar distribution as other staining techniques and FT-IRIS image. We also compared FT-IRIS mapping based on the inverted second derivative peak at 1204 cm^{-1} [49], but did not find any collagen-specific results (data not shown).

2.4.2 FT-IRIS to Map Collagen Deposition Density

Figure 2.4 shows correlation of local mean grey values, representing collagen deposition density, between immunohistochemical staining of type I collagen and FT-IRIS map of collagen deposition in a consecutive section for 6 different MI control samples. As demonstrated in these graphs and their corresponding correlation coefficient values, FT-IRIS maps of the collagen deposition density strongly correlates with immunohistochemical staining results (average correlation coefficient of 6 samples= 0.86 ± 0.07 , $p < 0.01$ for all samples). A similar strong correlation between the two methods was observed in samples treated with targeted delivery of VEGF to infarcted myocardium (data not shown).

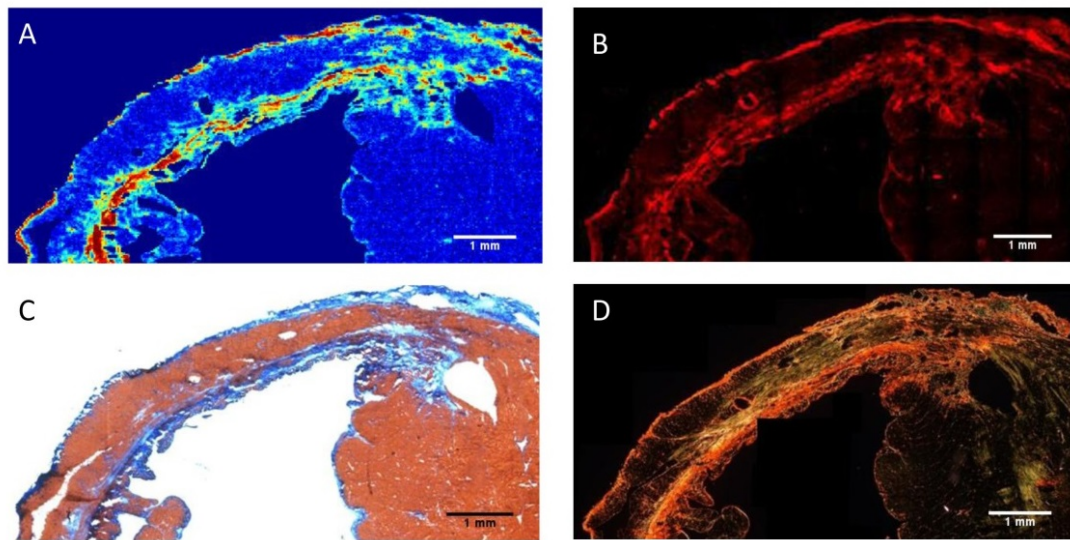
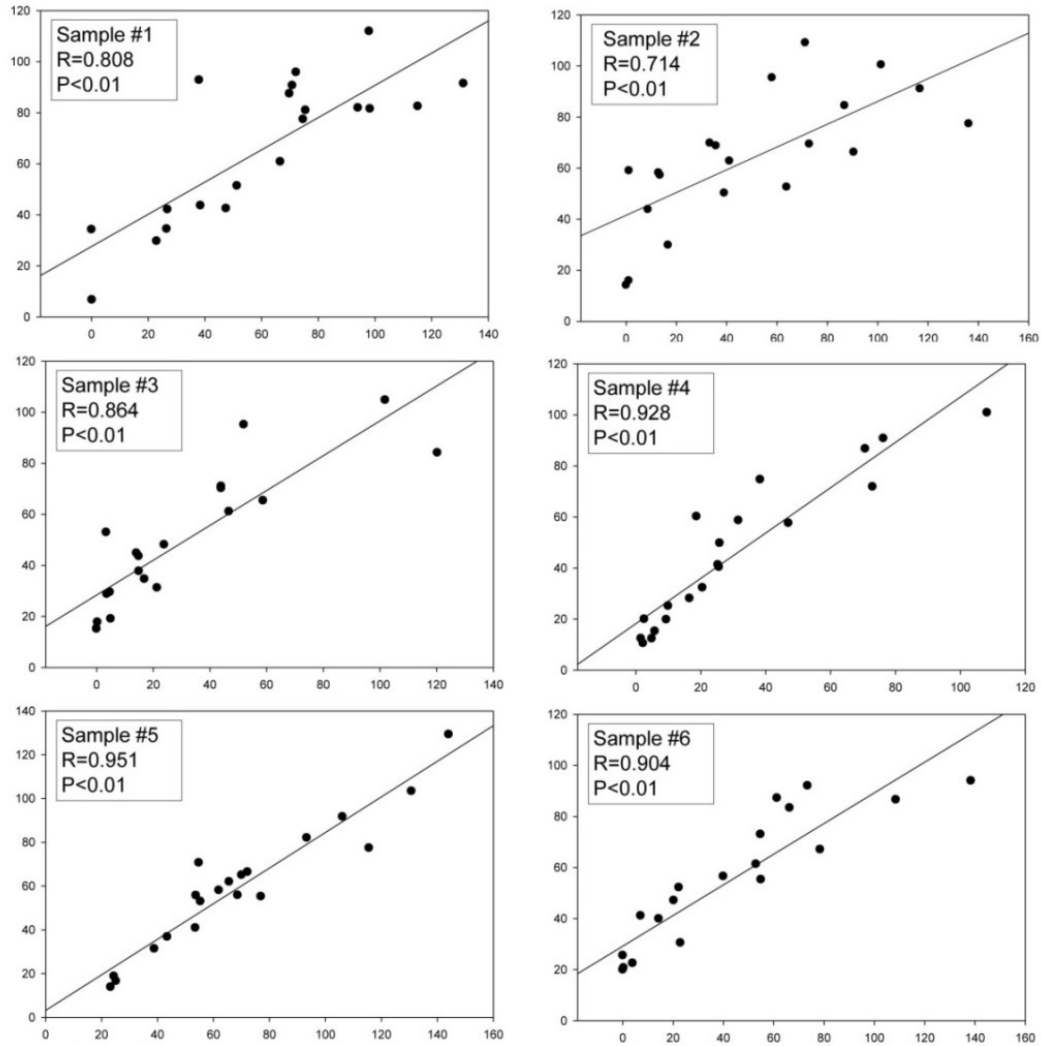


Figure 2.3 Collagen deposition is mapped in infarcted left ventricle using FT-IRIS imaging of the 1338 cm^{-1} absorbance (A), immunohistochemical staining of collagen type I (B), trichrome staining (C), and Picrosirius Red staining under polarized light (D).



In all graphs:
 X axis: mean intensity (grey value) of integrated area of the absorbance band centered at 1338 cm⁻¹
 Y axis: mean intensity (grey value) of Immunohistochemical staining for collagen type I

Figure 2.4 Pearson correlation for local collagen intensity between the FT-IRIS method and immunohistochemical staining in consecutive sections from 6 samples. In each sample, mean grey values of 20 sequential grid elements were measured and correlated in intensity images created from integrated area of the band centered at 1338 cm⁻¹ (X axis) versus immunohistochemical staining of collagen type I (Y axis) (average R for 6 samples=0.86 ±0.07, average p value for 6 samples= 0.00007).

2.5 Discussion

Cardiac remodeling involves cellular and structural processes affecting myocytes and their contractile proteins as well as extracellular matrix [77]. This matrix, primarily composed of collagen [21], [66], undergoes a remodeling process in most cardiac disease conditions resulting

in an increase in collagen deposition and fibrosis [21]. The extent of fibrosis and collagen scar is an important factor in the assessment of interventions aimed at treating cardiac diseases [66]. Hence an efficient and reliable measurement of collagen deposition in cardiac tissue is of great interest in the assessment of treatment strategies for cardiac pathologies. Because of several limitations and the variability experienced in staining techniques, we propose an alternative FT-IRIS methodology for detection and characterization of collagen deposition in cardiac tissue.

The FTIR absorbance band centered at 1338 cm^{-1} arises from the amino acid side chain vibrations in collagen and was first identified by Jackson et al [78]. They attributed this band to CH wagging vibration of proline side chains. Infrared spectra from different collagen types in previous studies also show the existence of this band in, e.g., collagen type I and III [79], type II [42] and type I and IV [80]. The intensity of this absorbance has been utilized to quantify triple helix collagen fibers in collagenase-induced cartilage degradation [81], as well as in osteoarthritic tissues [42], [82]. In the current study, the quantification of the local 1338 cm^{-1} band intensity across the section was utilized to map the extent of collagen deposition after myocardial infarction in rat heart tissue sections, and the results were comparable to conventional histology and immunohistochemical staining techniques. Other infrared absorbance bands, including the amide I carbonyl stretching mode of proteins, were investigated to assess collagen distribution, but only the 1338 cm^{-1} absorbance was found to be specific for collagen. As amide absorbance bands are found in all proteins, it is likely that the presence of the cardiac protein myosin, which also contains absorbances in these regions, precludes specificity of those bands for collagen in cardiac tissue.

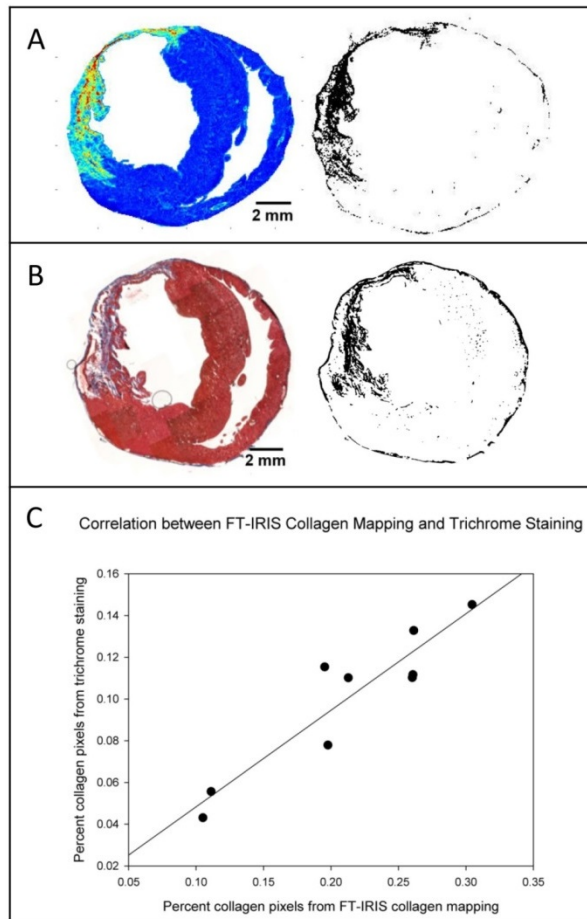


Figure 2.5 Comparison of FT-IRIS and trichrome staining. A: FT-IRIS mapping of collagen deposition in a typical sample (1338 cm⁻¹ area) and the corresponding binary image separating collagen from the rest of the myocardium. B: Trichrome staining of the sample tissue with the corresponding binary image. C: Percentage area of collagen deposition in tissue sections (number of pixels) from the two methods in a Pearson correlation model. (R=0.93, P=0.0003)

Trichrome staining techniques are widely used for differentiation of collagen from muscle tissue and assessment of collagen deposition [83]. Although several hypotheses have been proposed to explain the differential tissue coloring of these techniques, which use anionic dyes in association with heteropolyacids, the exact mechanism is not completely understood [84]. Previous studies have used these methods to visualize collagen deposition and measure the size of the scar in diseased cardiac tissues [24], [27], [85]. We have shown that the scar size

measured as percentage of tissue section showing collagen deposition from FT-IRIS analysis strongly correlated with the measurements achieved by trichrome staining of a section from same heart tissues. The fact that samples used in this analysis were comprised of two groups of animals; a treatment group with targeted delivery of VEGF to infarcted myocardium and a control untreated group, demonstrates the applicability of the methodology for different treatment conditions. We also used this methodology to show that a group of animals treated with targeted delivery of VEGF to infarcted myocardium, demonstrate a smaller collagen scar compared to controls, as was previously shown using conventional staining techniques. This provides an example of how this methodology could be used in the assessment of the size of the collagen scar in cardiac tissues independent of other staining techniques.

Picrosirius Red is another widely used staining method which interacts with collagen by the reaction of its sulphuric acid groups with the basic groups of collagen [86]. Picrosirius Red stains fibrillar collagen more specifically and more precisely than trichrome staining techniques [24], [27], especially when viewed under circularly polarized light since it no longer depends on the observation of a specific color but rather the birefringence of fibrillar collagen, which is a fundamental physical property [27]. Although the dependence of brightness to collagen fiber orientation with respect to transmission axis of linear polarizer can be mitigated by use of circularly polarized light, attempts to quantify collagen volume fraction from the level of birefringence brightness are limited by the dependence of brightness to collagen fiber orientation relative to the section plane [27]. Another complication with this technique is the necessity to exclude other non-collagen birefringent components of the tissue such as fibrin[87].

Immunohistochemical staining has been used to semi-quantitatively assess the amount of different collagen types in cardiac fibrosis and remodeling [88]–[90]. In our study, FT-IRIS and immunohistochemical staining of type I collagen were strongly correlated in a linear model, thus verifying that the intensity of the 1338 cm^{-1} band can be utilized to evaluate collagen deposition density. This finding is consistent with the fact that in both methods the intensity is linearly correlated to the target molecule concentration, following the Beer-Lambert law [39], [91]. Scattering of infrared radiation could also occur as a result of tissue thickness, which would result in intensity changes. However, as our spectral absorbance values were on the order of 1 absorbance unit or less, it is unlikely that this is a major concern in the current study. The small variation observed between the two methods may be due to different methodologies for tissue preparation and measurement, as well as the fact that staining and FT-IRIS data were obtained from successive sections of the same tissue. In addition, the phenomena that give rise to the image intensities are different; in the case of FT-IRIS, image intensity is a measure of molecular vibrations, whereas in immunofluorescence, the level of chromophore binding is being imaged. In our imaging system, we confirmed that the fluorescence intensity of the primary-secondary antibody complex is linearly correlated to the concentration of the primary antibody (data not shown).

Creation of collagen distribution maps using FT-IRIS technology has several advantages over commonly utilized staining techniques. The spectra are acquired in a single microscopic scanning step after sectioning, thus it requires minimal tissue preparation and no additional reagents or hazardous histology chemicals. Furthermore, after an initial identification and analysis of the corresponding band (or bands, in multivariate analysis) to molecules of interest, the procedure

could be repeated with additional tissue samples without variability among batches. In addition, since no target-specific staining is required, several different tissue components (e.g. different proteins, lipids, proteoglycans, etc.) can be studied on the same sample section as long as the corresponding absorbance bands are known. FTIR spectra can be acquired at pixel resolutions higher than 25 μm used in this study, and can be further enhanced in conjunction with an attenuated total reflectance (ATR) accessory [41]. For this study however, changes in the pixel resolution from 6.25 to 50 μm did not affect the results (data not shown), since collagen density was mapped in relatively large areas of cardiac tissue.

The percentage change in collagen deposition after myocardial infarction depends on the severity of infarction and the extent of the remodeling process. In the tissue samples evaluated in the current study, the infarct scar comprised an average of 21% of the tissue cross section. The correlations between the FT-IRIS results and staining techniques confirms that the FT-IRIS method developed is indeed sensitive to collagen deposition in the range that is normally observed within the infarct scar. The infarct scar, however, is predominantly composed of collagen [25]. If this technique is to be applied for the detection of very small percentages of collagen to other tissue components, a careful assessment of the sensitivity of the technique may be required. Previous studies have confirmed the sensitivity of FTIR in detection of very low (nM) concentrations of proteins using attenuated total reflectance methods [92]–[94], and concentrations on the order of $\sim 1\%$ in transmittance studies ([40], [95]).

The motivation for further investigation of FTIR spectra and their band signatures in cardiac tissue is two-fold. First, the capability of FTIR spectra in characterizing cardiac tissue is not limited to mapping collagen density. Although single absorbance band analysis was the focus of

the present study, there is a plethora of data in FTIR spectra, which if further investigated could yield valuable information about different cardiac proteins. Such information could answer some of the classical questions in cardiac remodeling and fibrosis such as differentiation and quantification of the ratio of different collagen types, or the extent and timeline of collagen cross-linking and maturity. The current FT-IRIS results do not distinguish between types I and III collagen, but it is possible that further investigations could result in this differentiation. The second potential lies in translation of this technology to in vivo diagnostic strategies. For example, this methodology can be used in the emerging area of catheter-based infrared fiber optics [96] to assist in the in vivo assessment of the health of cardiovascular tissues. In summary, the results presented support the further use, and clinical translation, of infrared spectral techniques for evaluation of cardiac pathologies and therapeutics.

CHAPTER 3

INFRARED SPECTROSCOPY TO MEASURE COLLAGEN AND ELASTIN IN AORTA USING MULTIVARIATE ANALYSIS

For the most part, sections presented in this chapter were published in Cheheltani et al. (2013) Infrared Spectroscopy to Measure Collagen and Elastin in Aorta Using Multivariate Analysis. 39th Annual Northeast Bioengineering Conference, 13–14 [97]. ©2013 IEEE. Reprinted, with permission.

3.1 Abstract

Pathological changes in extracellular matrix (ECM) occur in the context of abdominal aortic aneurysm disease. The objective of this study is to assess the capability of Fourier transform infrared spectroscopy (FTIR) to differentiate major aorta ECM components. Two partial least squares (PLS) models were developed using mixtures of matrix components in potassium bromide pellets. In the first model collagen and elastin powders were mixed in varying percentages. In the second model, pig aorta specimens were selectively degraded by enzymatic treatment of either collagen or elastin and used to prepare pellets. The results of the PLS model showed the ability of FTIR methodology for differentiation of elastin and collagen. These results lay the foundation for application of the methodology to assess the progression of AAA pathology.

3.2 Introduction

We have previously shown that infrared spectroscopy can be used to visualize cardiac collagen deposition after myocardial infarction using a univariate method [4]. One challenge in spectroscopic assessment of ECM, however, is the similarity of spectra for its different components [5], which calls for application of multivariate analysis techniques such as partial least square (PLS) regression for differentiation of spectroscopically similar components such as collagen and elastin. In this study, we demonstrate the ability of FTIR in conjunction with PLS to differentiate between major aorta components, namely elastin and collagen.

PLS is a multivariate regression method particularly suited for spectroscopy where the X matrix or matrix of predictors (spectra) has a large number of variables. PLS model optimizes the prediction of response matrix (Y) by finding the multidimensional direction in the X space that explains the maximum multidimensional variance direction in the Y space.

In this study, first potassium bromide (KBr) pellets were made using known concentrations of elastin and collagen powders and a PLS model (model A) was developed to predict the concentration of each component. Next, another PLS model (model B) was developed to predict elastin and collagen content in porcine aorta, in which collagen and elastin content was measured via biochemical assays.

3.3 Materials and Methods

3.3.1 Pure Component Pellets

KBr pellets of major aorta ECM components (collagen, elastin) were prepared by mixing 4 mg of pure component powder mixture with 196 mg of KBr and compressing the mixture into a pellet. The 4 mg pure component powder was prepared from a mixture of elastin/collagen powders in 0/100, 25/75, 50/50, 75/25 and 100/0 percentages by weight (n=6 for each percentage).

3.3.2 Porcine Aorta Pellets

Porcine aorta samples were acquired from a local slaughter house. Four aorta wall specimens were prepared by cutting strips of about 100 mg (wet weight). One specimen was cut from an anatomical position near the abdominal aorta and three specimens were cut from an anatomical position near the aortic arch. Of the latter, one specimen was treated for collagen degradation, one was treated for elastin degradation and one was left untreated. The specimen from abdominal aorta was left untreated. This resulted in four specimens with varying degrees of collagen and elastin content as shown in Table 3-1. After treatment, specimens were lyophilized and frozen milled to a fine powder. One mg of the resulting powder was mixed with 199 mg KBr to form one pellet. A total of 14 pellets were made.

3.3.3 Enzymatic Degradation of Aorta Specimens

Enzyme solutions were prepared in tris buffered Saline (TBS). One specimen was submerged in collagenase solution at 37°C, and one sample was submerged in elastase at room temperature. Untreated samples were submerged in TBS. All treatments were allowed to continue for 5 hours. To measure the amount of collagen and elastin, sample powders from each specimen

was used in hydroxyproline assay and Fastin elastin assay respectively. The results of these measurements are shown in Table 1-1

Table 3-1			
<i>Collagen and elastin content in aorta specimens</i>			
Specimen #	Specimen Treatment	Component content %(d/w)	
		Collagen	Elastin
1	Untreated aortic arch	13%	55%
2	Untreated abdominal aorta	12%	39%
3	Elastase treated	12%	23%
4	Collagenase treated	8%	40%

3.3.4 Data processing

Mid-IR spectra obtained from KBr pellets (X matrix) were combined with values of elastin/collagen components (Y matrix), and were analyzed using a PLS regression algorithm. Response values (Y) were obtained from either weighing the elastin/collagen concentration (model A) or biochemical assays (model B). Spectra were processed by a multiplicative scatter correction (MSC) and 41-point Savitzky–Golay second derivative calculation. The preprocessed values for frequencies in the region of 1000-1800 cm^{-1} were used as variables to predict collagen-elastin content. This range includes absorbances from both of these components. Full cross validation was used and the quality of the models was evaluated by assessment of the root mean square error (RMSE) of prediction, and the regression coefficient (R^2) of the cross validation model.

3.4 Results and Discussion

Summary of the results of PLS models are shown in Table 3-2. For model A, 1 factor was sufficient to separate pellets with varying levels of elastin/collagen concentration as shown in Figure 3.1-A. For model B, 5 factors seemed to give the best results; however, as shown in

Figure 3.1-B, even in score plot of factors 1 vs. 3, it is clear that the model is able to separate samples according to their elastin/collagen content.

Table 3-2				
<i>Summary of PLS Results</i>				
PLS Parameter	Model A		Model B	
	Collagen	Elastin	Collagen	Elastin
R ² of validation	0.98	0.86	0.97	0.94
RMSE of prediction	0.21	0.40	0.001	0.01
Number of factors	1	1	5	5

Both models were able to predict elastin/collagen content in strong correlations. The results of the present study demonstrate the ability of the infrared spectroscopy together with a PLS regression to predict elastin and collagen content in a mixture of these components, as well as in dried up aortic tissue specimens with selective protein degradation.

Infrared Spectroscopy has the potential for translation to a clinical environment to examine ECM changes in aorta in a minimally invasive fashion using fiber optic technology. This study creates a basis for next spectroscopic studies of aorta ECM proteins, where fiber optics will be used to collect spectra from aorta specimens to measure the level of ECM degradation as an indication of AAA progression. Furthermore, from the developed models, spectral features specific to different ECM components can be detected and utilized in other analysis methods such as cluster analysis to visualize these components in histological images.

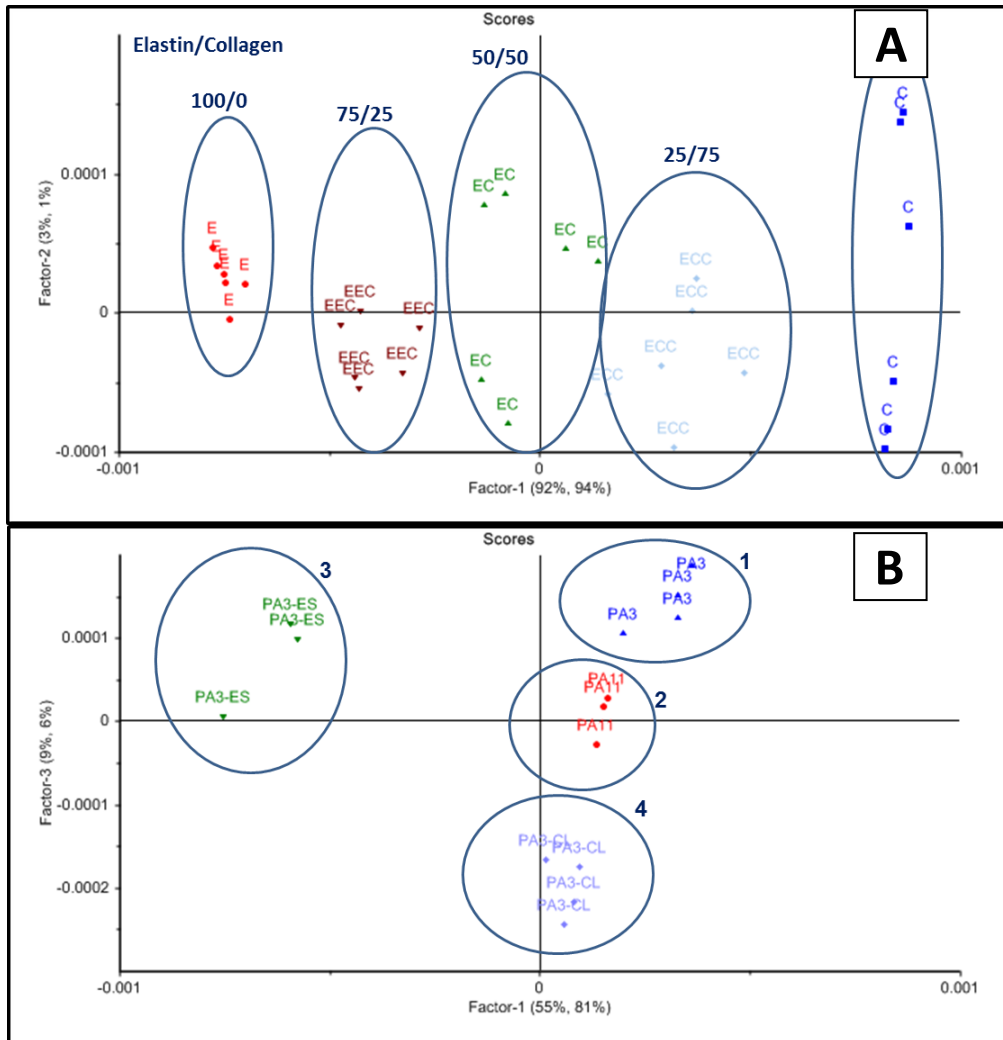


Figure 3.1 (A) Score plots of model A with the first two factors. PLS model has grouped the samples according to elastin/collagen percentages. (B) Score plot of factor 1 vs. 3 in PLS model B; with increasing elastin and collagen content being represented along factors 1 and 3 respectively. Number for each group is the specimen number as defined in Table 3-1.

CHAPTER 4

FOURIER TRANSFORM INFRARED SPECTROSCOPY TO QUANTIFY COLLAGEN AND ELASTIN DEGRADATION IN AN IN VITRO MODEL OF ABDOMINAL AORTIC ANEURYSM

For the most part, sections presented in this chapter will be submitted for a publication as Cheheltani et al. (2014) Fourier Transform Infrared Spectroscopy to Quantify Collagen and Elastin in an in vitro Model of Aortic Degradation, The Analyst.

4.1 Abstract

In this study, an infrared spectroscopic methodology has been developed to quantify collagen and elastin in aorta. Enzymatically degraded pig aorta samples were used as a model of ECM degradation in abdominal aortic aneurysm (AAA). After enzymatic treatment, Fourier transform infrared (FTIR) spectra of the aortic tissue were acquired by an infrared fiber optics probe (IFOP) and FTIR imaging spectroscopy (FT-IRIS). Collagen and elastin content were quantified biochemically and partial least squares (PLS) models were created to predict collagen and elastin content in aorta based on FTIR spectra. PLS models created from FT-IRIS spectra were able to predict elastin and collagen content of the samples with strong correlations ($R^2=0.90$ and 0.70 respectively), and IFOP spectra were successfully used to predict elastin content ($R^2=0.81$). The PLS regression coefficients from the FT-IRIS models were used to map collagen and elastin in tissue sections of degraded pig aortic tissue as well as a human AAA biopsy tissue, creating a similar map of each component compared to histologically stained images. These results support further application of FTIR spectroscopic techniques for evaluation of AAA tissues.

4.2 Introduction

The aorta is the major blood vessel for transport of oxygenated blood from the heart to the arteries of the systemic circulation, and aortic diseases are among the leading causes of death in developed countries. The aorta is composed of three distinct structural layers or tunics: the intima, media and adventitia, and the cellular and extracellular composition of these layers are related to their function [30]–[32]. The innermost layer, tunica intima, is essentially composed of a single layer of endothelial cells that are in direct contact with blood. The tunica media is composed of smooth muscle cells surrounded by an elastic extracellular matrix (ECM) of fibrous proteins; elastin and collagen. Elastin fibers provide the elastic properties and tensile strength of the aorta necessary for propulsion of the blood downstream. These fibers are arranged in concentric plates called elastic lamellae with a network of finer elastic fibers between lamellae. Collagen fibers, which are dispersed in the space between the lamellae, contribute to the strength and structural integrity of the aorta. The outermost layer of the aorta, tunica adventitia, is surrounded by loose connective tissue and mostly consists of bundles of thick collagen fibrils. In aging and disease, the fibrous structure and content of collagen and elastin in the aortic ECM change [15], [17], [31], [33], [34]. There is a direct relationship between the structural integrity of the compositional proteins and the healthy functionality of the aorta [98][38]. Therefore, characterization of the molecular changes in ECM has a critical role in the diagnosis and severity assessment of different pathological conditions. Moreover, such characterization provides useful information for deeper understanding of the pathophysiological mechanisms that underlie their onset and progression.

One of the common diseases of the aorta is the focal dilatation of the infrarenal aorta known as abdominal aortic aneurysm (AAA). AAA, predominantly found in men 65 years of age and older, is associated with progressive destruction of the ECM structure and its major constituents, collagen and elastin macromolecules [10][11], leading to wall weakening and dilatation [36], [101]. Left untreated, the gradual expansion of the aorta and weakness of the vessel wall may lead to rupture and consequent death [102]. In current clinical practice, the necessity for surgical intervention to prevent rupture is determined by the maximum diameter of the aneurysm. However, several studies have found biomechanical properties to be more reliable predictors of rupture risk [35], [102]–[105]. Since there is a direct relationship between the level of ECM protein integrity and mechanical properties of the aorta [38], [106], a methodology that provides detailed knowledge of the molecular composition and content of the aortic wall in AAA patients would be extremely beneficial for precise diagnosis and rupture risk assessment. In this study, we introduce a novel application of Fourier transform infrared spectroscopy (FTIR) for the quantification of collagen and elastin content in aorta.

Recent infrared microscopy and imaging studies applied to cardiovascular tissues include monitoring arterial remodeling after injury [64], identification and characterization of vulnerable plaques using characteristic absorption bands of lipids and total protein [41], [53], [54], study of collagen deposition in cardiomyopathic heart sections [50], [51] and in cardiac remodeling after myocardial infarction [48], [49]. In our laboratory, we have developed FTIR methodology to map collagen deposition in heart sections that had undergone cardiac remodeling after myocardial infarction [65]. In addition, FTIR has been used to characterize aneurysmal aortas on biopsies of human ascending aortas [57]–[59], [63]. These investigators demonstrated that normal and

aneurysmal human arterial tissue biopsies could be differentiated using the ratio of α -helical to β -sheet content and principal component analysis (PCA) [57], hierarchical cluster analysis (HCA) [58] and factorial discriminant analysis (FDA)[63]. Furthermore, curve-fitting was used to detect alteration of β structures in the protein spectral profile of pathological aortas [59]. Although this group of studies set the ground work for differentiation of pathological from healthy aortic tissues, there has been minimal confirmation with histology or biochemical analysis, and the relative degradation of the primary ECM components (elastin and collagen) associated with aneurysm conditions has not been specifically evaluated.

In this study, we develop multivariate regression models to quantify collagen and elastin in degraded aorta, using FTIR spectroscopic methods. The motivation for development of this methodology is twofold: first, FTIR has the potential of translation to a clinical diagnostic method through the use of infrared fiber optic (IFOP) technology [42], [68], [107]. For cardiovascular tissues specifically, the potential of catheter based IFOP probes for the characterization of atherosclerotic plaques has gained increasing attention [108]–[110]. As a second motivation, a better understanding of the pathophysiology of AAA is dependent on development of methods that can reliably measure content and distribution of various ECM components. Fourier transform infrared imaging spectroscopy (FT-IRIS) has been increasingly used to create chemical images of various components in biological tissues [53], [63], [65], [67]. Here, we have used these two modalities of FTIR analysis, IFOP on intact tissues, and FT-IRIS on histological tissue sections, to quantify collagen and elastin in proteolytically treated aorta samples as a model of AAA disease [38]. FTIR spectra collected from each modality were correlated to elastin or collagen content in multivariate models applying the partial least

squares (PLS) regression method. To demonstrate an application of the developed methodology, the FT-IRIS based PLS regression models were applied to aortic histological sections, resulting in a map of ECM components in these tissue sections. It should be emphasized that despite being presented in the context of AAA disease, this methodology is applicable to any aortic pathological condition that is identified with a change in the content of collagen or elastin in aortic ECM.

4.3 Material and Methods

4.3.1 Preparation of the aorta samples

Pig aortas were purchased from a local slaughterhouse and transferred on ice before being cut into rings of about 2-3 cm in length (Figure 4.1-A). Aorta rings were embedded in optimal cutting temperature (OCT) compound (Tissue Tek O.C.T, Sakura Finetek, Torrance, CA), flash frozen and kept at -80°C until being used for degradation experiments.

4.3.2 Enzymatic degradation of the aorta samples

Frozen aorta rings selected from different anatomical locations along the aorta were thawed and cut into circumferential strip samples of *ca.* 100 mg wet tissue weight (Figure 4.1-B).

Samples were then treated with collagenase, elastase or buffer (untreated) for 2, 5 or 24 hours for a total of 9 treatment groups. Collagenase treatment was applied by leaving the sample submerged in 500 ml of collagenase solution for the specified treatment time at 37°C.

Collagenase solution was prepared by dissolving purified collagenase (CLSPA, Worthington Biochemical, Lakewood, NJ) in tris-buffered saline (TBS, pH 8.0) at a concentration of 1 mg/ml.

Elastase treated samples were left in 500 ml of elastase solution for the specified treatment

time at room temperature. Elastase solution was prepared by dissolving purified elastase (ESFF, Worthington Biochemical, Lakewood, NJ) in TBS (0.5 mg/ml). Untreated samples were left in 500 ml of TBS at room temperature. A total of 81 samples were prepared. After the specified treatment time samples were washed with deionized water (DI) water and FTIR-IFOP data were collected as detailed below. Each sample was then cut in half along the aorta circumference. One half was put in OCT compound, flash frozen and stored at -80°C for further histologic sectioning. The remaining half was weighed (wet weight), minced into smaller tissue pieces, and lyophilized for use in biochemical assays of elastin and collagen content. Biochemically measured elastin and collagen contents were expressed as either mass percentage of wet tissue (%w/w) or mass percentage of dry matter after lyophilization (%d/w).

4.3.3 Biochemical analysis for quantification of elastin and collagen

Tissue samples were minced, lyophilized and their dry matter weight recorded before being used for biochemical assays. Elastin in the samples was converted to soluble cross-linked polypeptide elastin fragments, known as α -elastin [16], by 0.25 M oxalic acid extraction at 100°C. A total of four 1 hour extractions were necessary to completely dissolve the elastin in the aorta samples. The amount of α -elastin in the resulting solutions was measured using Fastin Elastin Assay (Biocolor, Carrickfergus, UK) according to the manufacturer instructions. For collagen quantification, the hydroxyproline content of the samples was measured [111]. Collagen content in the samples was estimated by assuming 12.5 g hydroxyproline/100 g collagen [112] after correction for hydroxyproline content in elastin (1.5g hydroxyproline/100g elastin [112]–[114]).

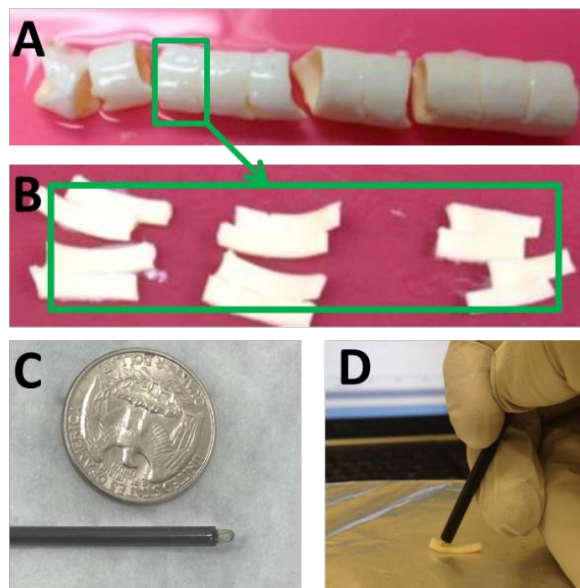


Figure 4.1 Experimental procedure. A) Pig descending aorta cut in 2-3 cm long rings. B) Aorta rings cut open and cut in smaller pieces for enzymatic degradation. C) Custom-made ATR sampling tip for FTIR-IFOP data collection next to an American quarter dollar coin. D) FTIR-IFOP data collection from an aorta sample.

4.3.4 FTIR Fiber optic probe (IFOP) data collection

IFOP spectra were collected with a custom-made silver halide attenuated total reflectance (ATR) sampling tip (Art Photonics, Berlin, Germany). The tip was mounted to the end of a 1 m silver halide fiber, which was connected to a Fibermate 2 fiber-optic probe launcher (Harrick Scientific Products, Pleasantville, NY). The launcher was coupled to a Nicolet iS5 spectrometer (Thermo Scientific, Madison, WI). The custom-made ATR sampling tip was 15 cm in length and had a diameter of 3 mm (Figure 4.1-C). Freshly treated samples were washed in DI water and excess water was removed before data collection. IFOP spectra were collected from 3 points on the intima and 3 points on the adventitia side of the sample. The sampling tip was held by hand in contact with the sample (Figure 4.1-D). Each spectrum was collected from $750\text{-}4000\text{ cm}^{-1}$ with 64 co-added scans and a spectral resolution of 8 cm^{-1} .

4.3.5 FT-IRIS data collection and analysis

Enzymatically degraded frozen aorta samples were cryosectioned (aortic cross section) at 9 μm , mounted on MirrIR low-e microscope slides (Kevley Technologies, Chesterland, OH) and fixed in 10% formalin for 10 minutes. OCT on the slide was washed off carefully with DI water. FT-IRIS images were acquired at 50 μm pixel resolution and 8 cm^{-1} spectral resolution with 2 co-added scans using a Perkin Elmer Spotlight 400 spectrometer (Shelton, CT). FT-IRIS data were analyzed in ISys 5.0 software (Malvern Instruments Ltd, Malvern, UK). For each sample, the average spectrum of all pixels in the image was calculated and used in PLS models to predict elastin and collagen dry weight content.

4.3.6 PLS models

PLS analysis and spectral preprocessing was performed in The Unscrambler X software (CAMO Software AS, Oslo, Norway). A total of four PLS models were created. The summary of these models and their abbreviations as used in this paper is presented in Table 1.

Table 4-1		
<i>Summary of the four PLS models and their abbreviations in this chapter</i>		
Model Abbreviation	Component	Mode of spectral collection
COL-IFOP	Collagen	Infrared fiber optics probe (IFOP)
ELAS-IFOP	Elastin	Infrared fiber optics probe (IFOP)
COL-FTIRIS	Collagen	Infrared imaging spectroscopy (FT-IRIS)
ELAS-FTIRIS	Elastin	Infrared imaging spectroscopy (FT-IRIS)

Two PLS models were created for collagen and elastin content prediction using IFOP spectra. The six spectra collected per sample (three from the intima side and three from the adventitia side) were averaged prior to spectral preprocessing. Spectral bands attributed to elastin and

collagen were apparent between 1000 and 1800 cm^{-1} ; this spectral region was subsequently used for analysis. An extended multiplicative scatter correction (EMSC) was applied to the spectra, followed by calculation of the second derivative of the spectra (polynomial order of 3 and 11 smoothing points). Two thirds of the samples (57 samples for ELAS model and 48 samples for COL model) were assigned to the calibration set and were correlated with reference content (%w/w) of collagen (COL-IFOP model) or elastin (ELAS-IFOP model) measured previously by biochemical assays. The average spectra of the remaining samples (27 samples for ELAS model and 24 samples for COL model) were used as the validation set. For these sets to be both representative of the whole range of the sample, they were carefully assigned such that both included samples from all treatment groups and samples from different anatomical positions of the aorta.

Two PLS models for collagen and elastin content were developed based on FT-IRIS spectra of sections from enzymatically degraded aorta specimens mounted on low-e elides. Average spectra per image for each specimen were used in the models and similar pre-processing methods as used for the IFOP models were applied. The second derivative was calculated with a polynomial order of 3 and 9 smoothing points. The same calibration and validation sets as used in PLS-IFOP models were used and FT-IRIS spectra were correlated with reference content (%d/w) of collagen (COL-FTIRIS model) or elastin (ELAS-FTIRIS model) measured previously by biochemical assays.

4.3.7 Pure component pellets

Potassium bromide pellets were prepared using pure powders of collagen (C206, Elastin Products Company, Owensville, MO) and elastin (SP46, Elastin Products Company, Owensville,

MO). The purchased collagen was in the form of shredded fibers and was milled into fine powder using a freezer mill 6770 (SPEX Sample Prep, Metuchen, NJ). Pellets were prepared by mixing 4 mg of component powder with 196 mg of KBr and compressing the mixture into a pellet. The 4 mg component powder was prepared from a mixture of elastin/collagen powders in 0/100, 50/50, 100/0 percentages by weight (n=6 for each percentage). FTIR Spectra of each pellet were acquired at 2 cm^{-1} spectral resolution with 64 co-added scans using the Perkin Elmer Spotlight 400 spectrometer. Spectra presented for each group were calculated by averaging the spectra of six pellets within each group.

4.3.8 Mapping components in aorta and human AAA sections

A 5 hour elastase treated sample and a 5 hour collagenase treated sample were selected and consecutive $9\text{ }\mu\text{m}$ sections were cryosectioned and mounted on to MirrIR low-e microscope slides and glass slides for FT-IRIS and histology respectively. Sections of a human AAA wall specimen were prepared similarly. This specimen was excised from an AAA patient during their elective surgical repair (obtained under University of Pittsburgh IRB approval for a previous study), paraffin embedded, and sectioned onto MirrIR low-e and glass slides. After deparaffinization, FT-IRIS images were collected at $6.25\text{ }\mu\text{m}$ pixel resolution and 8 cm^{-1} spectral resolution and each pixel was 2 co-added scans. Second derivative of the spectra in the images were calculated with polynomial order of 3 and 9 smoothing points similar to PLS-FTIRIS models mentioned above. Spectra were vector normalized and exported to MATLAB R2013a (Mathworks, Inc., Natick, MA). Regression coefficients of COL-FTIRIS and ELAS-FTIRIS PLS models were also imported and used to predict collagen and elastin content respectively for each image

pixel. Maps of elastin or collagen content in the sections were created by the scalar product of each pixel spectrum and the regression coefficients.

4.3.9 Histological staining

The histology sections from the 5 hour elastase treated specimen were stained using the Verhoeff-Van Gieson (VVG) staining protocol for elastic fibers stain kit (Polysciences Inc., Warrington, PA). The 5 hour collagenase treated specimen sections were stained with picosirius red stain kit (Polysciences Inc., Warrington, PA). The AAA wall sections were stained with Movat's pentachrome staining protocol. Histology images were acquired using a Nikon microscope equipped with a Nikon DS-Fi1 color camera and Nikon Element software (Nikon Instruments Inc., Mellville, NY). Images of collagen distribution in the picosirius red stained sections, were obtained under linearly polarized light as detailed previously [115].

4.4 Results and Discussion

4.4.1 Measured collagen and elastin content in aorta

The overall elastin and collagen contents of untreated aortas, measured using biochemical assays, were in agreement with previous studies [113], [114]. Average elastin content in different aortic rings ranged from 44.7% ($\pm 3.8\%$) to 58.6% ($\pm 5.0\%$) (%d/w). Samples from anatomical positions closer to the arch on average had higher values than those closer to abdominal section (Figure 4.2-A). The gradual decrease of elastin proportion in descending aorta from arch to abdominal has been reported in several mammals and has been associated with less elasticity needed in distal regions as the blood flows further from the heart [116]. Collagen proportion in different aorta rings ranged from 4.1% (± 0.1) to 19.8 ($\pm 1.1\%$). Collagen content

was lower in the samples from upper sections of the aorta and higher in samples closer to the abdominal section (Figure 4.2-B). In treated samples, elastin was lowest in samples treated with elastase for 24 hours (zero or close to zero) and highest in samples treated with collagenase for 24 hours. Collagen content was accordingly highest in elastase treated samples and lowest in collagenase treated samples. Since treatment with elastase for 24 hours resulted in almost complete degradation of elastin, samples within this treatment group lost about half of their dry matter weight. In these samples, the remaining mass after treatment was too low for two biochemical assays, and priority was given to elastin assay. As a result, these samples were not included in the PLS models for collagen content. The most prominent feature of ECM changes in AAA is a wide scale depletion of elastin [116], [117] and our elastase treated samples provide a good model for AAA disease condition in terms of elastin degradation.

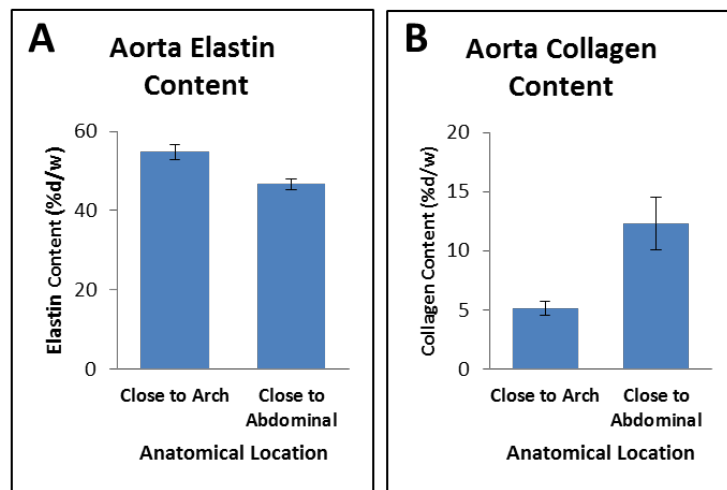


Figure 4.2 Elastin and collagen content in pig descending aorta in different anatomical locations (n=9 per group, error bars are standard deviation). A) Elastin content in the descending aorta decreases as the aorta descends (P=0.002). B) Collagen content in the descending aorta increases as the aorta descends (P=0.014).

4.4.2 FTIR Spectral features of Elastin, Collagen and Aorta Samples

The spectra of collagen and elastin show several similarities as seen in the KBr pellet spectra (Figure 4.3-A and Figure 4.3-B). They both have features that arise from their protein structure, such as amide I (approximately 1580-1718 cm^{-1}) and amide II (approximately 1480-1580 cm^{-1}) regions. More interesting was the observation that the peak at 1338 cm^{-1} , which we have previously shown to be a strong quantifying peak for collagen scar deposition in infarcted cardiac tissue sections [65], had a very similar absorbance in collagen and elastin spectra. This band has been assigned to the CH_2 wagging vibration of proline side chains [78], and the similar absorbance of this band in collagen and elastin could be originating from the similar proline content of collagen and elastin (119 and 115 residues in 1000 residues respectively [112]–[114]).

Despite the similarities, collagen and elastin had some distinct differences, such as the spectral features in the 1040-1100 cm^{-1} and 1380-1420 cm^{-1} regions. As expected, the spectra of aorta (Figure 4.3 C to F) and the spectra of its major constituents, collagen-elastin mixture (Figure 4.3 A and B), are similar in general features such as the prominent peaks of amide I and amide II bands. These spectral bands appear broader in KBr pellets due to scattering effects. Differences between collagen-elastin mixture spectra and aorta spectra are attributed to other minor aorta constituents, e.g. proteoglycan and glycoproteins of the ECM and actin and myosin proteins of the smooth muscle cells. One of the most prominent spectral features of decreasing elastin content in aorta is the shift in amide II peak toward higher wavenumbers (Figure 4.3 C and E). This could be explained by differences in amino acid compositions of collagen and elastin. For example, collagen has 9.5% glutamine [10], whereas elastin has 1.7% glutamine [14] and

glutamine has vibrational peaks at 1556-1560 cm^{-1} [118]. The shift in amide II towards higher vibrational peaks can be tentatively assigned to a spectral contribution from glutamine.

The underlying structure of the amide I band was resolved by examining second derivative spectra. Two peaks were observed in the amide I region of FT-IRIS and KBr pellet spectra. The peak at approximately 1630 cm^{-1} slightly shifted to higher wavenumbers with decreasing elastin content (Figure 4.3 B, D and F). This slight shift may be explained by the differences in secondary structures of collagen and elastin [57], [59], [60]. Collagen is composed mainly of α -helical structures, while elastin is primarily β -sheets; the amide I band of α -helical structures occurs between 1643-1667 cm^{-1} , and for β -sheet structures occurs between 1610-1645 cm^{-1} [57], [60].

There is a noticeable difference in the amide I/amide II intensity ratio between IFOP and FT-IRIS spectra, which can be attributed to the contribution of O-H bending vibration of water at 1640 cm^{-1} [78]; IFOP spectra were collected from freshly treated tissues containing water, whereas FT-IRIS spectra were collected from dehydrated tissue sections. There is also a decrease in intensity of amide I with lower elastin content seen in FT-IRIS (Figure 4.3-C) and pellet spectra (Figure 4.3-A) which is not noticeable in IFOP spectra (Figure 4.3-E). This may be due to the fact that samples with low elastin content, i.e. samples treated with higher treatment times with elastase, would lose their original solid structure and absorb water 3-4 times their original water content. This inverse relationship between elastin and water content in the elastase treated samples may have resulted in higher absorbance from higher water content balancing the effect of elastin loss in amide I region in these samples.

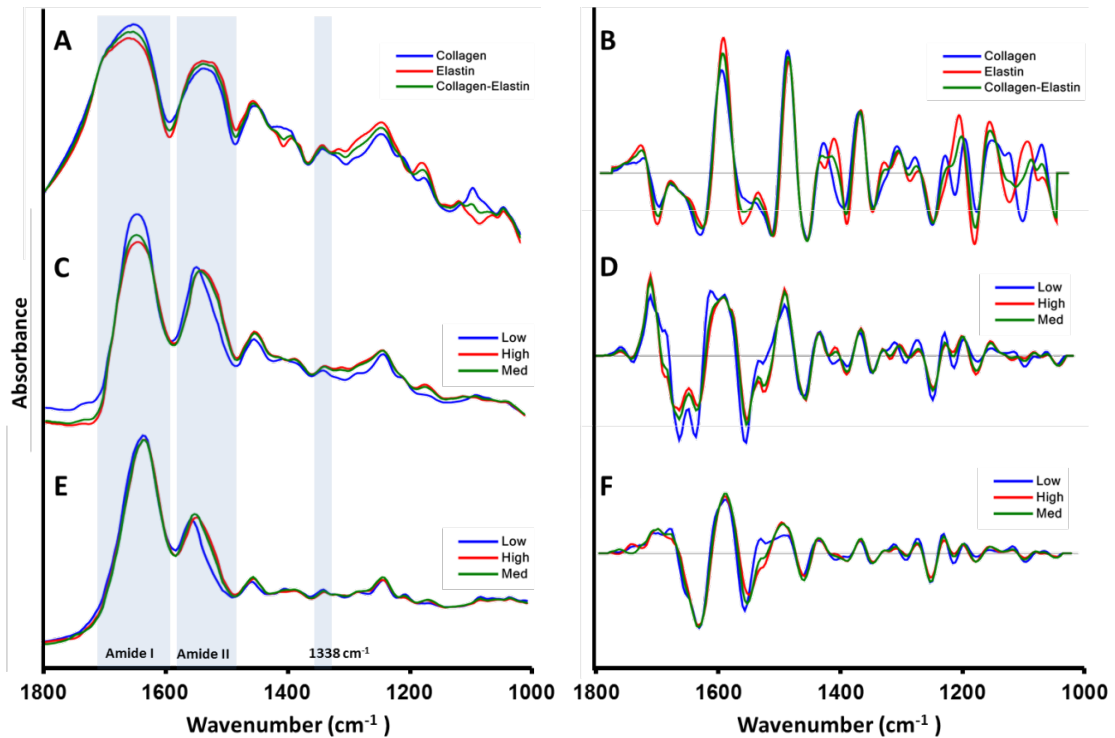


Figure 4.3 Average spectra of samples with low, medium and high elastin content. A) Reference spectra of collagen-elastin KBr pellets, and B) second derivative of (A). C) FT-IRIS spectra, D) second derivative of (C), E) FTIR-IFOP spectra, F) second derivative of (E). Samples in C and D were categorized into Low (0.0-25.8 %d/w), Medium (27.3-51.6 %d/w) and High (52.0 -78.2 %d/w) and samples in E and F were categorized into Low (0.0-5.3 %w/w) Medium (7.8-14.0 %w/w) and High (14.0-20.9 %w/w) elastin content as measure by Fastin elastin assay.

In addition, IFOP spectra were inherently different from spectra collected using the FT-IRIS imaging system. IFOP spectra were collected using an ATR technique; in ATR spectral data collection infrared light is directed at a sample through a high refractive index material, most of the light is totally internally reflected however a small amount of light penetrates into the sample, this is known as an evanescent wave. An ATR spectrum is based on the absorption profile of this evanescent wave and because of the depth penetration characteristics of this evanescent wave ATR spectra are different to those collected using the FT-IRIS imaging system. The depth of penetration of the evanescent wave is dependent on both wavelength and the refractive index of the sample such that penetration depth, and therefore effective pathlength,

is greatest at longer wavelengths. This greater effective pathlength results in an enhancement of absorption features at longer wavelengths [39]. ATR correction algorithms can be used in many ATR applications with crystal based ATR tips where the pathlength of the evanescent wave is known. However, in this study, due to the complicated loop-shaped geometry of the custom-made ATR tip (Figure 4.1-C) and the unknown pathlength of the wave, ATR correction could not be applied.

4.4.3 PLS Models

The results for PLS regression models are presented in Figure 4.4. As the plots show, in all models both calibration and validation sets span the whole range of the samples under study. The developed PLS models strongly correlated with measured numbers, with the R^2 for regression lines exceeding 0.7 for all but the COL-IFOP model. The error of prediction of the three strongest models was ~10% of the range of measurements. These results confirm that elastin and collagen concentration can be predicted in aorta samples using infrared imaging spectroscopy of their histology sections. Furthermore, elastin concentration can be estimated using infrared fiber optic probe spectra taken from bulk tissue samples.

In general, the models predicting elastin were more accurate than collagen models. Elastin is the major ECM component in aorta with quantities more than twice the amount of collagen quantity. Therefore, the greater contribution of elastin to the mid-infrared spectra means that variations in elastin content will be more obvious spectrally. In addition, the measurement error associated with collagen content was greater than elastin content. We estimated the collagen content in our samples by determining hydroxyproline concentration, which is a very well established method for estimating collagen content in biological tissues [111], [112], [114],

[119]. Because of the low hydroxyproline content of elastin, the contribution of elastin to total hydroxyproline is neglected in most applications of this method. However, in our study we applied enzymes to degrade collagen and elastin to varying degrees, and because of the varying ratio of elastin to collagen content in our samples we could not neglect the contribution of elastin to hydroxyproline concentration. For this reason, collagen was calculated from the hydroxyproline assay after the contribution from elastin was accounted for. While this approach would assure more realistic values for collagen content, the errors in the elastin assay were introduced into the estimation of collagen and add to intrinsic errors in the hydroxyproline assay. This could also explain a number of negative collagen values which were observed in samples treated with 24 hours collagenase. These samples were expected to have close to zero collagen content as confirmed with histology (data not shown), and the negative values could have resulted from the assumed hydroxyproline content in elastin (1.5 %) being an overestimation.

The higher signal to noise ratio of FT-IRIS spectra vs. IFOP spectra may also contribute to FT-IRIS models being stronger than IFOP models. IFOP spectra were collected and averaged from six points on the surface of the sample whereas FT-IRIS spectra were averaged from the pixels in the hyper-spectral images of the aortic wall cross section which were *ca.* 3500-9000 pixels for each sample. Furthermore, the proteolytically degraded samples were heterogeneous as the enzyme treatments degraded the aorta samples from the outer surfaces. This effect can be seen in the images from two typical samples treated with elastase and collagenase for 5 hours in Figure 4.6 A and Figure 4.6-B, respectively. Elastin lamina, as differentiated in black in the Verhoeff Van Geisen staining in Figure 4.6-A, has degraded completely in the peripheries, with

the core still packed with elastin lamina. In Figure 4.6-B, the same pattern exists for collagen fibers visualized as bright yellow in the picosirius red stain under polarized light. This spatial variation of components in the partially degraded samples could have resulted in sampling errors in collecting the spectra using the IFOP from the surface of the sample

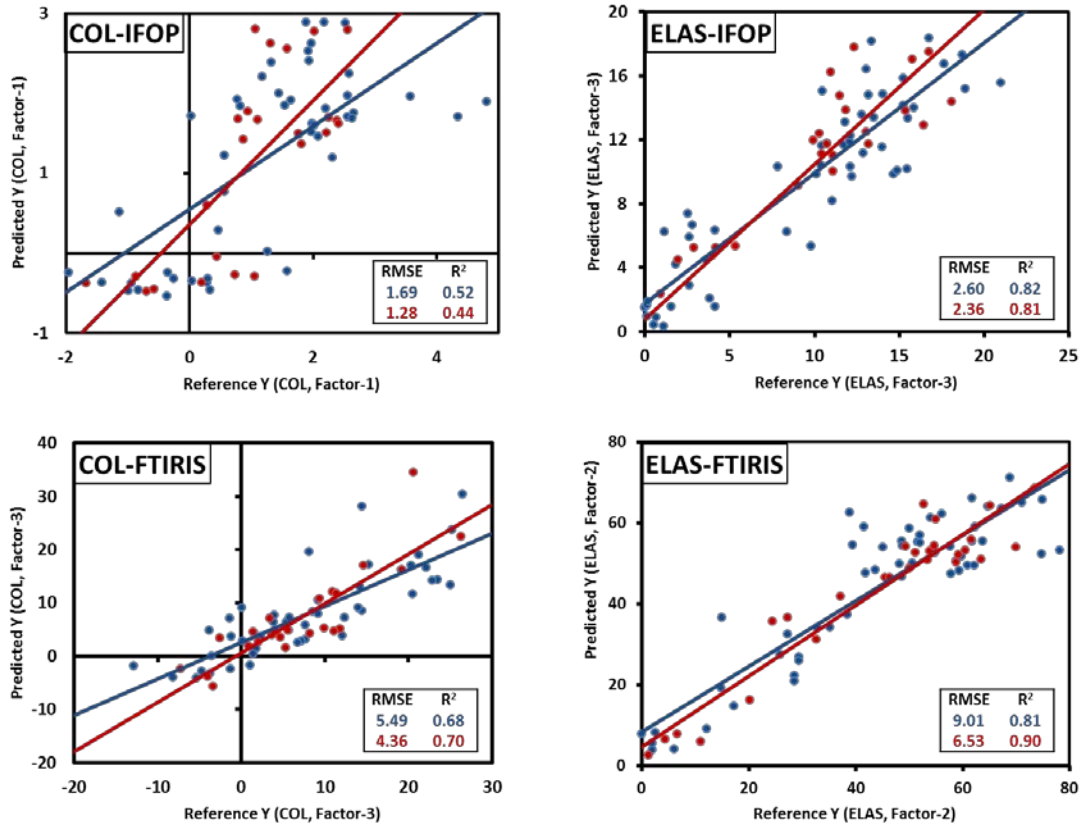


Figure 4.4 Predicted vs. reference values for the developed PLS models as detailed in Table 1. Calibration set is marked in blue and validation set is marked in red.

. Finally, contribution of water in the spectra could be another reason for a weaker correlation between content and spectra in IFOP models. IFOP spectra were collected from samples containing water, and in the case of elastase treated samples, additional water is likely to have been absorbed. Despite a lower sensitivity of IFOP spectral data collection compared to FT-IRIS, they each have distinct applications. IFOP data collection has the advantage that it is

transferrable to a clinical environment with further development of the technology. FT-IRIS is an imaging technology which is useful in mapping components at high spatial resolution on histological sections as observed in the example application below.

Factor 1 from FT-IRIS PLS models are shown in Figure 4.5. Since collagen and elastin are the major constituents of ECM, and our model was based on only degradation of these constituents, it is not surprising to see that the peaks that indicate increasing elastin content in ELAS model, are indicating decreasing collagen content in COL model and vice versa.

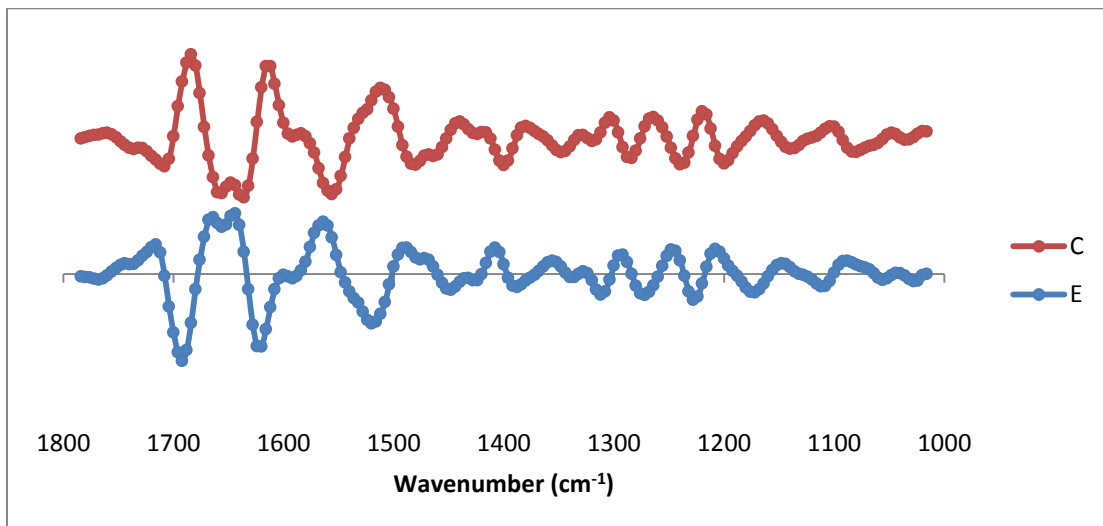


Figure 4.5 Comparison of factor 1 in PLS models predicting collagen (C) and elastin (E) from FT-IRIS spectra.

4.4.4 Mapping components in aorta sections and human AAA section

To further validate the results of the FT-IRIS PLS models, and to demonstrate their application for investigation of AAA disease, we used the results of these PLS models to create maps of elastin and collagen on histological sections of degraded aorta as well as sections from the aorta of a patient with an AAA.

Figure 4.6-C and Figure 4.6-D show the FT-IRIS mapping of elastin and collagen using the regression coefficient of the corresponding FT-IRIS PLS model as explained in the methods section. These images, similar to their corresponding histological sections (Figure 4.6 A and B), show a complete degradation of elastin or collagen in the peripheries that were in direct contact with the enzyme.

The histopathological features of AAA pathology are noticeable in the Movat's pentachrome section shown in Figure 4.6-E where the normal alignment of elastin and collagen fibers is absent. Instead of organized elastin lamella across the whole thickness of the section, elastin is only visible in a portion of the thickness as black aggregates, with the rest of the section completely depleted of elastin. The distribution of elastin determined using FT-IRIS and the ELAS-FTIRIS PLS model (Figure 4.6-F) and the distribution of collagen using COL-FTIRIS model (Figure 4.6-G) are comparable to Movat's pentachrome staining. The fact that the results of the PLS model based on enzymatically degraded swine aorta samples could be applied with this level of similarity to histology in this human AAA section, is a strong indication of the applicability of the developed models to human tissues.

4.4.5 Conclusion

FTIR spectroscopy is a viable method for predicting collagen and elastin content in aortic tissue. We have created PLS models that can be applied to histological sections of the aortic tissue. This methodology to map collagen or elastin in aortic tissue is a useful tool in studying changes of ECM in different aortic diseases, with minimal preparation of the sections compared to histological or immunohistochemical methods. Also, quantification of the content from images would be fast and easy without complications attributed to image processing methods of

histological images. We have also developed a PLS model to quantify elastin in “intact” aortic tissue using an infrared fiber optic probe. This methodology could prove useful when fiber optic technology advances to the point of being applicable *in vivo* for diagnosis or risk assessment of pathological conditions of the aorta including AAA.

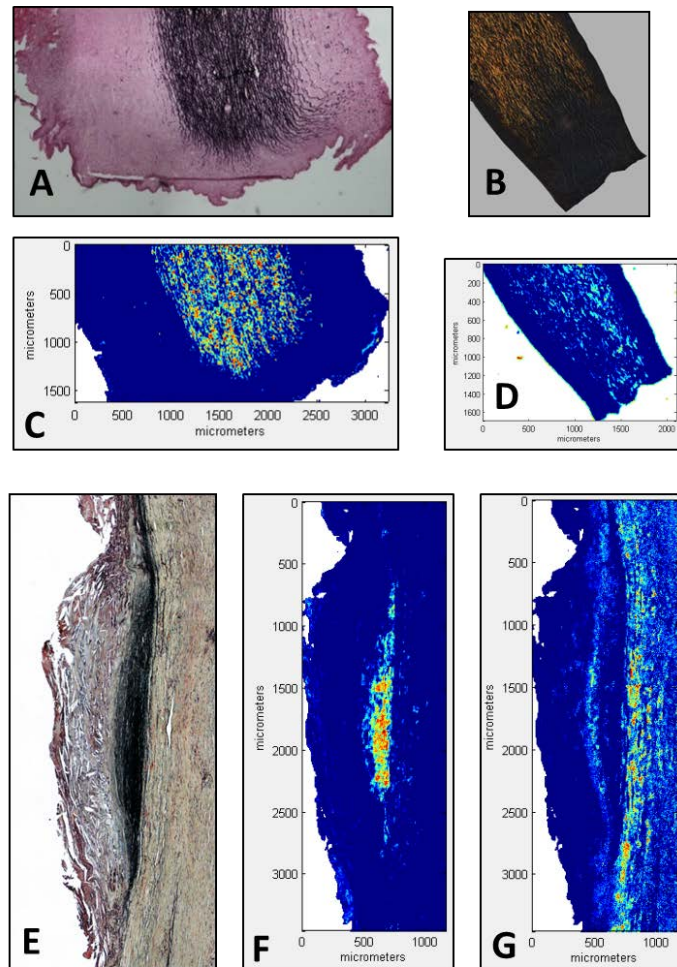


Figure 4.6 Histological and FT-IRIS images of aorta samples. FT-IRIS images are intensity images in pseudo-color increasing in intensity from blue to red. A) Verhoeff-Van Gieson (VVG) staining of a sample treated with elastase for 5 hours with elastin stained black. B) Polarized image of a picosirius red staining in a sample treated with collagenase for 5 hours with collagen fibers visualized as bright yellow-orange. C) FT-IRIS mapping of elastin in a consecutive section from the sample in (A). D) FT-IRIS mapping of collagen in a consecutive section from the sample in (B). E) Movat’s pentachrome staining of a section of a human AAA sample visualizing pathological aggregates of elastin fibers as black, collagen as yellow-brown, proteoglycans in blue and fibrin in red. F) FT-IRIS mapping of elastin in the sample in (E). G) FT-IRIS mapping of collagen in the sample in (E).

CHAPTER 5

CORRELATION OF FOURIER TRANSFORM INFRARED

SPECTROSCOPIC IMAGING-DERIVED PARAMETERS WITH

MECHANICAL PROPERTIES OF ABDOMINAL AORTIC ANEURYSM

5.1 Introduction

In this chapter, the FTIR methodology developed in CHAPTER 3 is applied to sections of abdominal aortic tissue from aneurysm patients. An overview of the disease and the relevant changes of aorta extracellular matrix, the effect of intraluminal thrombus and mechanical properties of aneurysmal aorta, will be discussed.

5.1.1 Abdominal Aortic Aneurysm

Abdominal aortic aneurysm (AAA) is a degenerative disease associated with dilation and weakening of the abdominal aorta [100]. If left untreated, the progressive weakening of the aorta may expand until the stresses acting on the wall exceed the strength of the aortic wall, at which point it will ultimately rupture. The rupture of an AAA results in death in 65% to 85% of the patients [120]. Several repair procedures have been developed to treat AAA's before rupturing; however, a decision to surgically intervene is complicated by the mortality risk, cost and post-procedural complications. Since in many cases the development of AAA and progression of the aortic dilation is accompanied by an increase in the diameter of the aorta, currently the maximum diameter of the aneurysm is used as the screening factor to identify at risk aneurysms, with 5-5.5cm being the limit. Studies however, have questioned the suitability of

maximum diameter criterion with reports of larger than 5 cm aneurysm that are stable, and a considerable percentage of smaller aneurysms rupturing [36].

The natural development of the AAA cannot be prevented by current available therapies, so there is a great need to understand more about the pathological mechanisms behind the disease. Current imaging and microscopy tools such as immunofluorescence microscopy, confocal microscopy, electron microscopy, histology, and immunohistochemistry (IHC) are either qualitative or based on subjective quantitative methods [121]. The aim in this chapter is to review the methodology we have developed for mapping collagen and elastin in AAA tissue sections and how that can apply to studying the health and functionality of the aorta and its mechanical properties.

5.1.2 AAA Extracellular Matrix

Elastic fibers and fibrillar collagen are the main structural proteins of the ECM in the aorta, and are significantly affected by the AAA disease. Since these structural proteins are responsible for the mechanical properties of the aorta, changes in their structure, composition and content is a major determinant of AAA disease progression, severity and rupture risk [17], [120].

AAA is an evolving and heterogeneous condition with several developmental stages that appear at a different pace and severity for each patient [122]. It has been suggested that factors contributing to AAA initiation and progression are distinct and AAA development can be viewed as having different developmental stages as proposed in Figure 5.1 [122].

As depicted in this model, one of the main aspects of AAA is the decrease and fragmentation of the elastic fibers [100], [117], [120], [123], [124]. This wide scale degradation of elastic fibers has been proposed in the literature to be among the earliest features in AAA development

[120], [125]. Loss of elastic fibers increases the dispensability of the aorta [122], [123], [126] which is one of the main factors in speeding the process to ultimate rupture [127].

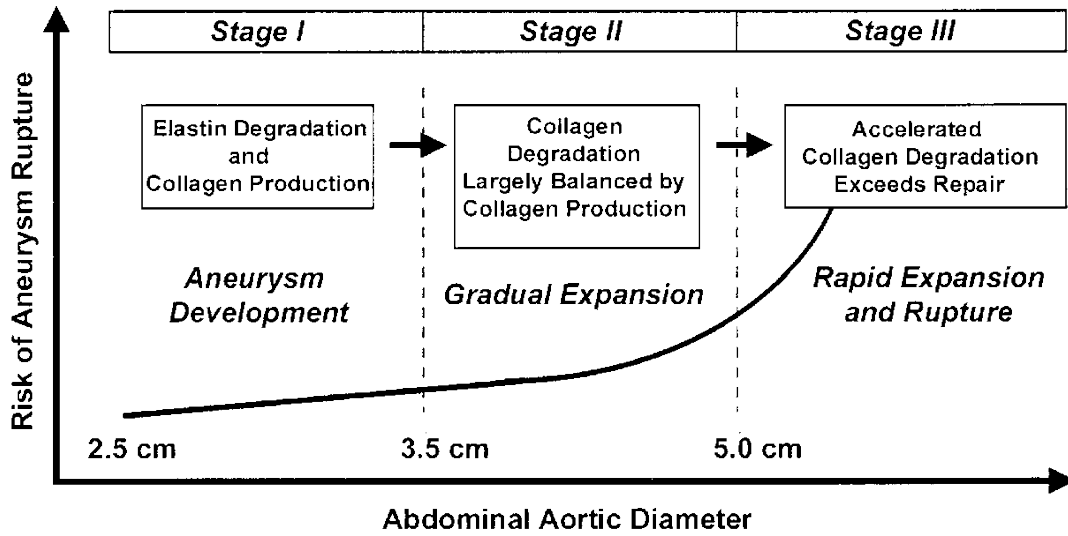


Figure 5.1 Proposed stages of AAA progression [122]

Another aspect of AAA also depicted in the model in Figure 5.1 is a change in collagen deposition and degradation. Collagen turnover has been shown to increase in AAA patients as evidenced by a serum marker of collagen metabolism [128]. Collagen content has been shown to increase in AAA [98], [117], [129], [130]. The increase in the production of collagen has been proposed to be a response to compensate for elastin degradation [131].

There is also a change in collagen organization associated with AAA disease. In a normal aorta collagen organization and structure in medial and adventitial layers are distinct. In the media collagen fibrils are interdispersed perpendicular to elastin lamella to assist in the elastic recoil whereas collagen in the adventitia is structured in ribbon-like bands highly organized to brace the medial and intima layers and provide resilience and prevent overstretching. In AAA vessel wall collagen structure is lost and disorganized, condensed and rigid sheets of collagen is formed

which is consistent with fibrosis, and there is no clear distinction between the medial and adventitial collagen network [98].

With the degradation of elastic fibers, the mechanical stability of the aorta and its ability to withstand stress depends on collagen and the balance between collagen production and degradation. In fact, although elastin degradation is necessary for aortic dilation and AAA development, the ultimate rupture has been proposed to be a function of the collagen degradation [100], [122], [132]. This means when collagen degradation exceeds its production at a rate that the strength of the existing collagen matrix is not sufficient to resist acting forces on the tissue, rupture happens.

5.1.3 Intraluminal Thrombus

Intraluminal thrombus is a common component of AAA that has been proposed to be an active biophysical environment and contributor to AAA condition [133], [134]. Histological examination of Intraluminal thrombus (ILT) showed that there are channels or canaliculi inside the ILT, increasing in area with increasing distance from the luminal surface. These networks create a fluid permeability in ILT that is three orders of magnitude higher than that of porcine aorta and articular cartilage. These canaliculi are suggested to act as a delivery system for macromolecules or cells across the aortic wall. This delivery across the ILT is limited to the first 1 cm of the ILT thickness and the presence of cells inside the thrombus decreases with distance from the lumen [133].

ILT has also been shown to induce hypoxia in the wall [134]. Hypoxia increase the bioreactivity and elastase production in macrophages, and the produced proteolytic enzymes could leech

from ILT and affect the collagen and elastin production of endothelial cells, smooth muscle cells and fibroblasts [134].

In terms of the rupture risk, ILT has a dual role. Rupture happens when strength of the wall is not enough to withhold stress and while ILT acts like a cushion that affects wall stress magnitude and distribution, it also creates weakening in the wall by creating an inflammatory environment rich in proteolytic enzymes that degrade collagen and elastin and thus adversely affects strength of the aorta [135]

5.1.4 Mechanical Properties in AAA

As mentioned in section 5.1.2, changes in the structure and content of structural proteins affects the mechanical properties of the aorta in AAA. With degradation of elastic fibers, collagen fibers become engaged in the load bearing process in lower stresses than they would in a normal aorta [136], causing increased stiffness of AAA tissue compared to normal aortic tissue[137].

Strength of AAA has been measured to be about 50% less than normal aorta [138]. The tensile strength decreases with increasing diameter [35] which is one of the signs of AAA development. Increased collagen turnover has also been found to correlate with reduced distensibility in AAA [126].

In order to predict rupture, studies have used computational methods, such as finite elements analysis, to mechanically model the structure of aorta, its mechanical strength and applied forces [37]. Although a patient-specific geometry of the aorta can be digitally recreated using current imaging techniques and implemented in these models, the technology to assess the molecular composition of the aorta for individual patients is not available and the constitutive

parameters of the aortic wall and other components of the AAA tissue such as ILT is being estimated from average properties from several AAA patients. However, there have been studies on the relationship between level of ECM protein degradation in aortic samples and their mechanical properties [38]. In this chapter, the methodology developed in CHAPTER 4 to quantify ECM structural proteins will be applied to map these components in the sections of AAA tissues and potential relations between components and mechanical properties available for these tissues is studied.

5.2 Material and Methods

5.2.1 AAA Tissue Preparation

Through our collaboration with Dr. David Vorp of the University of Pittsburgh, 26 AAA wall sections were surgically excised as pairs from 13 aneurysm patients during elective surgical repair of their aneurysms. Tissue specimens were paraffin embedded and sectioned on low-e slides and histology slides for FT-IRIS and histological staining respectively. FT-IRIS data collection was performed as detailed below. Histological sections were stained with Movat's pentachrome staining [139].

5.2.2 Mechanical Properties

For each AAA section a mean value for stress, strength, ILT thickness and rupture potential index was reported.

5.2.2.1 Tissue Stress

A complete geometry of AAA samples was modeled by reconstructing the CT-scan of patients taken before the surgery. A finite element model of each AAA was created based on the

geometry of the arterial wall and its thickness as well as the attaching ILT if existing as explained before [140]. The constitutive relation for AAA wall and ILT were based on the average parameters previously calculated for these tissues from several patients and it is the same for all samples. The reported stress for each AAA specimen was the mean stress value from the area the specimen was taken.

5.2.2.2 Tissue Strength

Strength in each specimen was calculated based on the model explained in [105] which takes into account local ILT thickness, local diameter normalized to the diameter of non-aneurysmal aorta estimated from the patient's age and sex, family history of AAA and gender. The reported strength for each specimen is the mean strength value of the specimen.

5.2.2.3 ILT Thickness

ILT thickness was measured from the CT-scans and the reported ILT thickness value reported is the mean value of local ILT thickness in the specimen.

5.2.2.4 Rupture Potential Index

Rupture Potential Index (RPI) was calculated by dividing local stress over local strength in the whole model and the reported RPI is the mean RPI value in the specimen[105].

5.2.3 FT-IRIS Data Collection and Analysis

Tissue sections on low-e slides were deparaffinized and FT-IRIS images were acquired at 25 μm pixel resolution (for whole section images) or 6.25 μm (for partial section images) and 8 cm^{-1} spectral resolution with 2 co-added scans using a Perkin Elmer Spotlight 400 (Shelton, CT). Second derivative of the spectra were calculated with polynomial order of 3 and 9 smoothing

points. Spectra were then exported to MATLAB R2013a (Mathworks, Inc.) for the next step of performing the scalar product of the reference spectral coefficients to the imaging spectra.

Using enzymatically degraded pig aorta samples (see 4.3) a PLS model was created to predict collagen and elastin content in FT-IRIS images. The regression coefficient from PLS models for collagen and elastin were imported in MATLAB and the scalar product of the regression coefficient and the second derivative spectra of each pixel was calculated. The resulting scalar values for each pixel were imported back into ISys software to create a map of collagen and elastin content.

Collagen maturity was calculated as the ratio of the peaks at 1660 cm^{-1} and 1690 cm^{-1} [67]. The ratio of these peaks has been shown to be an indication of collagen maturity [141]. The value for this parameter was averaged over areas of the samples with collagen values higher than zero.

5.3 Results

5.3.1 Elastin Distribution

In almost all AAA sections elastin was completely depleted in the media and normal elastic lamella were missing. Isolated or aggregated elastin fragments were visible for some samples by histology, but for the whole sections imaged at $25\text{ }\mu\text{m}$ pixel resolution, this spatial resolution was not high enough to detect the sparse elastin fragments. Only for a few exceptional regions were thick elastin fibers or aggregates visible, and when these regions were imaged at $6.25\text{ }\mu\text{m}$ pixel resolution, elastin could be mapped. An example of such an image is shown in Figure 5.2. This figure shows a neovessel formed in the adventitia of one of the samples, with thick elastic fibers formed around the vessel. Using the methodology described in Section 5.2.3, the elastin

distribution is mapped across the section (Fig 4-A) creating an image similar to the Movat's staining image (Fig 4-B).

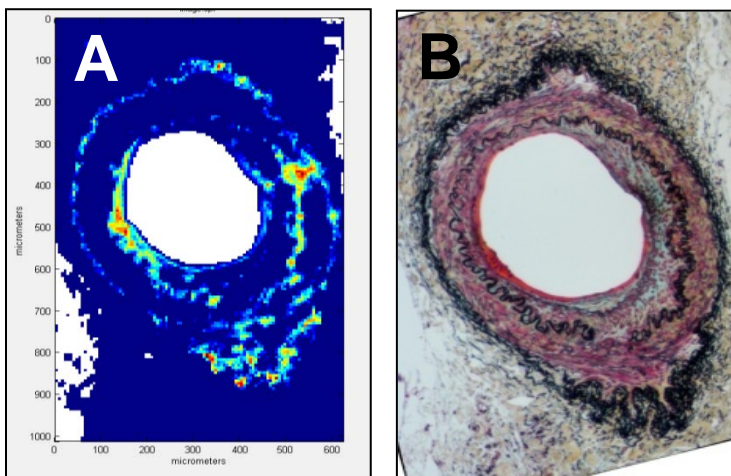


Figure 5.2 A neovessel formed in a human AAA wall sample. A) FT-IRIS mapping of elastin using the results of the PLS model explained in CHAPTER 4. B) Movat's staining of the region with elastin in black.

5.3.2 Collagen Distribution

Collagen distribution was mapped on whole tissue samples using the methodology described in Section 5.2.3. As shown in Figure 5.3, the distribution of collagen deposition using this FT-IRIS methodology correlates well with histological staining image (B).

Collagen deposition in all AAA samples was mapped using this method. Collagen in each image was normalized to total protein by dividing the value of collagen deposition in each pixel to the value of total protein from peak integration mapping of the amide I band. The mean value of the collagen deposition for each sample was calculated and compared to mechanical properties.

As mentioned in section 5.3.1, elastin was almost completely degraded in AAA samples. When the peak integration of the band centered at 1338 cm^{-1} was mapped across these sections as described in section 2.3.5, the mean value of this parameter for 26 samples was correlated

significantly with the mean value of collagen using the correlation coefficient from of PLS model as described above ($R=0.93$, $P<0.01$).

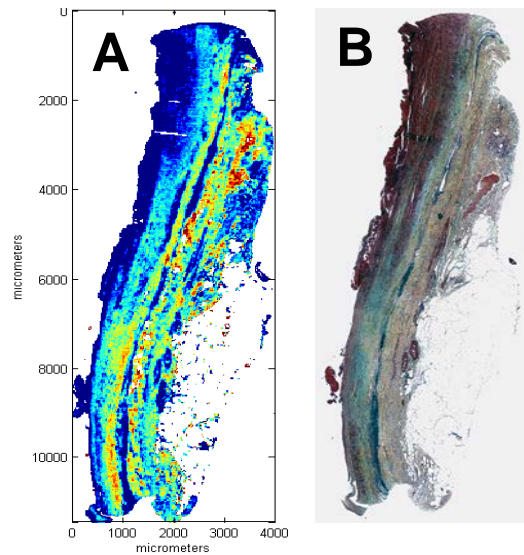


Figure 5.3 An example AAA sample. A) FT-IRIS mapping of collagen using the results of the PLS model explained in CHAPTER 4 . FT-IRIS images are intensity images in pseudo-color increasing in intensity from blue to red.. B) Movat's staining of the sample with collagen in yellow-brown staining.

5.3.3 Relationship between Collagen and Stress

Calculated value for collagen for each sample was correlated to the value of stress for each sample as shown in Figure 5.4. Images were also masked to separate media in the samples and the mean value of collagen in the media was calculated and correlated with stress values for each sample (Figure 5.5). From these figures the following trends are seen that when stress values for both samples in a pair are small (stress value lower than 5 N/m^2) the stress value and collagen do not appear to have a correlation. This could be because the two stress values for the pair of AAA samples from one patient are too close (the difference in stress values equal to or smaller than 4.1 N/m^2) to get a conclusive result. For samples with higher stress values, most of the pairs (7 pairs) show an increased stress with decreased collagen. Two pairs show a decrease

in stress with decreasing collagen. Relationship between collagen content and RPI followed the same trend as the relationship between collagen content and stress.

5.3.4 Relationship between Collagen and ILT Thickness

Calculated collagen content in the media was correlated to ILT thickness for each sample as shown in Figure 5.6. In three patients the difference in ILT thickness in the pair of samples is smaller than 0.004 cm so no conclusive correlation could be found. In the remaining pair of samples, collagen quantity increases with increasing ILT thickness in 8 patients and decreases with the ILT thickness in 2 patients.

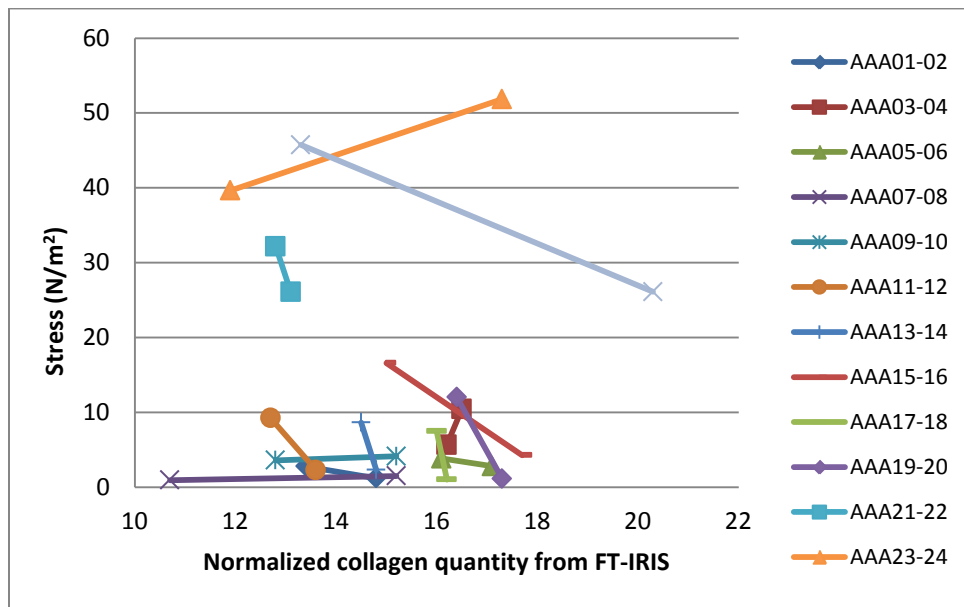


Figure 5.4 Collagen quantity vs. Stress in AAA samples. Each line represents the values for the pair of AAA samples from one patient.

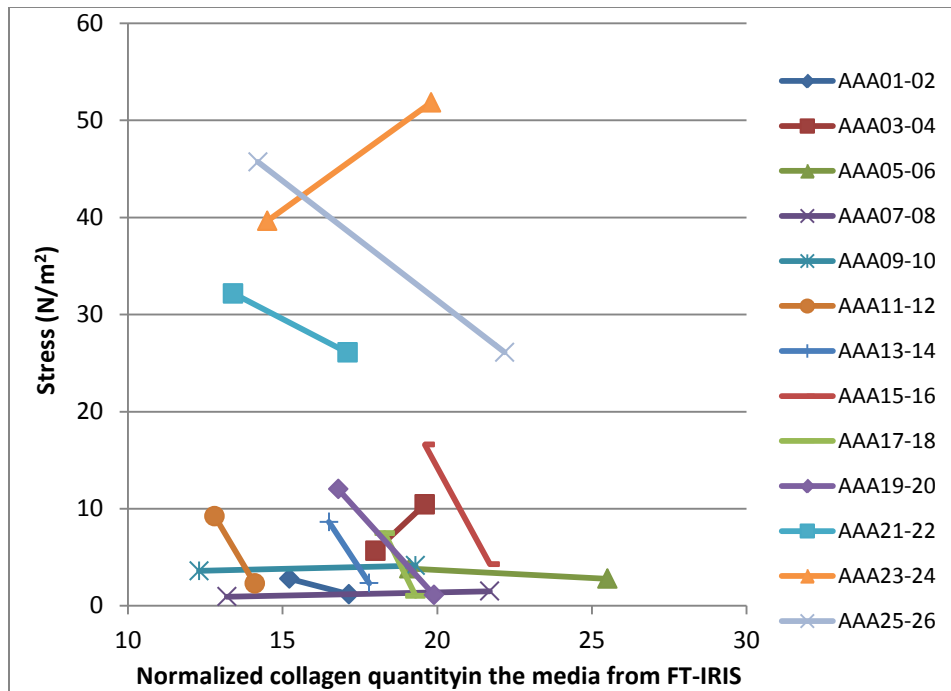


Figure 5.5 Collagen quantity vs. Stress in the media of AAA samples. Each line represents the values for the pair of AAA samples from one patient.

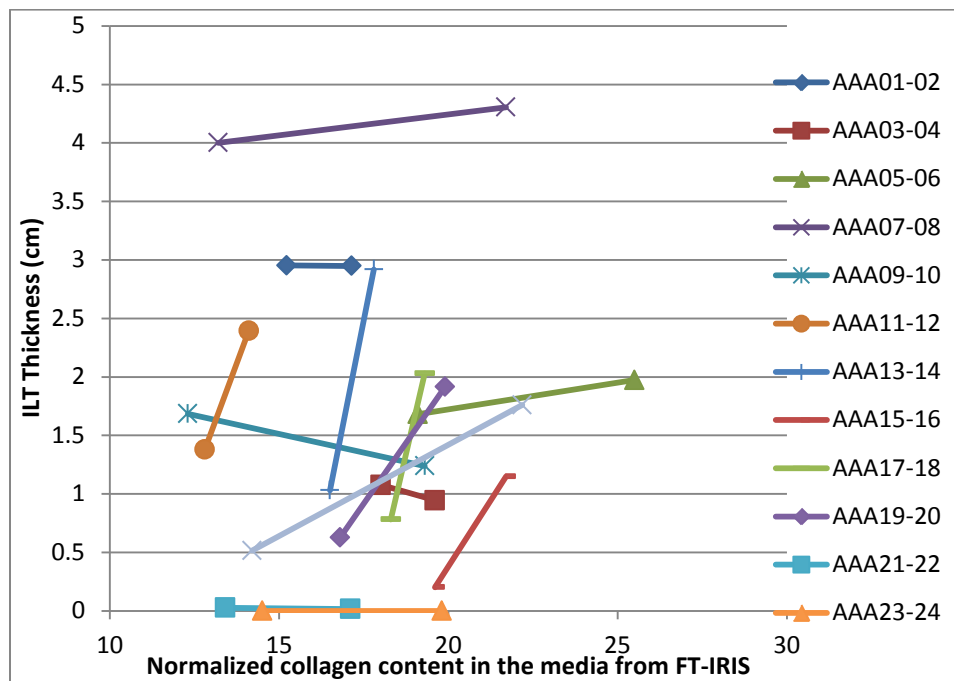


Figure 5.6 Collagen quantity in the media vs. ILT Thickness of AAA samples. Each line represents the values for the pair of AAA samples from one patient.

5.3.5 Relationship between Collagen Maturity and Content

Figure 5.7 shows the relationship between the mean value of collagen content and collagen maturity in AAA samples. There is a weak negative correlation ($R=-0.35$) seen between increasing collagen content and decreasing collagen maturity which tends towards significance ($P=0.08$). The statistical power for the correlation test was 0.41 which could mean a higher significance level could be achieved with higher number of samples.

The average collagen maturity index for all 26 AAA samples was 3.6. This parameter was 3.2 in normal human aortic tissues ($n=2$) taken from cadavers. This higher maturity index may be an indication pathologic turnover of collagen. The average collagen maturity index was also higher in comparison to collagen maturity index in infarcted rat heart tissues studied under CHAPTER 2 which was 3.2 ($n=12$).

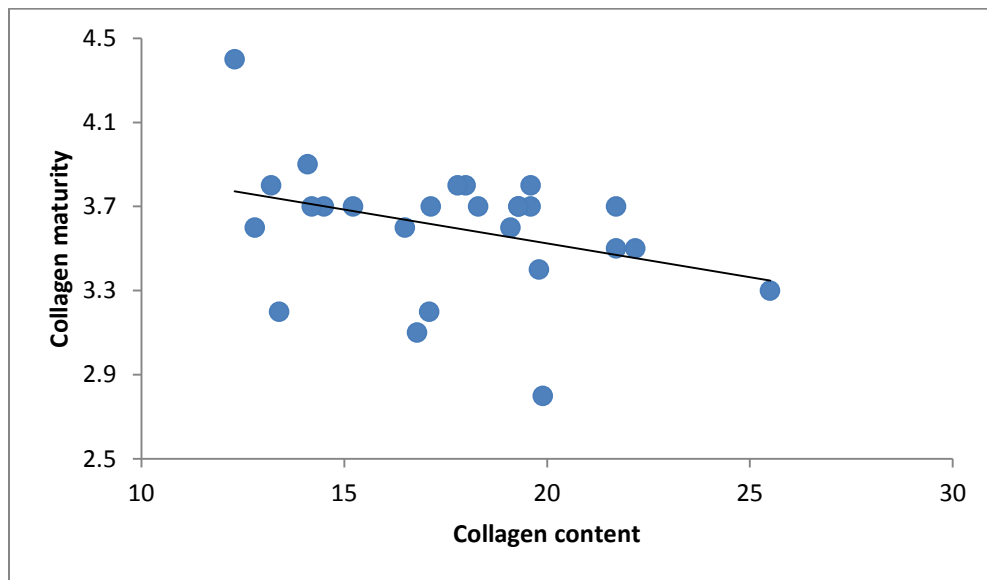


Figure 5.7 Relationship between collagen content and maturity

5.4 Discussion

AAA tissue environment is a complex pathological system. AAA samples used in this study were collected during the surgery of patients who were undergoing the elective repair of their aneurysms. The fact that these AAA patients were electing to have a surgical repair of their aneurysms suggests that these AAA samples were in the later stages of their aneurysm and they were not deemed stable aneurysms. This has multiple implications when the results of the current study are being discussed.

The histological features of these AAA samples was consistent with the known feature of the AAA tissue [100]. There was a complete disruption of the elastic lamella, with no evidence of order in their structure as in normal tissue. Most of the samples either completely lacked elastic fibers that would be visible from the staining under the microscope or they had fragmentation or aggregation of elastin in small patches. We have shown that although fragmented elastin could not be resolved with the available resolution of the FT-IRIS system, elastin in areas with patches of thick elastic fiber deposition could be mapped and we have created an image of the elastin content in the sample that was compatible with the histological image.

As expected, elastin was highly replaced by collagen in the media. We created images of collagen deposition and content in these AAA samples, again compatible with histological images. These findings demonstrate the capability of FT-IRIS in creating maps of components in the samples that could be more easily and reliably quantified compared to histology.

When collagen content was compared to stress value for the pair of samples from each patient, for most samples collagen was negatively correlated to stress. This observation is consistent with the growing aneurysms not being able to produce collagen effectively and sufficiently to

compensate for the forces acting on the aortic tissue, making the tissue weaker and more susceptible to further growth of the aneurysm and its ultimate rupture. A similar relationship between collagen deposition and forces acting on the tissue exists in cardiac remodeling after myocardial infarction. In cardiac remodeling, as a response to loss of muscle tissue due to infarction, a collagen scar is deposited in cardiac tissue to maintain structural integrity, but this increase in collagen and the resulting increase in stiffness cannot sufficiently compensate for the flexibility needed for cardiac function, and in time this could ultimately lead to cardiac failure [21], [24], [25].

The fact that collagen content was positively correlated with ILT thickness in most samples could be another indication of the fact that increased collagen deposition in AAA is not an effective process. ILT is a cause of hypoxia in the aortic wall which could affect the healthy production of collagen[134].

Another observation in these samples was the weak correlation between collagen deposition and maturity. This observation could be consistent with collagen turnover being higher in the AAA environment than in normal tissue; new (less mature) collagen is deposited in the aorta but since the environment of AAA is a degrading environment with abundance of proteolytic enzymes, deposited collagen is degraded and replaced by new collagen in an increasing rate. The observation that collagen in the media and collagen in the whole tissue section show the same relationship to stress, implies that the collagen deposition in these layers is probably of the same rate.

In this chapter we have provided an example of applying FTIR methodology we developed based on an in vitro model of AAA (CHAPTER 4) to characterize tissue components and examine possible relationships between the components and mechanical properties of the AAA tissue.

CHAPTER 6

SUMMARY AND CONCLUSION

Motivated by limitations in the current methods for characterization of extracellular matrix components in cardiovascular diseases, in this dissertation we developed FTIR methodologies to complement the current available techniques in cardiovascular research, specifically in quantifying major ECM components.

In cardiac tissue after myocardial infarction, dead muscle tissue is replaced by a collagen scar in the process of cardiac remodeling. The extent of the collagen deposition is a determinant of the severity of the remodeling. For this reason, one of the major steps in research efforts targeted at alleviating the severity of this condition for patients surviving myocardial infarction is to demonstrate the efficacy of the proposed treatment in addressing the level of cardiac remodeling. For this, researches usually rely on staining methods to visualize collagen deposition in cardiac sections. We have developed an FT-IRIS methodology based on univariate quantification of the peak centered at 1338 cm^{-1} , arising from amino acid side chain vibrations in collagen, to visualize and quantify collagen deposition in infarcted cardiac tissues. We confirmed the validity of our methodology with conventional histology and immunohistochemical staining. Use of FTIR based methodologies has several advantages. It needs minimal sample preparation, does not use hazardous chemicals needed for many histological staining protocols and does not rely on expensive reagents and time-consuming procedures as those associated with immunohistochemical staining methods.

In the second arm of the dissertation, we focused on alteration of collagen and elastin in the aorta in the context of abdominal aortic aneurysm disease. We used an *in vitro* model of enzymatic degradation of these components in pig aorta and developed a multivariate analysis method using partial least squares (PLS) regression which was calibrated by measurements from biochemical assays. We applied two different FTIR modalities of FT-IRIS and IFOP. In the PLS models based on FT-IRIS spectra, the predicted values of collagen and elastin strongly correlated with the reference values of these components. We also applied the regression coefficients to map these components in degraded pig aorta samples as well as actual human AAA tissue sections. Images created using this methodology were consistent with histology images. The PLS regression model for elastin based on IFOP spectra was also successful in predicting elastin content of the degraded pig aorta. Our model confirms that elastin degradation in bulk tissue can be predicted using IFOP technology. This is mainly important because IFOP has a potential to be used for the diagnosis of different pathologies *in vivo* upon further development of the technology.

In the final chapter of this dissertation we presented an example of the application of our developed methodology in AAA research. We mapped collagen in human AAA samples and demonstrated how it can be useful in better understanding of this disease.

The methodologies we have developed in this dissertation advance the field of biomedical engineering in two major approaches:

1. FT-IRIS methods can be applied as useful tools to replace or complement conventional staining methods in studying ECM components in cardiovascular research.

2. IFOP methods demonstrate the feasibility of this technology for the assessment of ECM components in cardiovascular tissue and set ground work for its further advancement until its applicability for *in vivo* diagnosis.

There are some limitations associated with this dissertation project. In degrading the aortic ECM components we only focused on structural proteins, collagen and elastin. Aortic media includes several other components such as proteoglycans or other minor proteins of the cardiovascular ECM, and smooth muscle cells, inclusion of which could improve the precision and applicability of the FTIR models. A limitation of correlating mechanical properties with collagen content in AAA samples is that it does not provide any information about the quality of the deposited collagen. Inclusion of other structural properties such as crosslinking and fiber orientation will provide a more realistic picture of the pathological condition of structural proteins in AAA and their relation with mechanical stability and strength. Another limitation in our degradation models and quantifying structural proteins was a lack of differentiation between collagen types. Collagen is formed in different collagen types with distinct structures, functions and properties, which we did not address in our study.

Future research in this area could include other components of disease process including the proteolytic enzymes such as elastase and MMP's to create a better understanding of the disease progression. Another expansion of this research could be the application of fiber optic based FTIR data collection and analysis in an animal model of AAA. Application of the methodology in AAA samples as presented in this dissertation is at its very initial stages and will be further developed to produce more decisive conclusions with regards to the relationship between ECM components and mechanical properties.

REFERENCES

- [1] W. M. Becker, L. J. Kleinsmith, J. Hardin, and G. P. Bertoni, *The World of The Cell*. San Francisco, CA: Pearson Education Inc, 2009.
- [2] M. Chiquet and J. Engel, "An Overview of Extracellular Matrix Structure and Function," in *The Extracellular Matrix: an Overview*, R. P. Mecham, Ed. Berlin, Heidelberg: Springer Berlin Heidelberg, 2011, pp. 1–39.
- [3] D. E. Birk and P. Bruckner, "Collagens, Suprastructures, and Collagen Fibril Assembly," in *The Extracellular Matrix: an Overview*, R. P. Mecham, Ed. Berlin, Heidelberg: Springer Berlin Heidelberg, 2011, pp. 77–115.
- [4] R. O. Hynes, "The extracellular matrix: not just pretty fibrils.," *Science*, vol. 326, no. 5957, pp. 1216–9, Nov. 2009.
- [5] P. Fratzl, "Collagen: Structure and Mechanics, an Introduction," in *Collagen Structure and Mechanics*, P. Fratzl, Ed. New York: Springer, 2008, pp. 1–13.
- [6] D. J. . Hulmes, "Collagen Diversity, Synthesis and Assembly," in *Collagen Structure and Mechanics*, P. Fratzl, Ed. New York: Springer, 2008, pp. 15–47.
- [7] D. E. Birk and F. H. Silver, "Collagen fibrillogenesis in vitro: comparison of types I, II, and III.," *Arch. Biochem. Biophys.*, vol. 235, no. 1, pp. 178–85, Nov. 1984.
- [8] D. J. S. Hulmes, "Building collagen molecules, fibrils, and suprafibrillar structures.," *J. Struct. Biol.*, vol. 137, no. 1–2, pp. 2–10, 2002.
- [9] K. Beck and B. Brodsky, "Supercoiled protein motifs: the collagen triple-helix and the alpha-helical coiled coil.," *J. Struct. Biol.*, vol. 122, no. 1–2, pp. 17–29, Jan. 1998.
- [10] P. Szpak, "Fish bone chemistry and ultrastructure: implications for taphonomy and stable isotope analysis," *J. Archaeol. Sci.*, vol. 38, no. 12, pp. 3358–3372, Dec. 2011.
- [11] N. C. Avery and A. J. Bailey, "Mechanical Properties of Collagen Fibers," in *Collagen Structure and Mechanics*, P. Fratzl, Ed. New York: Springer, 2008, pp. 81–110.
- [12] B. A. Kozel, R. P. Mecham, and J. Rosenbloom, "Elastin," in *The Extracellular Matrix: an Overview*, R. P. Mecham, Ed. Berlin, Heidelberg: Springer Berlin Heidelberg, 2011.
- [13] R. P. Mecham, "Methods in elastic tissue biology: elastin isolation and purification.," *Methods*, vol. 45, no. 1, pp. 32–41, May 2008.
- [14] W. H. Ladislas Robert, *Elastin and Elastases*, 1st ed. CRC Press, 1989.

- [15] J. E. Wagenseil and R. P. Mecham, "Elastin in Large Artery Stiffness and Hypertension.," *J. Cardiovasc. Transl. Res.*, no. January, Jan. 2012.
- [16] L. Debelle and a M. Tamburro, "Elastin: molecular description and function.," *Int. J. Biochem. Cell Biol.*, vol. 31, no. 2, pp. 261–72, Feb. 1999.
- [17] A. Tsamis, J. T. Krawiec, and D. A. Vorp, "Elastin and collagen fibre microstructure of the human aorta in ageing and disease: a review.," *J. R. Soc. Interface*, vol. 10, no. 83, p. 20121004, Jun. 2013.
- [18] A. Y. Lee, B. Han, S. D. Lamm, C. a Fierro, and H.-C. Han, "Effects of elastin degradation and surrounding matrix support on artery stability.," *Am. J. Physiol. Heart Circ. Physiol.*, vol. 302, no. 4, pp. H873–84, Feb. 2012.
- [19] M. Gacko, "Elastin: Structure, properties and metabolism," *Cell. Mol. Biol. Lett.*, vol. 5, no. 3, pp. 327–348, 2000.
- [20] C. M. Kielty, M. J. Sherratt, and C. A. Shuttleworth, "Elastic fibres.," *J. Cell Sci.*, vol. 115, no. Pt 14, pp. 2817–28, Jul. 2002.
- [21] K. T. Weber, "Cardiac interstitium in health and disease: the fibrillar collagen network.," *J. Am. Coll. Cardiol.*, vol. 13, no. 7, pp. 1637–52, Jun. 1989.
- [22] M. Eghbali and K. T. Weber, "Collagen and the myocardium: fibrillar structure, biosynthesis and degradation in relation to hypertrophy and its regression.," *Mol. Cell. Biochem.*, vol. 96, no. 1, pp. 1–14, Jul. 1990.
- [23] C. Delcayre and B. Swynghedauw, "Molecular mechanisms of myocardial remodeling. The role of aldosterone.," *J. Mol. Cell. Cardiol.*, vol. 34, no. 12, pp. 1577–84, Dec. 2002.
- [24] Y. Sun and K. T. Weber, "Animal models of cardiac fibrosis.," *Methods Mol. Med.*, vol. 117, no. III, pp. 273–90, Jan. 2005.
- [25] Y. Sun, M. F. Kiani, A. E. Postlethwaite, and K. T. Weber, "Infarct scar as living tissue.," *Basic Res. Cardiol.*, vol. 97, no. 5, pp. 343–7, Sep. 2002.
- [26] V. L. Roger, A. S. Go, D. M. Lloyd-Jones, E. J. Benjamin, J. D. Berry, W. B. Borden, D. M. Bravata, S. Dai, E. S. Ford, C. S. Fox, H. J. Fullerton, C. Gillespie, S. M. Hailpern, J. a Heit, V. J. Howard, B. M. Kissela, S. J. Kittner, D. T. Lackland, J. H. Lichtman, L. D. Lisabeth, D. M. Makuc, G. M. Marcus, A. Marelli, D. B. Matchar, C. S. Moy, D. Mozaffarian, M. E. Mussolino, G. Nichol, N. P. Paynter, E. Z. Soliman, P. D. Sorlie, N. Sotoodehnia, T. N. Turan, S. S. Virani, N. D. Wong, D. Woo, and M. B. Turner, "Executive summary: heart disease and stroke statistics--2012 update: a report from the American Heart Association.," *Circulation*, vol. 125, no. 1, pp. 188–97, Jan. 2012.

- [27] P. Whittaker, R. a Kloner, D. R. Boughner, and J. G. Pickering, "Quantitative assessment of myocardial collagen with picosirius red staining and circularly polarized light.," *Basic Res. Cardiol.*, vol. 89, no. 5, pp. 397–410, 1994.
- [28] R. T. Miller, "Technical Immunohistochemistry: Achieving Reliability and Reproducibility of Immunostains," in *Society for Applied Immunohistochemistry*, 2001, pp. 0–56.
- [29] J.-M. Fritschy, "Is my antibody-staining specific? How to deal with pitfalls of immunohistochemistry.," *Eur. J. Neurosci.*, vol. 28, no. 12, pp. 2365–70, Dec. 2008.
- [30] T. C. Gasser, R. W. Ogden, and G. a Holzapfel, "Hyperelastic modelling of arterial layers with distributed collagen fibre orientations.," *J. R. Soc. Interface*, vol. 3, no. 6, pp. 15–35, Feb. 2006.
- [31] G. a Antoniou, G. S. Georgiadis, S. a Antoniou, F. a Granderath, A. D. Giannoukas, and M. K. Lazarides, "Abdominal aortic aneurysm and abdominal wall hernia as manifestations of a connective tissue disorder.," *J. Vasc. Surg. Off. Publ. Soc. Vasc. Surg. [and] Int. Soc. Cardiovasc. Surgery, North Am. Chapter*, vol. 54, no. 4, pp. 1175–81, Oct. 2011.
- [32] J. E. Wagenseil and R. P. Mecham, "Vascular Extracellular Matrix and Arterial Mechanics," *Physiol. Rev.*, vol. 89, no. 3, pp. 957–989, 2009.
- [33] G. Vieira-Damiani, D. P. Ferro, R. L. Adam, A. A. de Thomaz, V. Pelegati, C. L. Cesar, and K. Metze, "Elastic fibers and collagen distribution in human aorta," 2011, p. 79030B–79030B–8.
- [34] T. Toda, N. Tsuda, I. Nishimori, D. E. Leszczynski, and F. A. Rummerow, "Morphometrical analysis of the aging process in human arteries and aorta," *Cells Tissues Organs*, vol. 106, no. 1, pp. 35–44, 1980.
- [35] D. A. Vorp and J. P. Vande Geest, "Biomechanical determinants of abdominal aortic aneurysm rupture.," *Arterioscler. Thromb. Vasc. Biol.*, vol. 25, no. 8, pp. 1558–66, Aug. 2005.
- [36] J. P. Vande Geest, E. S. Di Martino, A. Bohra, M. S. Makaroun, and D. a Vorp, "A biomechanics-based rupture potential index for abdominal aortic aneurysm risk assessment: demonstrative application.," *Ann. N. Y. Acad. Sci.*, vol. 1085, pp. 11–21, Nov. 2006.
- [37] B. J. Doyle, A. J. Cloonan, M. T. Walsh, D. A. Vorp, and T. M. McGloughlin, "Identification of rupture locations in patient-specific abdominal aortic aneurysms using experimental and computational techniques.," *J. Biomech.*, vol. 43, no. 7, pp. 1408–16, May 2010.

- [38] J. a Kratzberg, P. J. Walker, E. Rikkers, and M. L. Raghavan, "The effect of proteolytic treatment on plastic deformation of porcine aortic tissue.," *J. Mech. Behav. Biomed. Mater.*, vol. 2, no. 1, pp. 65–72, Jan. 2009.
- [39] B. C. Smith, *Fundamentals of Fourier transform infrared spectroscopy*, 2nd ed. Boca Raton, FL: CRC Press, 2011.
- [40] N. P. Camacho, P. West, P. a Torzilli, and R. Mendelsohn, "FTIR microscopic imaging of collagen and proteoglycan in bovine cartilage.," *Biopolymers*, vol. 62, no. 1, pp. 1–8, Jan. 2001.
- [41] S. G. Kazarian and K. L. a Chan, "Applications of ATR-FTIR spectroscopic imaging to biomedical samples.," *Biochim. Biophys. Acta*, vol. 1758, no. 7, pp. 858–67, Jul. 2006.
- [42] P. a West, M. P. G. Bostrom, P. a Torzilli, and N. P. Camacho, "Fourier transform infrared spectral analysis of degenerative cartilage: an infrared fiber optic probe and imaging study.," *Appl. Spectrosc.*, vol. 58, no. 4, pp. 376–81, Apr. 2004.
- [43] B. Mizaikoff, "Peer Reviewed: Mid-IR Fiber-Optic Sensors," *Anal. Chem.*, vol. 75, no. 11, p. 258 A–267 A, Jun. 2003.
- [44] Å. Rinnan, F. Van Den Berg, and S. B. Engelsen, "Review of the most common pre-processing techniques for near-infrared spectra," *TrAC Trends Anal. Chem.*, vol. 28, no. 10, pp. 1201–1222, Nov. 2009.
- [45] kim H. Esbensen, D. Guyot, W. Frank, and L. P. Houmoller, *Multivariate data analysis : in practice : an introduction to multivariate data analysis and experimental design*, 5th ed. Oslo, Norway: CAMO, 2002.
- [46] B. C. Smith, *Quantitative Spectroscopy: Theory and Practice*. Academic Press, 2003, p. 212.
- [47] "The Unscrambler X." CAMO Software, Oslo, Norway, 2011.
- [48] K. Lui, M. Jackson, M. G. Sowa, H. Ju, I. M. Dixon, and H. H. Mantsch, "Modification of the extracellular matrix following myocardial infarction monitored by FTIR spectroscopy.," *Biochim. Biophys. Acta*, vol. 1315, no. 2, pp. 73–7, Mar. 1996.
- [49] K. Z. Liu, I. M. Dixon, and H. H. Mantsch, "Distribution of collagen deposition in cardiomyopathic hamster hearts determined by infrared microscopy.," *Cardiovasc. Pathol.*, vol. 8, no. 1, pp. 41–7, 1999.
- [50] P. S. Bromberg, K. M. Gough, and I. M. C. Dixon, "Collagen remodeling in the extracellular matrix of the cardiomyopathic Syrian hamster heart as assessed by FTIR attenuated total reflectance spectroscopy," *Can. J. Chem.*, vol. 77, no. 11, pp. 1843–1855, 1999.

- [51] K. M. Gough, D. Zelinski, R. Wiens, M. Rak, and I. M. C. Dixon, "Fourier transform infrared evaluation of microscopic scarring in the cardiomyopathic heart: effect of chronic AT1 suppression.," *Anal. Biochem.*, vol. 316, no. 2, pp. 232–42, May 2003.
- [52] T. T. Yang, S. F. Weng, N. Zheng, Q. H. Pan, H. L. Cao, L. Liu, H. D. Zhang, and D. W. Mu, "Histopathology mapping of biochemical changes in myocardial infarction by Fourier transform infrared spectral imaging.," *Forensic Sci. Int.*, vol. 207, no. 1–3, pp. e34–9, Apr. 2011.
- [53] C. S. Colley, S. G. Kazarian, P. D. Weinberg, and M. J. Lever, "Spectroscopic imaging of arteries and atherosclerotic plaques.," *Biopolymers*, vol. 74, no. 4, pp. 328–35, Jul. 2004.
- [54] F. Palombo, S. G. Cremers, P. D. Weinberg, and S. G. Kazarian, "Application of Fourier transform infrared spectroscopic imaging to the study of effects of age and dietary L-arginine on aortic lesion composition in cholesterol-fed rabbits.," *J. R. Soc. Interface*, vol. 6, no. 37, pp. 669–80, Aug. 2009.
- [55] I. Mamarelis, K. Pissaridi, V. Dritsa, P. Kotileas, V. Tsiligiris, V. Tzilalis, and J. Anastassopoulou, "Oxidative stress and atherogenesis. An FT-IR spectroscopic study.," *In Vivo*, vol. 24, no. 6, pp. 883–8, 2010.
- [56] A. Urbas, M. W. Manning, A. Daugherty, L. a Cassis, and R. a Lodder, "Near-infrared spectrometry of abdominal aortic aneurysm in the ApoE^{-/-} mouse.," *Anal. Chem.*, vol. 75, no. 14, pp. 3650–5, Jul. 2003.
- [57] F. Bonnier, S. Rubin, L. Ventéo, C. M. Krishna, M. Pluot, B. Baehrel, M. Manfait, and G. D. Sockalingum, "In-vitro analysis of normal and aneurismal human ascending aortic tissues using FT-IR microspectroscopy.," *Biochim. Biophys. Acta*, vol. 1758, no. 7, pp. 968–73, Jul. 2006.
- [58] S. Rubin, F. Bonnier, C. Sandt, L. Venteo, M. Pluot, B. Baehrel, M. Manfait, and G. D. Sockalingum, "Analysis of structural changes in normal and aneurismal human aortic tissues using FTIR microscopy," *Biopolymers*, vol. 89, no. 2, pp. 160–169, 2007.
- [59] F. Bonnier, S. Rubin, L. Debelle, L. Ventéo, M. Pluot, B. Baehrel, M. Manfait, and G. D. Sockalingum, "FTIR protein secondary structure analysis of human ascending aortic tissues.," *J. Biophotonics*, vol. 1, no. 3, pp. 204–14, Aug. 2008.
- [60] W. Y. Sun, J. L. Fang, M. Cheng, P. Y. Xia, and W. X. Tang, "Secondary structure dependent on metal ions of copper,zinc superoxide dismutase investigated by Fourier transform IR spectroscopy.," *Biopolymers*, vol. 42, no. 3, pp. 297–303, Sep. 1997.
- [61] L. Debelle, a J. Alix, S. M. Wei, M. P. Jacob, J. P. Huvenne, M. Berjot, and P. Legrand, "The secondary structure and architecture of human elastin.," *Eur. J. Biochem.*, vol. 258, no. 2, pp. 533–9, Dec. 1998.

- [62] L. Debelle, a J. Alix, M. P. Jacob, J. P. Huvenne, M. Berjot, B. Sombret, and P. Legrand, "Bovine elastin and kappa-elastin secondary structure determination by optical spectroscopies," *J. Biol. Chem.*, vol. 270, no. 44, pp. 26099–103, Nov. 1995.
- [63] F. Bonnier, D. Bertrand, S. Rubin, L. Ventéo, M. Pluot, B. Baehrel, M. Manfait, and G. D. Sockalingum, "Detection of pathological aortic tissues by infrared multispectral imaging and chemometrics.," *Analyst*, vol. 133, no. 6, pp. 784–90, Jun. 2008.
- [64] B. C. Herman, R. Kundi, D. Yamanouchi, K. C. Kent, B. Liu, and N. Pleshko, "Molecular analysis of arterial remodeling: a novel application of infrared imaging," *Proc. SPIE*, vol. 7182, pp. 7182H1–7182H–12, 2009.
- [65] R. Cheheltani, J. M. Rosano, B. Wang, A. K. Sabri, N. Pleshko, and M. F. Kiani, "Fourier transform infrared spectroscopic imaging of cardiac tissue to detect collagen deposition after myocardial infarction.," *J. Biomed. Opt.*, vol. 17, no. 5, p. 056014, May 2012.
- [66] S. de Jong, T. a B. van Veen, J. M. T. de Bakker, M. a Vos, and H. V. M. van Rijen, "Biomarkers of myocardial fibrosis.," *J. Cardiovasc. Pharmacol.*, vol. 57, no. 5, pp. 522–35, May 2011.
- [67] A. Boskey and N. Pleshko Camacho, "FT-IR imaging of native and tissue-engineered bone and cartilage.," *Biomaterials*, vol. 28, no. 15, pp. 2465–78, May 2007.
- [68] D. L. Wetzel, L. H. Wetzel, M. D. Wetzel, and R. A. Lodder, "Imminent cardiac risk assessment via optical intravascular biochemical analysis," *Analyst*, vol. 134, no. 6, pp. 1099–1106, 2009.
- [69] C. Krafft, "Vibrational Spectroscopic Imaging of Soft Tissue," in in *Infrared and Raman Spectroscopic Imaging*, H. W. S. Reiner Salzer, Ed. Weinheim, Germany: Wiley-VCH Verlag GmbH & Co. KGaA, 2009, pp. 113–147.
- [70] K. A. Morris, Michael D.; Schulmerich, Matthew V.; Dooley, Kathryn A.; Esmonde-White, "Vibrational Spectroscopic Imaging of Hard Tissues," in in *Infrared and Raman Spectroscopic Imaging*, H. W. S. Reiner Salzer, Ed. Weinheim, Germany: Wiley-VCH Verlag GmbH & Co. KGaA, 2009, pp. 149–171.
- [71] H. C. Canuto, K. W. Fishbein, A. Huang, S. B. Doty, R. a Herbert, J. Peckham, N. Pleshko, and R. G. Spencer, "Characterization of skin abnormalities in a mouse model of osteogenesis imperfecta using high resolution magnetic resonance imaging and Fourier transform infrared imaging spectroscopy.," *NMR Biomed.*, vol. 25, no. 1, pp. 169–176, Aug. 2011.
- [72] R. C. Scott, J. M. Rosano, Z. Ivanov, B. Wang, P. L.-G. Chong, A. C. Issekutz, D. L. Crabbe, and M. F. Kiani, "Targeting VEGF-encapsulated immunoliposomes to MI heart improves vascularity and cardiac function.," *FASEB J.*, vol. 23, no. 10, pp. 3361–7, Oct. 2009.

- [73] R. C. Scott, B. Wang, R. Nallamothu, C. B. Pattillo, G. Perez-liz, A. Issekutz, L. Del Valle, G. C. Wood, and M. F. Kiani, "Targeted Delivery of Antibody Conjugated Liposomal Drug Carriers to Rat Myocardial Infarction," *Biotechnology*, vol. 96, no. 4, pp. 795–802, 2007.
- [74] B. Wang, R. Ansari, Y. Sun, A. E. Postlethwaite, K. T. Weber, and M. F. Kiani, "The scar neovasculature after myocardial infarction in rats.," *Am. J. Physiol. Heart Circ. Physiol.*, vol. 289, no. 1, pp. H108–13, Jul. 2005.
- [75] I. Adt, A. Kohler, S. Gognies, J. Budin, C. Sandt, A. Belarbi, M. Manfait, and G. D. Sockalingum, "FTIR spectroscopic discrimination of *Saccharomyces cerevisiae* and *Saccharomyces bayanus* strains.," *Can. J. Microbiol.*, vol. 56, no. 9, pp. 793–801, Sep. 2010.
- [76] A. C. Ruifrok and D. A. Johnston, "Quantification of histochemical staining by color deconvolution.," *Anal. Quant. Cytol. Histol.*, vol. 23, no. 4, pp. 291–9, Aug. 2001.
- [77] J. N. Cohn, R. Ferrari, and N. Sharpe, "Cardiac remodeling--concepts and clinical implications: a consensus paper from an international forum on cardiac remodeling. Behalf of an International Forum on Cardiac Remodeling.," *J. Am. Coll. Cardiol.*, vol. 35, no. 3, pp. 569–82, Mar. 2000.
- [78] M. Jackson, L. P. Choo, P. H. Watson, W. C. Halliday, and H. H. Mantsch, "Beware of connective tissue proteins: assignment and implications of collagen absorptions in infrared spectra of human tissues.," *Biochim. Biophys. Acta*, vol. 1270, no. 1, pp. 1–6, Jan. 1995.
- [79] D. L. Wetzel, G. R. Post, and R. a. Lodder, "Synchrotron infrared microspectroscopic analysis of collagens I, III, and elastin on the shoulders of human thin-cap fibroatheromas.," *Vib. Spectrosc.*, vol. 38, no. 1–2, pp. 53–59, Jul. 2005.
- [80] C. Petibois, G. Gouspillou, K. Wehbe, J.-P. Delage, and G. Déléris, "Analysis of type I and IV collagens by FT-IR spectroscopy and imaging for a molecular investigation of skeletal muscle connective tissue.," *Anal. Bioanal. Chem.*, vol. 386, no. 7–8, pp. 1961–6, Dec. 2006.
- [81] P. a West, P. a Torzilli, C. Chen, P. Lin, and N. P. Camacho, "Fourier transform infrared imaging spectroscopy analysis of collagenase-induced cartilage degradation.," *J. Biomed. Opt.*, vol. 10, no. 1, p. 14015, 2005.
- [82] X. Bi, X. Yang, M. P. G. Bostrom, D. Bartusik, S. Ramaswamy, K. W. Fishbein, R. G. Spencer, and N. P. Camacho, "Fourier transform infrared imaging and MR microscopy studies detect compositional and structural changes in cartilage in a rabbit model of osteoarthritis.," *Anal. Bioanal. Chem.*, vol. 387, no. 5, pp. 1601–12, Mar. 2007.

- [83] D. C. Sheeshan and B. B. Hrapchak, *Theory and Practice of Histotechnology*. Saint Louis: The C. V. Mosby Company, 1980.
- [84] J. Kiernan, *Histological and histochemical methods : theory and practice*, 4th ed. Bloxham [UK]: Scion, 2008.
- [85] J. Chen, S. K. Lee, W. R. Abd-Elgaliel, L. Liang, E.-Y. Galende, R. J. Hajjar, and C.-H. Tung, "Assessment of cardiovascular fibrosis using novel fluorescent probes.," *PLoS One*, vol. 6, no. 4, p. e19097, Jan. 2011.
- [86] L. C. Junqueira, G. Bignolas, and R. R. Brentani, "Picrosirius staining plus polarization microscopy, a specific method for collagen detection in tissue sections.," *Histochem. J.*, vol. 11, no. 4, pp. 447–55, Jul. 1979.
- [87] L. Rich and P. Whittaker, "COLLAGEN AND PICROSIRIUS RED STAINING : A POLARIZED LIGHT ASSESSMENT OF FIBRILLAR HUE AND SPATIAL DISTRIBUTION," *Brazilian J. Morphol. Sci.*, vol. 22, no. 2, pp. 97–104, 2005.
- [88] M. Kitamura, M. Shimizu, H. Ino, K. Okeie, M. Yamaguchi, N. Funjono, H. Mabuchi, and I. Nakanishi, "Collagen remodeling and cardiac dysfunction in patients with hypertrophic cardiomyopathy: the significance of type III and VI collagens.," *Clin. Cardiol.*, vol. 24, no. 4, pp. 325–9, Apr. 2001.
- [89] N. Morishita, S. Kusachi, S. Yamasaki, J. Kondo, and T. Tsuji, "Sequential Changes in Laminin and Type IV Collagen in the Infarct Zone," *Jpn. Circ. J.*, vol. 60, no. 2, pp. 108–114, 1996.
- [90] S. Wei, L. T. Chow, I. O. Shum, L. Qin, and J. E. Sanderson, "Left and right ventricular collagen type I/III ratios and remodeling post-myocardial infarction.," *J. Card. Fail.*, vol. 5, no. 2, pp. 117–26, Jun. 1999.
- [91] R. Wayne, *Light and video microscopy*. Amsterdam ;;Boston: Academic Press/Elsevier, 2009.
- [92] F.-N. Fu, M. P. Fuller, and B. R. Singh, "Use of Fourier Transform Infrared/Attenuated Total Reflectance Spectroscopy for the Study of Surface Adsorption of Proteins," *Appl. Spectrosc.*, vol. 47, no. 1, pp. 98–102, Jan. 1993.
- [93] B. R. Singh and M. P. Fuller, "FT-IR in Combination with the Attenuated Total Reflectance Technique: A Very Sensitive Method for the Structural Analysis of Polypeptides," *Appl. Spectrosc.*, vol. 45, no. 6, pp. 1017–1021, 1991.
- [94] K. a Oberg and a L. Fink, "A new attenuated total reflectance Fourier transform infrared spectroscopy method for the study of proteins in solution.," *Anal. Biochem.*, vol. 256, no. 1, pp. 92–106, Feb. 1998.

- [95] M. Carbonaro and a Nucara, "Secondary structure of food proteins by Fourier transform spectroscopy in the mid-infrared region.," *Amino Acids*, vol. 38, no. 3, pp. 679–90, Mar. 2010.
- [96] S. Waxman, S. R. Dixon, P. L'Allier, J. W. Moses, J. L. Petersen, D. Cutlip, J.-C. Tardif, R. W. Nesto, J. E. Muller, M. J. Hendricks, S. T. Sum, C. M. Gardner, J. a Goldstein, G. W. Stone, and M. W. Krucoff, "In vivo validation of a catheter-based near-infrared spectroscopy system for detection of lipid core coronary plaques: initial results of the SPECTACL study.," *JACC. Cardiovasc. Imaging*, vol. 2, no. 7, pp. 858–68, Jul. 2009.
- [97] R. Cheheltani, C. M. McGoverin, M. Kiani, and N. Pleshko, "Infrared Spectroscopy to Measure Collagen and Elastin in Aorta Using Multivariate Analysis," *2013 39th Annu. Northeast Bioeng. Conf.*, pp. 13–14, Apr. 2013.
- [98] J. H. N. Lindeman, B. A. Ashcroft, J.-W. M. Beenakker, M. van Es, N. B. R. Koekkoek, F. A. Prins, J. F. Tielemans, H. Abdul-Hussien, R. A. Bank, and T. H. Oosterkamp, "Distinct defects in collagen microarchitecture underlie vessel-wall failure in advanced abdominal aneurysms and aneurysms in Marfan syndrome.," *Proc. Natl. Acad. Sci. U. S. A.*, vol. 107, no. 2, pp. 862–5, Jan. 2010.
- [99] G. T. Jones, "The Pathohistology of Abdominal Aortic Aneurysm," in in *Diagnosis, Screening and Treatment of Abdominal, Thoracoabdominal and Thoracic Aortic Aneurysms*, R. Grundmann, Ed. InTech, 2011, pp. 53–74.
- [100] F. a M. V. I. Hellenthal, W. a Buurman, W. K. W. H. Wodzig, and G. W. H. Schurink, "Biomarkers of AAA progression. Part 1: extracellular matrix degeneration.," *Nat. Rev. Cardiol.*, vol. 6, no. 7, pp. 464–74, Jul. 2009.
- [101] E. S. Di Martino, A. Bohra, J. P. Vande Geest, N. Gupta, M. S. Makaroun, and D. a Vorp, "Biomechanical properties of ruptured versus electively repaired abdominal aortic aneurysm wall tissue.," *J. Vasc. Surg. Off. Publ. Soc. Vasc. Surg. [and] Int. Soc. Cardiovasc. Surgery, North Am. Chapter*, vol. 43, no. 3, pp. 570–6; discussion 576, Mar. 2006.
- [102] D. A. Vorp, "Biomechanics of abdominal aortic aneurysm.," *J. Biomech.*, vol. 40, no. 9, pp. 1887–902, Jan. 2007.
- [103] J. Hua and W. R. Mower, "Simple geometric characteristics fail to reliably predict abdominal aortic aneurysm wall stresses.," *J. Vasc. Surg.*, vol. 34, no. 2, pp. 308–15, Aug. 2001.
- [104] M. F. Fillinger, S. P. Marra, M. L. Raghavan, and F. E. Kennedy, "Prediction of rupture risk in abdominal aortic aneurysm during observation: wall stress versus diameter.," *J. Vasc. Surg.*, vol. 37, no. 4, pp. 724–32, Apr. 2003.

- [105] J. P. Vande Geest, D. H. J. Wang, S. R. Wisniewski, M. S. Makaroun, and D. a Vorp, "Towards a noninvasive method for determination of patient-specific wall strength distribution in abdominal aortic aneurysms," *Ann. Biomed. Eng.*, vol. 34, no. 7, pp. 1098–106, Jul. 2006.
- [106] E. Fonck, G. Prod'hom, S. Roy, L. Augsburg, D. a Rufenacht, and N. Stergiopoulos, "Effect of elastin degradation on carotid wall mechanics as assessed by a constituent-based biomechanical model," *Am. J. Physiol. Heart Circ. Physiol.*, vol. 292, no. 6, pp. H2754–63, Jun. 2007.
- [107] S.-S. Kim, C. Young, and B. Mizaikoff, "Miniaturized mid-infrared sensor technologies," *Anal. Bioanal. Chem.*, vol. 390, no. 1, pp. 231–7, Jan. 2008.
- [108] L. a Cassis and R. a Lodder, "Near-IR imaging of atheromas in living arterial tissue," *Anal. Chem.*, vol. 65, no. 9, pp. 1247–56, May 1993.
- [109] R. J. Dempsey, L. a Cassis, D. G. Davis, and R. a Lodder, "Near-infrared imaging and spectroscopy in stroke research: lipoprotein distribution and disease," *Ann. N. Y. Acad. Sci.*, vol. 820, pp. 149–69, May 1997.
- [110] P. R. Moreno, "Detection of Lipid Pool, Thin Fibrous Cap, and Inflammatory Cells in Human Aortic Atherosclerotic Plaques by Near-Infrared Spectroscopy," *Circulation*, vol. 105, no. 8, pp. 923–927, Feb. 2002.
- [111] R. E. Neuman and M. A. Logan, "The determination of Hydroxyproline," *J. Biol. Chem.*, vol. 184, p. 299, 1950.
- [112] C. A. Edwards and W. D. O'Brien, "Modified assay for determination in a tissue hydrolyzate of hydroxyproline," *Clin. Chim. Acta*, vol. 104, pp. 161–167, 1980.
- [113] R. E. Neuman and M. A. Logan, "The determination of Collagen and Elastin in Tissues," *J. Biol. Chem.*, vol. 186, no. 2, p. 549, 1950.
- [114] R.A. Grant, "Content and distribution of aortic collagen, elastin and carbohydrate in different species," vol. 7, no. 4, pp. 463–472, 1967.
- [115] J. M. Rosano, R. Cheheltani, B. Wang, H. Vora, M. F. Kiani, and D. L. Crabbe, "Targeted Delivery of VEGF after a Myocardial Infarction Reduces Collagen Deposition and Improves Cardiac Function.," *Cardiovasc. Eng. Technol.*, vol. 3, no. 2, pp. 237–247, Jun. 2012.
- [116] J. S. Campa, R. M. Greenhalgh, and J. T. Powell, "Elastin degradation in abdominal aortic aneurysms," *Atherosclerosis*, vol. 65, no. 1–2, pp. 13–21, May 1987.

- [117] R. J. Rizzo, W. J. McCarthy, S. N. Dixit, M. P. Lilly, V. P. Shively, W. R. Flinn, and J. S. Yao, "Collagen types and matrix protein content in human abdominal aortic aneurysms.," *J. Vasc. Surg.*, vol. 10, no. 4, pp. 365–73, Oct. 1989.
- [118] a Barth, "The infrared absorption of amino acid side chains.," *Prog. Biophys. Mol. Biol.*, vol. 74, no. 3–5, pp. 141–73, Jan. 2000.
- [119] L. Robert, A. Kadar, and B. Robert, "The macromolecules of the intercellular matrix of the arterial wall: collagen, elastin, proteoglycans, and glycoproteins.," *Adv. Exp. Med. Biol.*, vol. 43, no. 0, pp. 85–123, Jan. 1974.
- [120] N. Sakalihan, R. Limet, and O. D. Defawe, "Abdominal aortic aneurysm.," *Lancet*, vol. 365, no. 9470, pp. 1577–89, 2005.
- [121] S. Saatchi, J. Azuma, N. Wanchoo, S. J. Smith, P. G. Yock, C. a Taylor, and P. S. Tsao, "Three-dimensional microstructural changes in murine abdominal aortic aneurysms quantified using immunofluorescent array tomography.," *J. Histochem. Cytochem.*, vol. 60, no. 2, pp. 97–109, Feb. 2012.
- [122] R. Thompson, "Abdominal Aortic Aneurysms: Basic Mechanisms and Clinical Implications," *Curr. Probl. Surg.*, vol. 39, no. 2, pp. 110–230, Feb. 2002.
- [123] M. Carmo, L. Colombo, a Bruno, F. R. M. Corsi, L. Roncoroni, M. S. Cuttin, F. Radice, E. Mussini, and P. G. Settembrini, "Alteration of elastin, collagen and their cross-links in abdominal aortic aneurysms.," *Eur. J. Vasc. Endovasc. Surg.*, vol. 23, no. 6, pp. 543–9, Jun. 2002.
- [124] V. Samouillan, J. Dandurand, C. Lacabanne, A. Stella, M. Gargiulo, A. Degani, A. Gandaglia, and M. Spina, "Characterization of aneurysmal aortas by biochemical, thermal, and dielectric techniques.," *J. Biomed. Mater. Res. A*, vol. 95, no. 2, pp. 611–9, Nov. 2010.
- [125] R. Canfield and P. Dobrin, "Elastase, collagenase, and the biaxial elastic properties of dog carotid artery," *Am. J. Physiol.*, vol. 247, no. 1, pp. H124–H131, 1984.
- [126] K. a Wilson, J. S. Lindholt, P. R. Hoskins, L. Heickendorff, S. Vammen, and a W. Bradbury, "The relationship between abdominal aortic aneurysm distensibility and serum markers of elastin and collagen metabolism.," *Eur. J. Vasc. Endovasc. Surg.*, vol. 21, no. 2, pp. 175–8, Feb. 2001.
- [127] K. a Wilson, A. J. Lee, P. R. Hoskins, F. G. R. Fowkes, C. V. Ruckley, and A. W. Bradbury, "The relationship between aortic wall distensibility and rupture of infrarenal abdominal aortic aneurysm.," *J. Vasc. Surg.*, vol. 37, no. 1, pp. 112–7, Jan. 2003.

- [128] J. Satta, T. Juvonen, K. Haukipuro, M. Juvonen, and M. I. Kairaluoma, "Increased turnover of collagen in abdominal aortic aneurysms, demonstrated by measuring the concentration of the aminoterminal propeptide of type III procollagen in peripheral and aortal blood samples.," *J. Vasc. Surg.*, vol. 22, no. 2, pp. 155–60, Aug. 1995.
- [129] S. Menashi, J. S. Campa, R. M. Greenhalgh, and J. T. Powell, "Collagen in abdominal aortic aneurysm: typing, content, and degradation.," *J. Vasc. Surg. Off. Publ. Soc. Vasc. Surg. [and] Int. Soc. Cardiovasc. Surgery, North Am. Chapter*, vol. 6, no. 6, pp. 578–82, Dec. 1987.
- [130] L. Eberlová, Z. Tonar, K. Witter, V. Křížková, L. Nedorost, M. Korabečná, P. Tolinger, J. Kočová, L. Boudová, V. Třeška, K. Houdek, J. Moláček, J. Vrzalová, M. Pešta, O. Topolčan, and J. Valenta, "Asymptomatic abdominal aortic aneurysms show histological signs of progression: a quantitative histochemical analysis.," *Pathobiology*, vol. 80, no. 1, pp. 11–23, Jan. 2013.
- [131] M. Folkesson, A. Silveira, P. Eriksson, and J. Swedenborg, "Protease activity in the multi-layered intra-luminal thrombus of abdominal aortic aneurysms.," *Atherosclerosis*, vol. 218, no. 2, pp. 294–9, Oct. 2011.
- [132] P. B. Dobrin, "Pathophysiology and pathogenesis of aortic aneurysms. Current concepts.," *Surg. Clin. North Am.*, vol. 69, no. 4, pp. 687–703, Aug. 1989.
- [133] R. Adolph, D. a Vorp, D. L. Steed, M. W. Webster, M. V Kameneva, and S. C. Watkins, "Cellular content and permeability of intraluminal thrombus in abdominal aortic aneurysm.," *J. Vasc. Surg. Off. Publ. Soc. Vasc. Surg. [and] Int. Soc. Cardiovasc. Surgery, North Am. Chapter*, vol. 25, no. 5, pp. 916–26, May 1997.
- [134] D. A. Vorp, P. C. Lee, D. H. Wang, M. S. Makaroun, E. M. Nemoto, S. Ogawa, and M. W. Webster, "Association of intraluminal thrombus in abdominal aortic aneurysm with local hypoxia and wall weakening.," *J. Vasc. Surg. Off. Publ. Soc. Vasc. Surg. [and] Int. Soc. Cardiovasc. Surgery, North Am. Chapter*, vol. 34, no. 2, pp. 291–9, Aug. 2001.
- [135] D. H. J. Wang, M. S. Makaroun, M. W. Webster, and D. a Vorp, "Effect of intraluminal thrombus on wall stress in patient-specific models of abdominal aortic aneurysm," *J. Vasc. Surg.*, vol. 36, no. 3, pp. 598–604, Sep. 2002.
- [136] A. P. Tierney, D. M. Dumont, A. Callanan, G. E. Trahey, and T. M. McGloughlin, "Acoustic radiation force impulse imaging on ex vivo abdominal aortic aneurysm model.," *Ultrasound Med. Biol.*, vol. 36, no. 5, pp. 821–32, May 2010.
- [137] J. P. Vande Geest, M. S. Sacks, and D. a Vorp, "The effects of aneurysm on the biaxial mechanical behavior of human abdominal aorta.," *J. Biomech.*, vol. 39, no. 7, pp. 1324–34, Jan. 2006.

- [138] D. a Vorp, M. L. Raghavan, S. C. Muluk, M. S. Makaroun, D. L. Steed, R. Shapiro, and M. W. Webster, "Wall strength and stiffness of aneurysmal and nonaneurysmal abdominal aorta," *Ann. N. Y. Acad. Sci.*, vol. 800, pp. 274–6, Nov. 1996.
- [139] H. K. Russell, "A modification of Movat's pentachrome stain.," *Arch. Pathol.*, vol. 94, no. 2, pp. 187–91, Aug. 1972.
- [140] J. P. Vande Geest, D. E. Schmidt, M. S. Sacks, and D. a Vorp, "The effects of anisotropy on the stress analyses of patient-specific abdominal aortic aneurysms.," *Ann. Biomed. Eng.*, vol. 36, no. 6, pp. 921–32, Jun. 2008.
- [141] D. Farlay, M.-E. Duclos, E. Gineyts, C. Bertholon, S. Viguier-Carrin, J. Nallala, G. D. Sockalingum, D. Bertrand, T. Roger, D. J. Hartmann, R. Chapurlat, and G. Boivin, "The ratio 1660/1690 cm^{-1} measured by infrared microspectroscopy is not specific of enzymatic collagen cross-links in bone tissue.," *PLoS One*, vol. 6, no. 12, p. e28736, Jan. 2011.